

For Reference

NOT TO BE TAKEN FROM THIS ROOM

Ex libris
UNIVERSITATIS
ALBERTIANÆ



THE UNIVERSITY OF ALBERTA

RELEASE FORM

NAME OF AUTHOR PETER BAUMGARTNER
TITLE OF THESIS THE EFFECT OF JOINT
..... FABRIC ON ROCK MASS
..... CAVING
DEGREE FOR WHICH THESIS WAS PRESENTED M.Sc.
YEAR THIS DEGREE GRANTED 1979

Permission is hereby granted to THE UNIVERSITY OF ALBERTA LIBRARY to reproduce single copies of this thesis and to lend or sell such copies for private, scholarly or scientific research purposes only.

The author reserves other publication rights, and neither the thesis nor extensive extracts from it may be printed or otherwise reproduced without the author's written permission.

THE UNIVERSITY OF ALBERTA

THE EFFECT OF JOINT FABRIC ON ROCK MASS CAVING

by

PETER BAUMGARTNER



A THESIS

SUBMITTED TO THE FACULTY OF GRADUATE STUDIES AND RESEARCH

IN PARTIAL FULFILMENT OF THE REQUIREMENTS FOR THE DEGREE

OF MASTER OF SCIENCE

IN

MINING ENGINEERING

DEPARTMENT OF MINERAL ENGINEERING

EDMONTON, ALBERTA

FALL, 1979

THE UNIVERSITY OF ALBERTA
FACULTY OF GRADUATE STUDIES AND RESEARCH

The undersigned certify that they have read, and
recommend to the Faculty of Graduate Studies and Research,
for acceptance, a thesis entitled THE EFFECT OF JOINT FABRIC
ON ROCK MASS CAVING
.....
.....
submitted by P. Baumgartner
.....
in partial fulfilment of the requirements for the degree of
Master of Science

This thesis is dedicated to the poor souls
searching for a true understanding of rock mass
behavior.

ABSTRACT

The primary mechanisms of rock mass failures in an underground environment are unknown since they cannot be observed by any known means once moderately small movements have occurred.

This dissertation exams large scale underground movements by a two-dimensional physical modelling technique. A base friction machine that could tilt so as to add or subtract a component of gravity, was constructed to examine the progressive collapse of a jointed rock mass structure when a limiting excavation span had been exceeded.

The development of the tilting base friction machine which incorporates certain scaling laws was a necessary tool to examine qualitatively the the multi-parameter block interactions of a rock mass. Simulated rock masses with differing structural orientations and spacings were cast and failed on this machine.

The series of model tests identifies inter-block sliding, rotation, and crushing as the primary failure modes caused by the mass failure mechanisms of rock mass sliding, beam-column buckling, kink-band formation and intact material failure.

ACKNOWLEDGEMENTS

I wish to thank all the people who aided and encouraged me in my work:

my wife, Evelina, for her love and support in completing this project;

my parents, for their love, patience and encouragement;

Dr. B. Stimpson, for introducing the base friction modelling technique and for all his advise and support;

Gerry Chaisson, for the construction of the machine and its innovative design features;

Lin Yuen Ding, for the drafting of some very tedious figures;

Fred Eves, for his work on the Discrete Element Method and contribution to Appendix IV;

The Dept. of Mineral Engineering staff, for their advise, support and friendship;

Luscar Ltd., for a two-year mining scholarship;

my employer, Inco Metals Ltd., for allowing me to return to complete the project;

all those people, who had to put up with me during the project.

TABLE OF CONTENTS

CHAPTER	PAGE
INTRODUCTION	1
1.0. Rock Mass Caving	1
1.1. The Nature of Rock Masses and Failure Modes	5
1.2. Scope of the Investigation	8
THE MECHANICS OF JOINTED ROCK MASSES	9
2.0. Introduction	9
2.1. Continuous Joint Systems	10
2.1.1. Block Sliding	10
2.1.2. Block Rotation	14
2.1.3. Buckling	20
2.1.4. Intact Rock Failure	21
METHODS FOR STUDYING THE STABILITY OF JOINTED ROCK MASSES AND THEIR APPLICABILITY TO CAVING STUDIES ...	25
3.0. Introduction	25
3.1. Closed-Form Solutions	26
3.2. Physical Models	27
3.3. The Limit Equilibrium Method	28
3.4. Numerical Methods	29
3.4.1. Finite Element Method	30
3.4.2. Finite Difference Method	32
3.4.3. Discrete Element Method	33
3.5. Elastic Approach	33
3.6. Conclusion	36

TABLE OF CONTENTS continued

A QUALITATIVE PHYSICAL MODEL STUDY OF ROCK MASS CAVING ..	38
4.0. Introduction	38
4.1. Base Friction Model Technique	39
4.1.1. Model Technique	39
4.1.2. Machine Description	39
4.1.3. Model Material	44
4.1.4. Model Scaling	47
4.1.5. Model Preparation	51
4.2. Base Friction Model Study	52
4.2.1. Test #001	54
4.2.2. Test #002	57
4.2.3. Test #003	61
4.2.4. Test #004	65
4.2.5. Test #009	65
4.2.6. Test #013	71
4.2.7. Test #014	74
4.2.8. Test #015	74
4.2.9. Test #016	79
4.2.10. Test #017	82
4.2.11. Test #018	82
4.2.12. Test #019	87
4.2.13. Test #020	87
4.2.14. Test #005	92
4.2.15. Test #006	92
4.2.16. Test #008	92
4.2.17. Test #010	96
4.2.18. Test #007	96

TABLE OF CONTENTS continued

4.2.19. Test #012	99
4.2.20. Test #011	99
4.2.21. Test #024	99
4.2.22. Test #021	103
4.2.23. Test #025	103
4.2.24. Test #023	106
4.2.25. Test #022	106
4.2.26. Test #026	106
CONCLUSION AND RECOMMENDATION	110
BIBLIOGRAPHY	114
APPENDIX I	118
APPENDIX II	125
APPENDIX III	127
APPENDIX IV	132

LIST OF TABLES

Table	Description	Page
4.1.	GEOMETRY OF BASE FRICTION MODEL TESTS	54

LIST OF FIGURES

Figure	Page
1.1 Caving Induced by Longwall Mining	2
1.2a Stress Distribution Around a Longwall Panel (after Whittaker)	2
1.2b Stress Distribution Throughout a Room-and-Pillar Panel	2
1.3 Ingress of Waste, Diluting Ore	4
1.4 Schematic of Block Caving	4
1.5 Subsidence Due to Block Caving	6
2.1a Continuous Orthogonal Jointing	11
2.1b Continuous and Discontinuous Jointing (i.e. Columnar Basalt)	11
2.2 Shear Failure Curve	13
2.3 Shear Failure Envelope	13
2.4 Bi-Linear Shear Failure Envelope (after Patton)	13
2.5 Small Block Rotations	16
2.6 Shear Strain Due to Rotations in a Layer of Continuous Parallelopipeds (after Nascimento and Teixeira)	16
2.7 Effect of the Number to Joint Blocks, Driving Ratio T/N and Aspect Ratio	16
2.8 Kink-Band	18
2.9 Kink-Band Hinge Detail	18
2.10 Maximum Load for Column with Initial Deflection or Load Eccentricity (after Chapman and Slatford)	22
2.11 Theoretical Maximum Spans for Self-Supporting "Linear Arches" (after Woodruff)	22
2.12 Local Contact Crushing	24

LIST OF FIGURES continued

2.13 Indirect Point Load Tensile Failure	24
2.14 Extreme Fibre Tensile Failure Due to Bending	24
3.1 Finite Element Model	31
3.2 Some Typical Systones	35
3.3a Simple Systone of Disks	35
3.3b Forces Applied to a Systone Element (after Trollope)	35
4.1 Schematic of a Base Friction Model	40
4.2 Uniaxial Load-Deformation Curves of Oil, Flour and Sand Model Materials	46
4.3 Uniaxial Stress-Strain Curve of Flour and Methanol Model Material	48
4.4 Base Friction Vertical Stress as a Function of Machine Rotation θ and Kinematic Angle of Friction ϕ	50
4.5 Base Friction Machine Rotation θ as a Function of the Kinematic Angle of Friction ϕ	50
4.6 Arching Supported by Block Protrusions	58
4.7 Converging Kink-Bands	64
4.8 End Conditions Affecting Beam-Column Stability	70
6.1 Base Friction Stress Analysis	119
7.1 Model Material Properties	126
8.1 Kink Band Hinge Rotations	128
8.2 Vertical Mechanical Dilation	128

LIST OF PHOTOGRAPHIC PLATES

Plate	Description	Page
1	Base Friction Machine	42
2	Base Friction Machine Details	45
3	Test #001	55
4	Test #001 (con't)	56
5	Test #002	59
6	Test #002 (con't)	60
7	Test #003	62
8	Test #003 (con't)	63
9	Test #004	66
10	Test #004 (con't)	67
11	Test #009	68
12	Test #009 (con't)	69
13	Test #013	72
14	Test #013 (con't)	73
15	Test #014	75
16	Test #014 (con't)	76
17	Test #015	77
18	Test #015 (con't)	78
19	Test #016	80
20	Test #016 (con't)	81
21	Test #017	83
22	Test #017 (con't)	84
23	Test #018	85

LIST OF PHOTOGRAPHIC PLATES continued

24 Test #018 (con't)	86
25 Test #019	88
26 Test #019 (con't)	89
27 Test #020	90
28 Test #020 (con't)	91
29 Test #005	93
30 Test #006	94
31 Test #008	95
32 Test #010	97
33 Test #007	98
34 Test #012	100
35 Test #011	101
36 Test #024	102
37 Test #021	104
38 Test #025	105
39 Test #023	107
40 Test #022	108
41 Test #026	109

CHAPTER 1

INTRODUCTION

1.0. ROCK MASS CAVING

Rock mass caving or simply caving represents the loss of structural stability of an underground excavation. This usually implies a large downward displacement of rock material into the excavation. Mine excavations often cave with time, since they are often unsupported or only temporarily supported.

It is not sufficient to know whether or not the excavation will fail, but if it is designed to cave, how will it do so? If it does not fail, what must be done to encourage such action?

With certain mining systems, caving can result in significant stress relief around an excavation and thereby can reduce the amount of costly ground support. This phenomenon is of particular value in longwall mining where the superincumbent strata are allowed to cave behind the mining face and the immediate roof support equipment (fig. 1.1). Stress concentrations exist at the active mining boundaries only and not throughout the entire development area as in room-and-pillar mining (fig. 1.2 a-b).

In other mining systems, caving must be prevented and the extraction must be carried out in a controlled cyclic fashion. For example, only a portion of ground can be

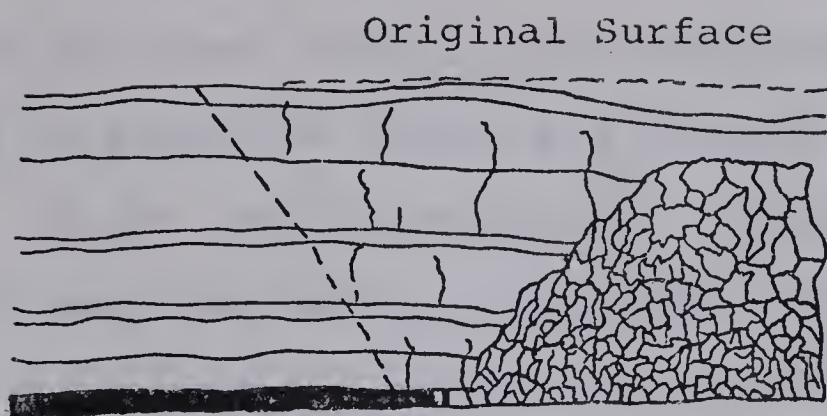


Fig. 1.1

Caving Induced by Longwall Mining

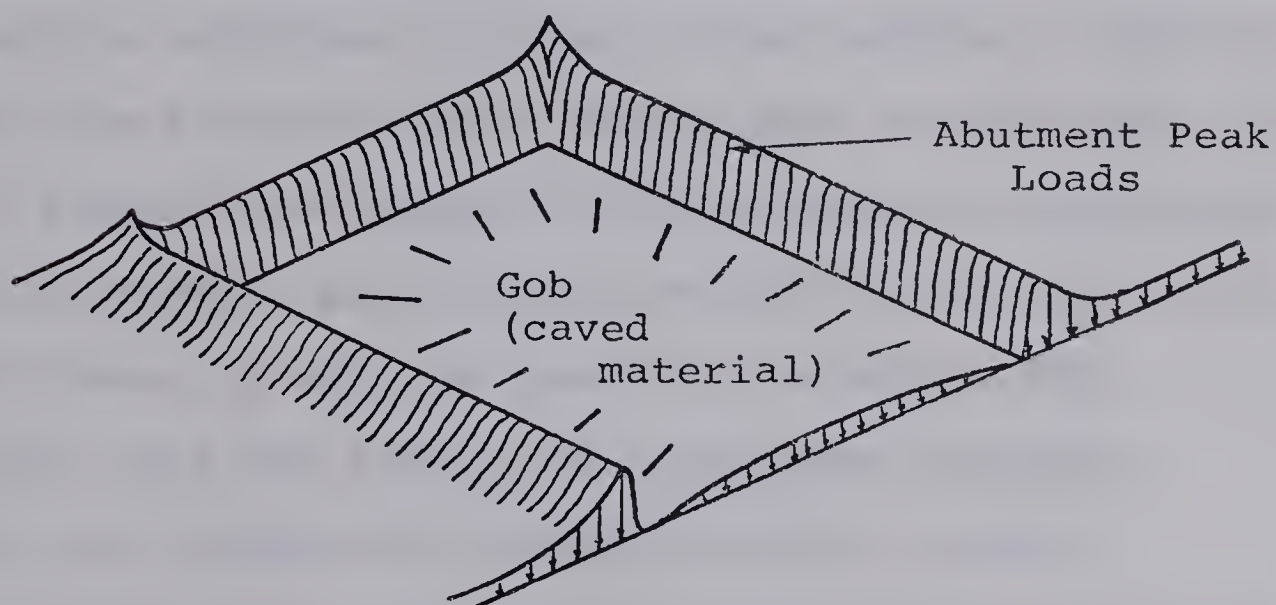


Fig. 1.2(a)

Stress Distribution Around A Longwall Panel (after Whittaker)

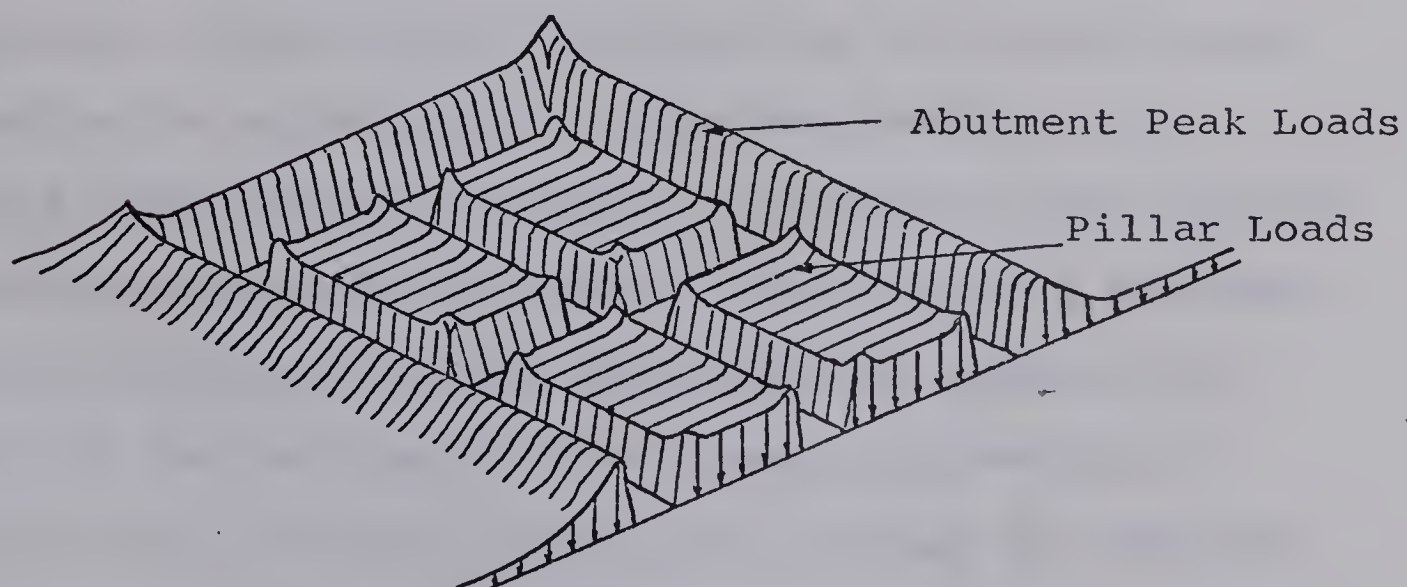


Fig. 1.2(b)

Stress Distribution Throughout a Room & Pillar Panel

excavated at any one time, such as in a cut-and-fill cycle, which must then be supported before any further excavation can take place. If the excavation becomes too large, instability may occur and must be prevented by installing a support system which provides a safe work environment and maintains the opening. In other cases, if the excavation boundaries are defined by a waste/ore contact, the broken muck must be withdrawn in a controlled fashion in order to minimize the dilution from a caving roof or wall (fig. 1.3).

In massive ore bodies and thick seams, an excavation technique known as block caving employs the caving action of the rock mass. If undercut rooms are excavated with sufficient span and length, the rock mass collapses, ideally, in a progressive fashion beyond a stable configuration. This caving action will stop if the broken material is not removed (fig. 1.4).

In the case of in-situ extraction of ores, liquids and gases, caving increases the rock mass void space and, consequently, increases the permeability of the rock mass surrounding the excavation or fragmentation zone. The increased communication between the extraction zone and the surrounding environment can affect salt and metal leaching, oil shale retorting and coal gasification. Reagents and products of the reactions have a greater propensity to escape from the intended regions. In the case of retorting and gasification, the gas phase reactants and products are particularly mobile due to low densities and viscosities.

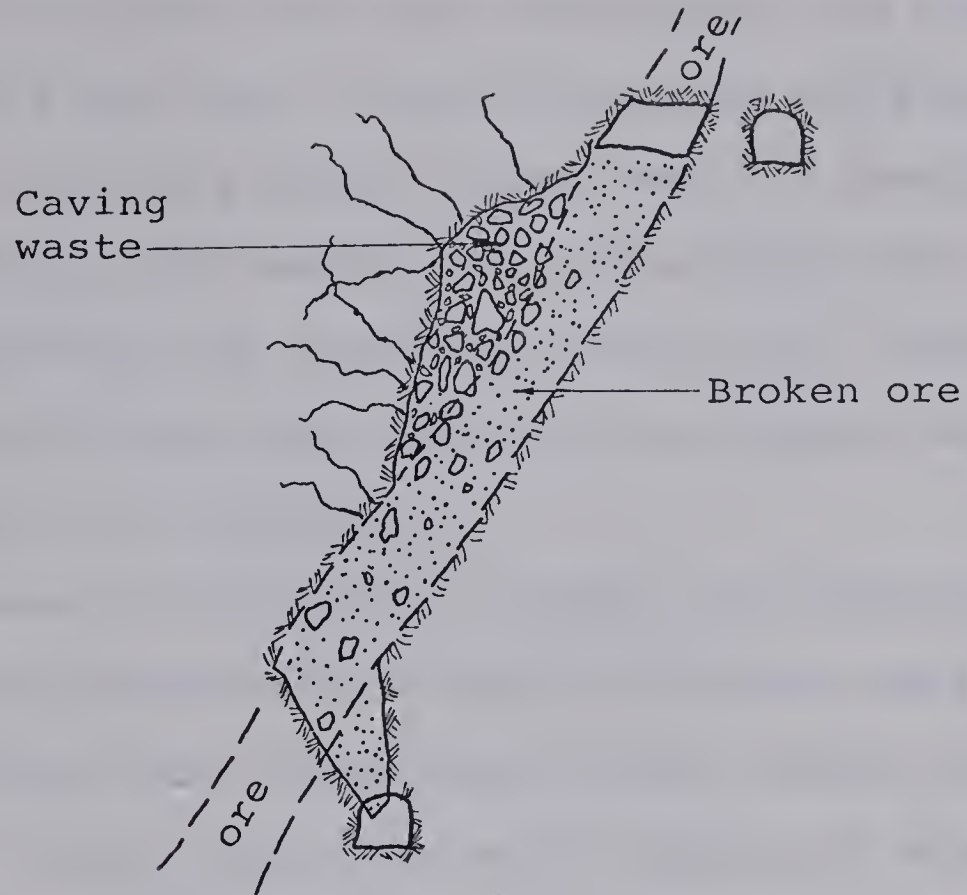


Fig. 1.3

INGRESS OF WASTE DILUTING ORE

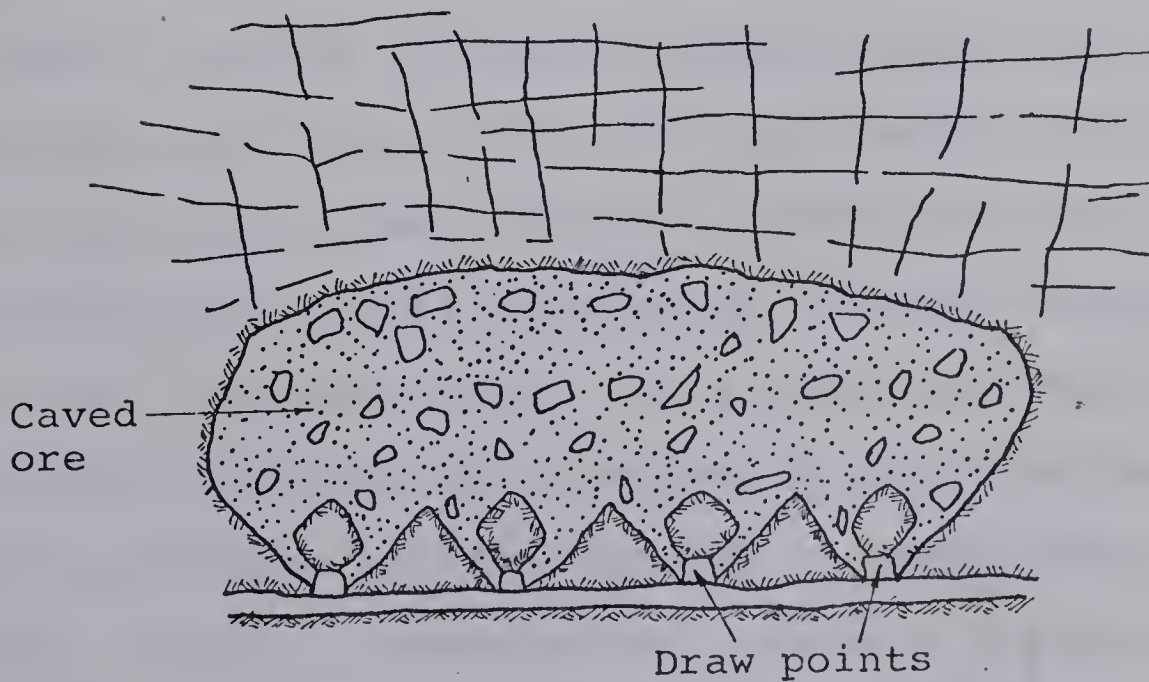


Fig. 1.4

SCHEMATIC OF BLOCK CAVING

Injected combustion air may 'short circuit' through a caved zone around the fire front. The environment may also enter the reaction zone, such as caved materials and excessive groundwater which may dilute and/or cool the reaction zone.

Relatively large amounts of caving invariably result in surface subsidence and 'sinkholes' (fig. 1.5). Shafts and surface installations must obviously be located beyond the subsidence zone of influence.

The causes and effects of caving, as illustrated above, must be better understood in order to develop safe and efficient large scale underground mining methods and to reduce unit costs. The mechanics of caving and progressive failure must be examined so as to better define the parameters which control caving and which ultimately influence the structural stability or instability of underground excavations.

1.1. THE NATURE OF ROCK MASSES AND FAILURE MODES

Early analyses of caving examined intact rock rupture (Bucky 1956 and Coates 1970). The engineering properties of intact rock (i.e. shear strength, tensile strength, modulus of rupture and uniaxial compressive strength, modulus of elasticity, Poisson's ratio, etc.) were considered as the controlling variables for classical elastic analyses. For lamellar geological structures such as bedded deposits, a modified analysis considered the strata as a system of rigidly clamped beams or plates (Obert and Duvall 1967).

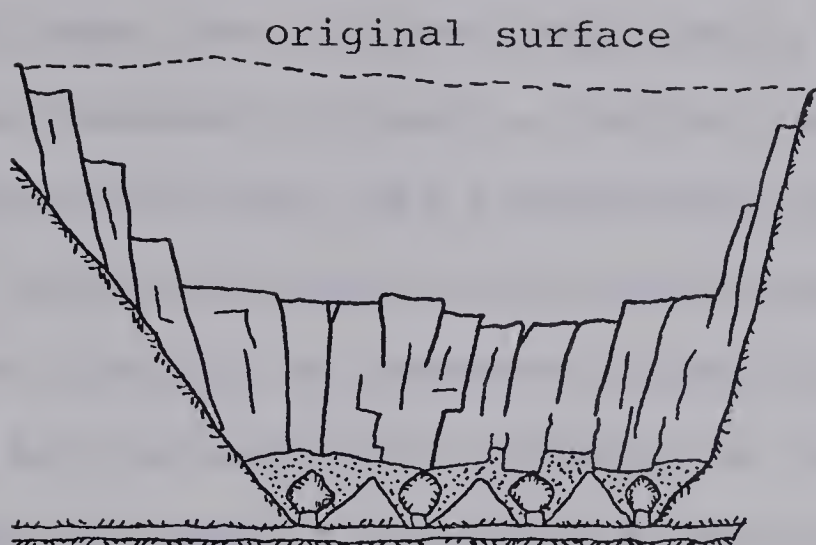


Fig. 1.5
Subsidence Due to Block Caving

However, both methods considerably overestimated stability since the strata was assumed to have some tensile strength.

Rock masses, particularly those in which economic minerals are found, are not monolithic but are constituted of intact rock weakened by joints, faults, bedding planes and other discontinuities. The discontinuities may be in random or in preferred orientations, continuous or discontinuous, singular or numerous. Though these planes of weakness may not be continuous, directly or indirectly they produce a mass of intact rock blocks by the intersection of these continuous or discontinuous planes.

Slope stability and underground studies indicate that the mechanical properties of the rock discontinuities and infilling materials (i.e. peak and residual friction angles, dilation, shear strength and intact rock strength of asperities) and the rock block geometry control the shear failure mode of the rock mass. Studies by Hammett (1974) show that the geometry of the rock mass with respect to the excavation controls the feature known as the mechanical dilation of the rock mass. This is dilation produced by the physical rotation of blocks within the mass as opposed to dilation produced by the overriding of joint surface asperities.

Another mode of failure related to block rotation is that of buckling instability of block beam-columns, beam-columns being long axial members subjected to both axial and transverse loads. Axial and transverse loads applied to rock

beam-columns, coupled with the no-tension carrying ability of the included fractures, can deflect and therefore rotate the members into the excavation.

It should also be noted that in caving, progressive failure occurs, caused by a combination of rock creep, continuing fracture propagation, a transient stress field in the mass, a transient groundwater regime, slaking and weathering, etc.. Since mining excavation is a quasi-static process, the influence of stress re-distributions or transient stress fields would appear to be an important consideration in the analysis of progressive failure.

1.2. SCOPE OF THE INVESTIGATION

Since the mechanics of caving are so complex and are rarely directly observable in-situ, the author chose to examine the influence of continuous joints and uniform joint spacings on the caving of rock masses by means of model studies. A two-dimensional physical model of a simplified block cave was developed to examine the effect of rock block interactions on stability and, in particular, on instability.

CHAPTER 2

THE MECHANICS OF JOINTED ROCK MASSES

2.0. INTRODUCTION

The strength of rock masses is reduced by planes of weakness (e.g. bedding planes, faults, joints, schistosity, foliation, unconformities, etc.). The planes of weakness can be classed into three groups: (a) large scale structures such as faults and unconformities which are usually singular planes within a mine excavation: (b) small scale structures such as bedding, cleavage and joint planes which occur as multitudinous surfaces within the excavation, and (c) macroscopic structures such as schistosity and foliation which also are multitudinous planes of weakness, but are often considered features of intact rock anisotropy since they tend to have greater cohesive strengths than the other structures.

The small scale structures which are prevalent within the mass can strongly affect its mechanical behavior. The systems of discontinuities such as joints and bedding planes determine the shape and size of the intact rock blocks in a rock mass. It has been widely observed that joint spacing shows some dependence upon the degree of geological deformation and the intact rock strength (Price 1966). Joint spacing increases with intact rock strength, all other things being equal. However, many other properties also

affect joint spacing (e.g. bed thickness in sedimentary strata). Joints frequently occur in two or more sets (i.e. a set being a system of semi-parallel planes) and can be relatively continuous (e.g. bedding) or discontinuous (e.g. hexagonal joints in basalt or dessicated clays) (fig.2.1 a-b). For simplicity, the term 'joint' will be used to include all planes of weakness such as cleavage, as well as true joints. If jointing is continuous and a free surface exists, essentially four singular or combined modes of failure can occur involving; (i) block sliding, (ii) block rotation, (iii) member buckling instability and (iv) intact rock block failure.

2.1. CONTINUOUS JOINT SYSTEMS

The simplest system to examine is that of continuous, through-going joints since well defined planes of potential movement can be assumed. During deformation, the individual blocks can: (i) slide, (ii) rotate or (iii) slide and rotate, with respect to one another.

2.1.1. BLOCK SLIDING

Direct shear strength tests of natural rough joints provide shear load - shear deformation curves from which the peak and residual strengths of the material can be derived (fig.2.2). A number of such tests for a range of normal loads produces a non-linear shear strength envelope (fig.2.3) for which Patton (1966) gives a simplified

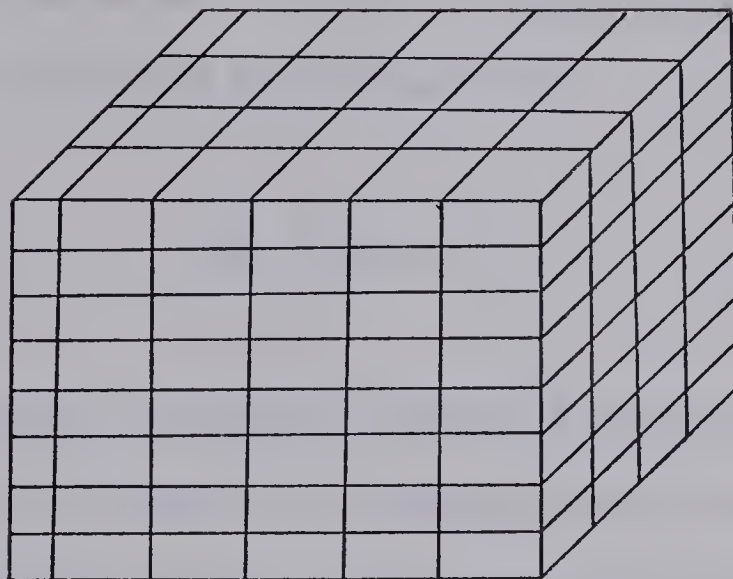


Fig. 2.1(a)
Continuous Orthogonal
Jointing

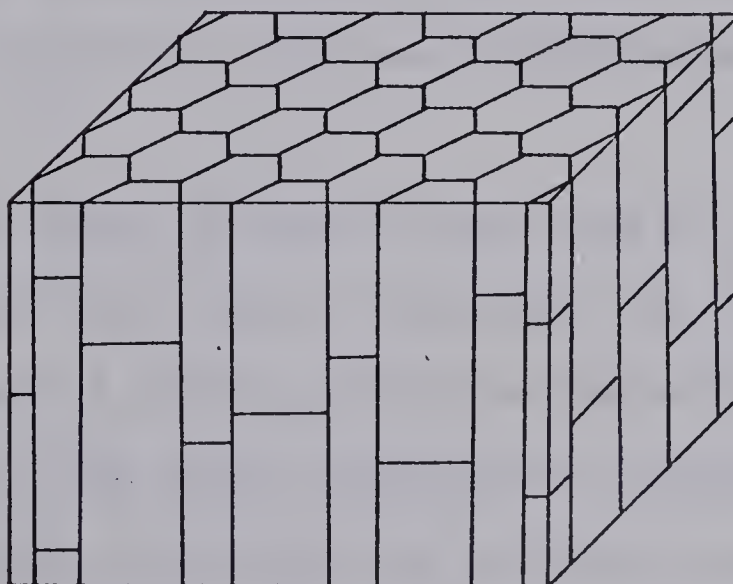


Fig. 2.1(b)
Continuous and Discontinuous
Jointing (i.e. Columnar Basalt)

explanation. By testing model joints with asperities set at a uniform spacing, height and angle of inclination i to the joint plane, he produced a bi-linear shear strength envelope (fig.2.4). At low normal loads the peak shear strength envelope is at an angle ϕ_p defined by:

$$\phi_p = \phi_r + i$$

where ϕ_r = effective residual angle of friction

i = angle of asperity inclination to the joint plane.

At high normal loads, the stresses on the asperities exceed the material strength and the asperities fail. The shear strength envelope then reduces to an angle ϕ_r .

Strength envelopes from real rough joints are non-linear, not bi-linear since the joint surface irregularities, unlike Patton's saw-tooth joint have a range of sizes, inclinations, internal strengths and coefficients of friction.

Laboratory shear strength tests are of small scale compared to the field scale. The effect of large scale surface roughness is difficult to estimate for the incorporation in the limit equilibrium analyses for rock slopes. With large joint spacing relative to the excavation dimensions, these analyses appear to be adequate for most cases.

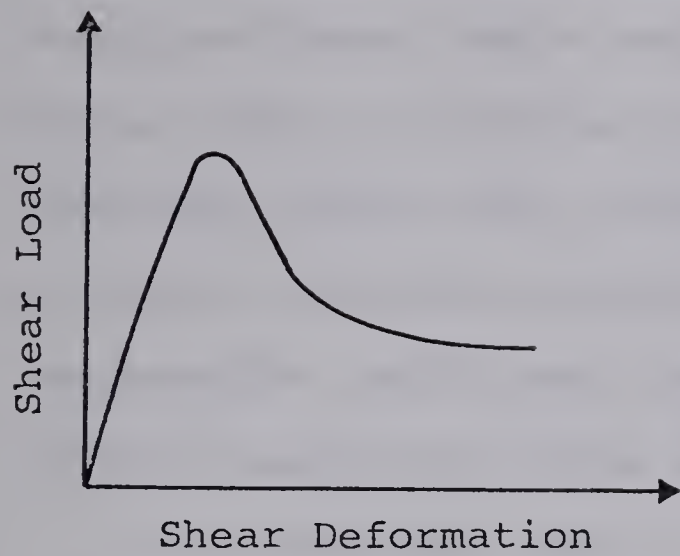


Fig. 2.2
Shear Failure Curve

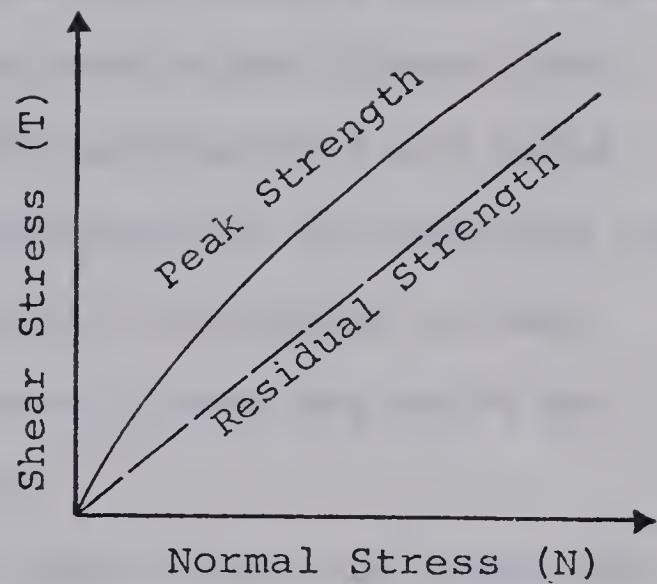


Fig. 2.3
Shear Failure Envelope

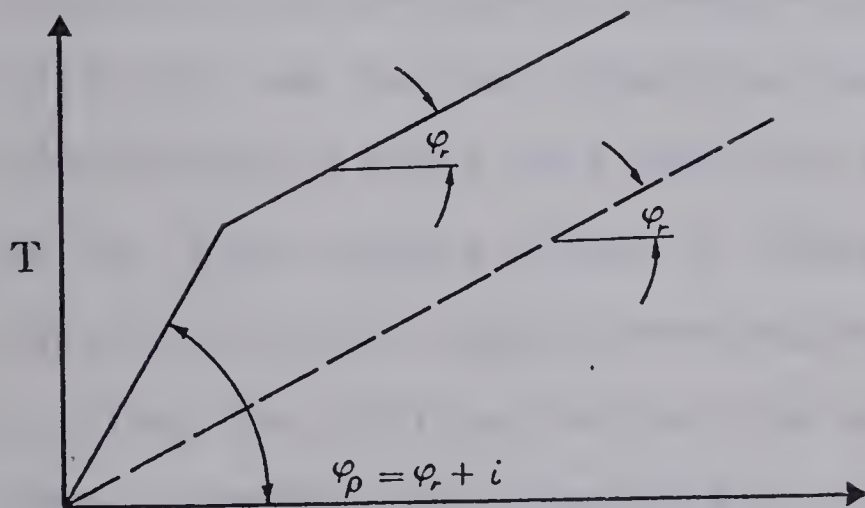


Fig. 2.4(a)
Bi-Linear Shear Failure Envelope
(after Patton)

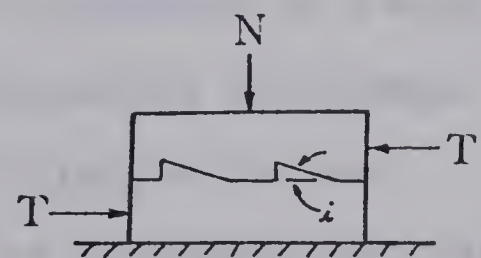


Fig. 2.4(b)

2.1.2. BLOCK ROTATION

When joint spacings are small relative to the size of the excavation, sliding mechanisms are complex and obscure. Normal and shear loads acting on constrained intact rock blocks induce non-uniform stress distributions and block rotations. Since joint stiffnesses tend to be less than that of intact materials, particularly if the joints contain compressible infillings, the intact blocks may shift and rotate a small but finite amount.

On a potential shear plane parallel to the joint set, block sliding becomes progressively difficult with shear displacement. The shifted and rotated intact blocks along this plane generate mechanical asperities due to the protruding block edges and corners into the shear plane. No longer can a single plane of failure be assumed since the disruption of one block disrupts its nearest neighbors (fig.2.5) and the net effect is the creation of a zone of disturbance. Within this zone the joint roughness or i-angle of the joint planes alters as shear deformation continues. Depending on the system constraints of dilation due to sliding, the driving forces, the asperity strengths and the joint geometry, the possibility of sliding as a primary mechanism becomes increasingly remote and rotations become dominant (Ladanyi and Archambault 1972).

Nascimento and Teixeira (1971) investigated joint block rotations of a single layer of blocks resting on a smooth, continuous joint plane as a possible shear displacement

mechanism (fig.2.6) and noted a vertical mechanical dilation accompanying block rotation. Also, horizontal dilation occurred when all the blocks rotated in-phase (i.e. all blocks rotated by the same angle). This simple model showed that if horizontal dilation was constrained then rotation was unlikely. They did not investigate the mechanics of several layers of blocks undergoing rotation.

Hammett (1974) extended this work, developing a mathematical relationship between the driving forces required for rotation, the number of blocks along the shear plane and the aspect ratio (ratio of block height to width) of individual blocks (fig.2.7). For a single layer of joint blocks between two continuous, intact joint surfaces, the net result was that, for a long failure plane, rotation along the joint planes was not kinematically possible and that translational sliding was the sole mechanism of displacement. The limiting length of the failure plane for which rotation can occur is approximately:

$$nb = 2 a / b$$

where n = no. of blocks

b = block width

a = block height

For example, if a / b is 5, then the maximum failure plane length is approximately $10b$ units before rotation is superceded by sliding. To be more exact, the driving forces

of simple sliding must be compared to Hammett's relationship:

$$\frac{T}{N} = \frac{n(a \cos \theta - b \sin \theta) + \frac{(1+2+\dots+(n-1)(b \tan \phi)(\tan \theta + \tan \phi)}{(1+\tan^2 \phi) \cos \theta}}{n(b \cos \theta + a \sin \theta) + \frac{(1+2+\dots+(n-1)(b)(\tan \theta + \tan \phi)}{(1+\tan^2 \phi) \cos \theta}}$$

where θ = block rotation angle

ϕ = friction angle

T = shear force

N = normal force

if:

$$T/N < \tan \phi$$

then rotation will take place but not when:

$$T/N \geq \tan \phi.$$

Tests conducted by Ladanyi and Archambault (1972) and those of the author show that kink-bands form with high aspect ratio composite blocks rotating on a plane oblique to the joint directions. An examination of this phenomenon (fig.2.8) shows that there is no contact between the kink-band columns (i.e. there is no lateral dilation force along the failure plane). This situation differs from the case of Nascimento's or Hammett's models.

Closer examination of the kink-band hinge (fig.2.9)

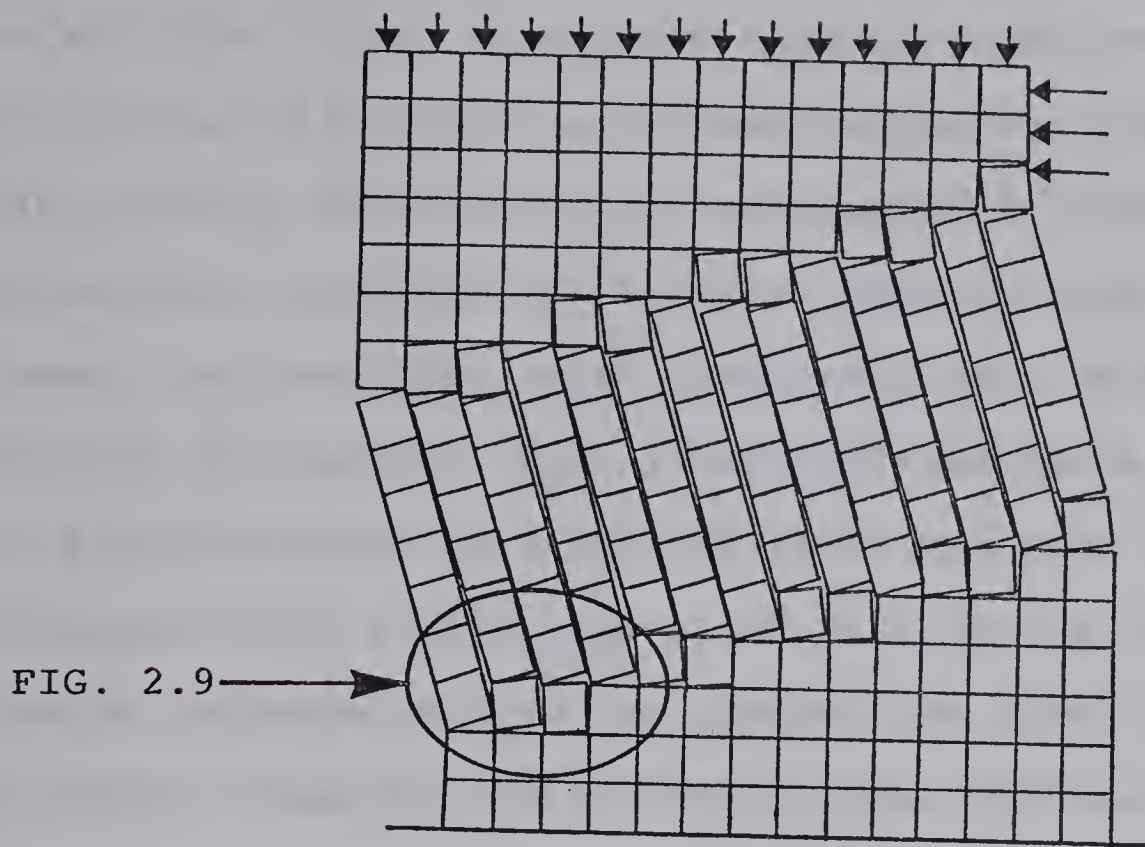


Fig. 2.8

Kink-Band

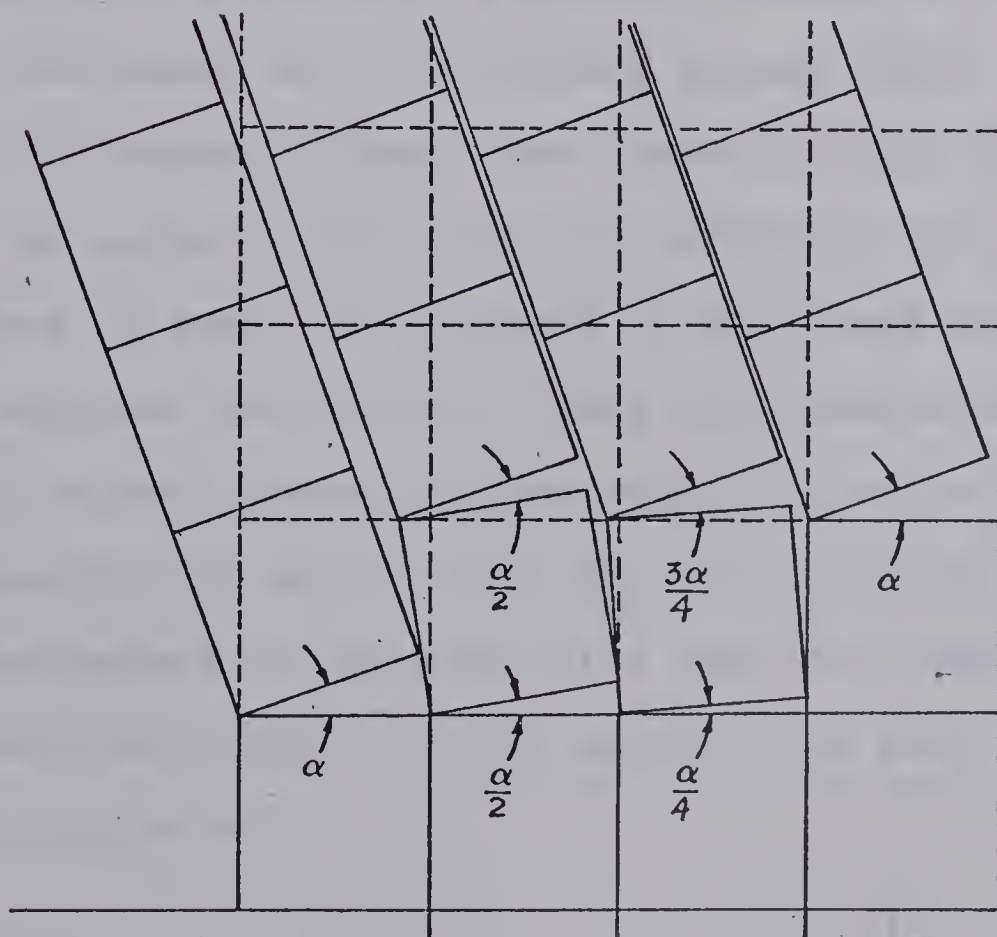


Fig. 2.9

Kink-Band Hinge Detail

shows why this is the case. On one joint plane, the first block rotates at α -degrees. The next adjoining block, if no sliding occurs, can rotate to a maximum of $\alpha/2$ -degrees (See Appendix III). In order for the kink band columns to remain in-phase, the overlying joint block must make up the difference in rotation (i.e. rotate $\alpha/2$ -degrees also). The next adjoining block on the joint plane can then rotate only $\alpha/4$ -degrees and its overlying block must rotate $3\alpha/4$ -degrees to remain in-phase. Due to the loadings at block hinges, local stress concentrations induce corner deformation and crushing. Therefore, at some point the next adjoining block does not rotate and then the upper block must rotate α -degrees in order to again remain in-phase with the kink-band.

The vertical mechanical dilation, caused by block rotations, decreases with increasing aspect ratio of individual kink-band columns (See Appendix III). In the limit, as the aspect ratio tends to infinity, the vertical dilation goes to zero. The effects at the block hinges limits or negates the dilation since the corners deform due to the high stress concentrations and the local crushing.

The possibility exists that the width of the kink-band might be determined by the condition that the total vertical dilation less the corner contact deformation must be equal to or less than zero.

2.1.3. BUCKLING

Kink-bands may also be examined as a phenomenon of column or beam-column instability, a field which has been well researched and documented for most civil engineering materials and structures (Timoshenko and Gere 1961). However, very little work has been undertaken for the problem of weak (i.e. having low or zero tensile strength) materials without reinforcement.

It is well-known that if a simple pin-ended column experiences a concentric axial load, the critical load P_{cr} required to buckle the column is:

$$P_{cr} = \frac{\pi^2 EI}{L^2}$$

where E = modulus of elasticity

I = section modulus

L = length of column.

Chapman and Slatford (1956) found that this is also true for brittle columns under the same boundary condition of concentric loading on a perfectly straight column. If the column has an initial deflection or if the load is applied in an eccentric manner, the maximum load carrying capacity is greatly reduced (fig.2.10).

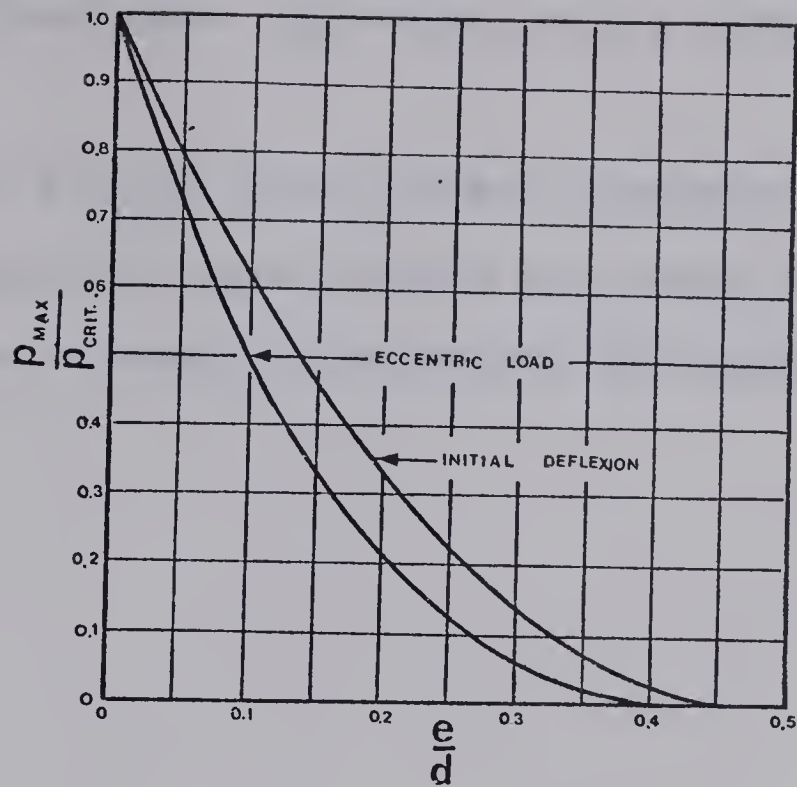
However, no definitive relationships exist for eccentric or transverse loadings or the effects of end conditions on brittle members. The problem is further

complicated by the high stress concentrations and local crushing at the joint block corners. Structural analysis of these problems may lead to methods for estimating the width and direction of kink-bands.

Another application of beam-column instability is that of roof support and caving. As mentioned at the beginning of Section 1.1, roof sections have been treated as linear elastic beams or plates. This approach was taken by Evans (1941) who represented the roof as a Voussoir Beam. His analysis results in large overestimates of spans. Woodruff (1966) modified this approach by introducing the effects of lateral abutment strains. His theoretical maximum spans for self-supporting linear arches (fig. 2.11) do not appear realistic. The study of beam-column instability may be a more realistic approach to estimating maximum roof spans.

2.1.4. INTACT ROCK FAILURE

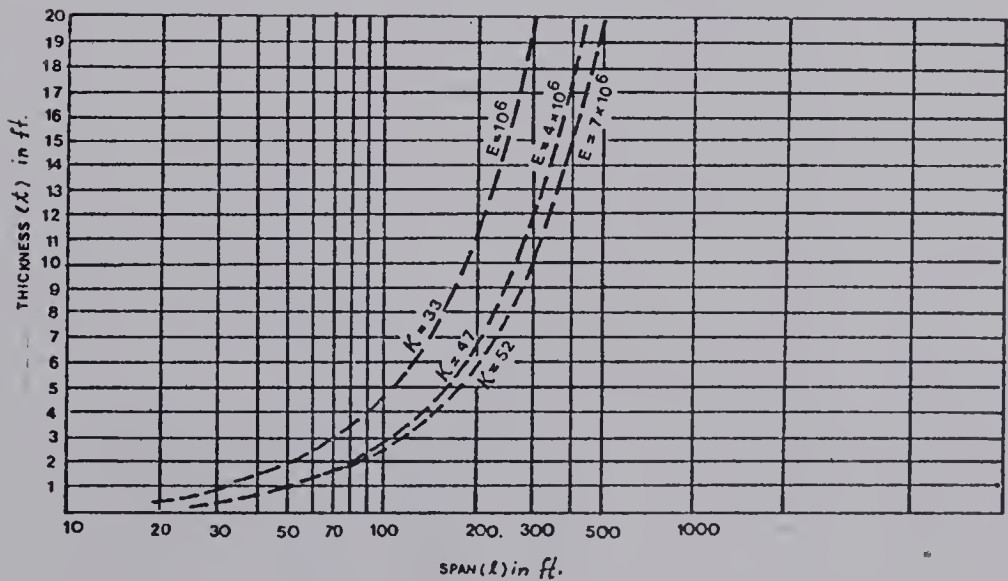
As has been noted, joint block rotations play an important role in the mechanics of ground stability and movement around excavations. As blocks rotate, edge-face contacts result. If a sufficiently large normal force is transmitted by an edge of one block to a face of an adjacent block, local crushing of the edge as well as to the face can occur (fig. 2.12). If another edge applies a load to an opposite face of the same block, tensile stresses may develop within the block due to the point-loading condition (fig. 2.13). If the tensile stress exceeds the tensile



e = eccentricity
 d = column thickness

Maximum Load for Column With Initial Deflexion or Load Eccentricity
(After Chapman & Slatford)

Fig. 2.10.

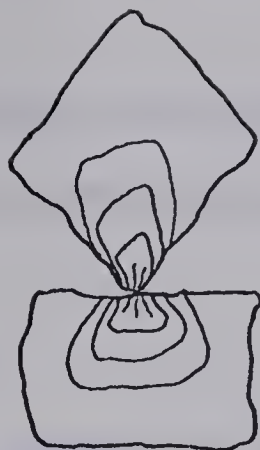


Theoretical Maximum Spans for Self-Supporting "linear arches".
(after Woodruff)

Fig. 2.11

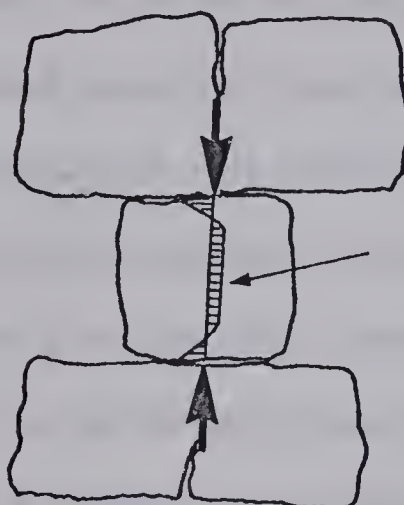
strength of the block, splitting of the intact block will occur.

Further, if the joint blocks experience multiple point loading (fig.2.14), beam flexure can occur. If the extreme fibre tensile strength is exceeded, the block will fracture.



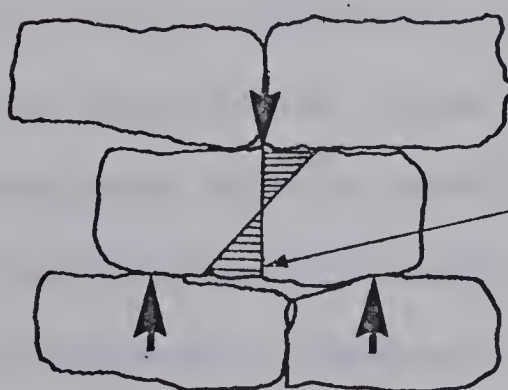
High stress concentrations
and local crushing

Fig. 2.12. Local Contact Crushing



Induced tension normal
to load direction

Fig. 2.13. Indirect Point Load Tensile
Failure



Tensile stress

Fig. 2.14 Extreme Fibre Tensile
Failure Due to Bending.

CHAPTER 3

METHODS FOR STUDYING THE STABILITY OF JOINTED ROCK MASSES AND THEIR APPLICABILITY TO CAVING STUDIES

3.0. INTRODUCTION

In order to achieve an underground structural design, the three elements of stability, usability and economy of the structure must be studied and analyzed.

Stability analyses are employed solely for the purpose of examining structural stability. Displacements of the structure are not determined in the examination. The primary goal is to create a structure where the failure resistance of the structure is greater than the applied driving forces. The ratio of the failure resistance to the driving forces is commonly known as the factor of safety. An acceptable design is one where only a fraction of the available failure strength of the rock is mobilized (i.e. the factor of safety is greater than one). Stability analyses are inadequate in many cases, for they do not take into account the load-deformation response of the rock mass. For example, rock bolt support methods in many mines are designed on the basis of dead load suspension. Seldomly does the effect of stress redistribution and the associated deformations due to adjacent excavations enter into the design.

The aim of usability analyses is to limit or control the rock mass displacements. The formulation of such

problems requires both the equations of equilibrium for an element of the rock mass, the constitutive equations governing the material behavior and the boundary conditions. The above discussion deals solely with the maintenance of a stable structure. However, in certain mining systems, rock mass stability is undesirable and failure is encouraged. The analyses must not only contend with the fact that failure must occur but must also include the identification of the failure modes and show the sequence of failure events.

Finally, the economy analyses is the economic optimization of various structural designs. The structures are examined in terms of application, allowable deformation, safety and overall costs.

The potential of various methods of studying caving mechanics will now be discussed. These include: closed-form solutions; physical models; the limit equilibrium method; numerical methods; and the clastic approach.

3.1. CLOSED-FORM SOLUTIONS

The classical theories of linear elasticity and plasticity were the first means used to examine the stability of underground structures. Up to the yield point, the rock mass was assumed to be a linear elastic continuum and the openings were simple geometric shapes, since more complex shapes were difficult to describe in terms of the appropriate mathematical boundary conditions. For very simple geometric cases, anisotropy could be introduced

(Lekhnitskii 1963). The analyses fail when the stresses exceed the material strength parameters. Whenever a situation arises where a given geometric shape, under given applied loads, fails locally in a rock mass, the method fails, not because the structure loses all stability (i.e. the roof may cave to a stable configuration), but because the closed-form solutions cannot predict the ultimate geometric failure configuration and corresponding stress field and deformations.

The theory of plasticity has been used to study ductile materials (e.g. soil, highly fractured, weak or weathered rock) which, unlike brittle rock, can be deformed to a much greater degree before total failure occurs. This theory assumes that the material behaves as a continuum and flows rather than fails in a catastrophic manner.

The applicability of these classical techniques to rock mass caving is extremely limited. They cannot solve the problems of a discontinuum, and whatever solutions are generated, are implicit in nature; that is, the process from the initial problem configuration to the final solved configuration is not observable in a time-step sequence.

3.2. PHYSICAL MODELS

Physical models are small, scaled analogues of real structures. The model materials employed are scaled directly or in a known distorted manner to the real material properties (Fumagalli 1968). They are then formed into a

structure and scaled loads are applied to simulate the studied structure. With appropriate instrumentation, loads and deformations can be observed and analyzed.

Compared to closed-form solutions, physical models can readily incorporate discontinuities into their make-up. For surface structures such as dams, dam abutments, slopes, etc., three-dimensional models and analyses can be made.

However, physical models have many disadvantages. The many material properties needed are so difficult to attain simultaneously that the results of load-deformation studies are somewhat questionable quantitatively. As for closed-form solutions, simplifications must be made for underground structures since they cannot readily be generated or analyzed as three-dimensional models. Two-dimensional plane strain or plane stress models are created making extrapolations to the real case somewhat difficult.

Costs of model techniques increase rapidly with the degree of complexity of the models, loading systems and instrumentation systems.

The fact that the failure mechanisms are directly observable and that zones of particular interest are indicated, can often greatly outweigh the disadvantages and costs.

3.3. THE LIMIT EQUILIBRIUM METHOD

A limit equilibrium analysis is a stability analysis. In this method, the shape of the failure surface is assumed

at the outset, such as along a discontinuity which represents a plane of weakness. The driving forces within the rock mass are estimated. Next, the available resisting forces along the discontinuity are determined and compared to the driving forces. If the available resisting forces are greater than the driving forces, the structure will be stable (i.e. in the limit, a factor of safety greater than one). Various failure surfaces must be investigated in order to determine the most critical one along which failure may occur.

It is a relatively simple stable/unstable analysis and is almost exclusively used in slope design in rock and soils. Unfortunately, the technique is difficult to apply for very complex and confined underground situations. If the mechanisms of beam-column buckling and kink-band formation could be quantified, then perhaps it might find some application underground.

The limit equilibrium method is an implicit analysis and does not predict deformations. Due to its semi-empirical nature, it cannot be applied in determining caving mechanisms and directions, since it requires that an initial assumption be made about the potential failure mechanism.

3.4. NUMERICAL METHODS

With the advent of high speed digital computers, finite element, finite difference and discrete element numerical techniques have greatly expanded in use in solving problems.

Complex problems dealing with discontinuous rock masses with non-linear, elasto-plastic material properties embodying complex geometric openings supported by rock bolts and concrete linings can now be analyzed. However, limitations still exist and will be further discussed.

3.4.1. FINITE ELEMENT METHOD

The finite element method is an implicit technique that currently cannot be used for problems involving large displacements. The technique makes use of the equations of equilibrium for an element of a rock mass as in the classical techniques but also can accommodate the constitutive equations governing the material behavior (Zienkiewicz 1971). The elements are then composed into a numerical model of the structure to be analyzed (fig.3.1). Plastic, no-tension carrying ability and non-linear elastic behavior for many different materials and configurations can be accommodated. Time-dependant phenomena, the effects of sequential excavation, support installation and therefore stress redistribution can also be examined.

As mentioned previously, the technique is implicit in nature and can solve a geotechnical problem if the mass remains in a stable condition. In caving, stability is not wanted and the technique gives no ready indication of the failure mechanism or direction that caving will occur. Its use is limited to evaluating the stability of adjacent openings subjected to high stresses induced by the caving

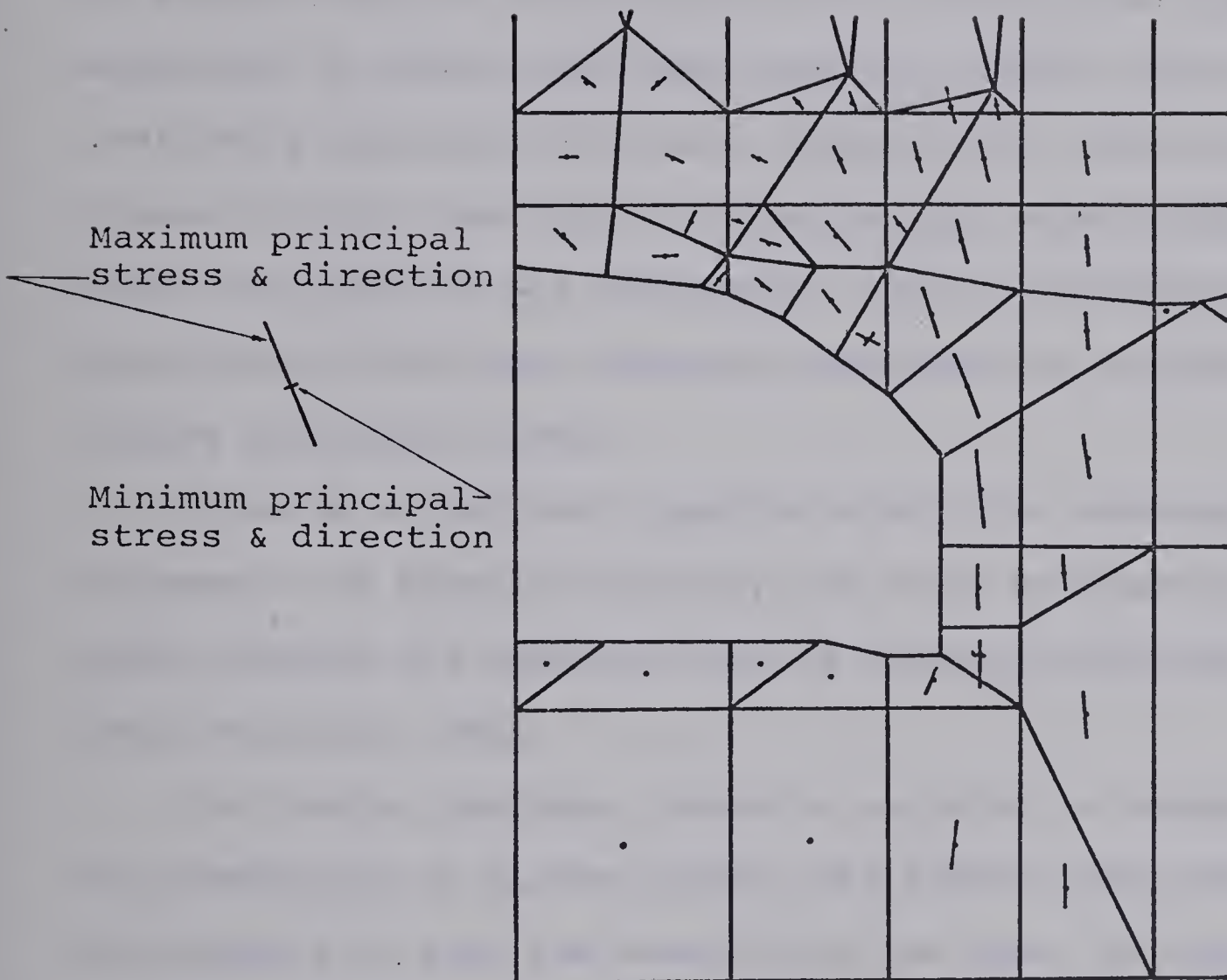


FIG. 3.1 Finite Element Model.

zone.

3.4.2. FINITE DIFFERENCE METHOD

The finite difference technique as applied to a discontinuous rock mass is based on its dynamic response. The behavior of the material can be described by an equation of motion combined with some form of constitutive law. The equations of motion deal with momentum effects and the continuity equations with mass conservation. These are linked through some form of stress-strain relationship and then are solved by the fundamental partial differential equations of continuum mechanics expressed in explicit finite difference forms.

Time is an explicit quantity within the mathematical expression of dynamic behavior, and large deformations can occur because the deformed grid is updated continually after each iteration cycle.

For static problems, there is no point to compare the two techniques of finite element and finite difference, for the results of each are essentially the same. However, when large deformations are expected to occur in a sequential manner as in rock mass caving, finite difference techniques have a distinct advantage.

Hammett (1974) with the use of the PISCES codes has examined discontinua problems involving sequential structural collapse. The PISCES codes proved disappointing for discontinuous masses due to problems in the modelling of

joints, but showed more promise in dealing with a continuum such as soil.

3.4.3. DISCRETE ELEMENT METHOD

The discrete element method developed by Cundall (1971, 1974) describes a rock mass as an assemblage of discrete, interacting blocks. Deformations occur only along block boundaries defined by incremental force/displacement relationships. All deformation occurs at edge-to-corner contacts and the shear and normal forces are calculated for each corner of each block.

The current technique has some small but 'dirty' approximations incorporated in order to make the program faster (i.e. all blocks have equal inertial masses though the gravitational masses are unaffected). The program provides relative magnitudes for forces and displacements but no real material property values other than the joint friction angle are used. Until the program is 'calibrated' to provide absolute forces and displacements, the method is only suitable for providing mechanisms of failure. In its present form, the discrete element method is, nevertheless, an important development for examining structural instability and caving modes of discontinuous ground.

3.5. CLASTIC APPROACH

Clastic mechanics assumes that rock masses can be described as an assemblage of unit building blocks of any

shape and size. Depending on the shape of the block boundaries, the units will tend to group into systematically packed zones (i.e. systones (fig.3.2)) and the theorem of centroid reactions states that all lines of action of contact forces must pass through the centroid of each unit. Stress transmission and failure criteria in discontinua are the main foci of attention. Only the stress transmission analysis will be discussed since the failure criteria deal with intact rock and this problem is not included in this study.

In a simple systone of disks (fig.3.3a) with applied forces p , q and r (fig.3.3b), it may be shown theoretically, that q is directly proportional to p :

$$q = kp$$

With the further restriction of a 'no-tension' criterion, then:

$$0 < k < 1$$

The condition $k = 1$ is the no-arching condition and $k = 0$ is the full-arching condition. There is no requirement for k to be constant throughout the mass, but $k = 0$ and $k = 1$ represent the extreme stress state solutions. The theory demonstrates that with relatively very small deformations,

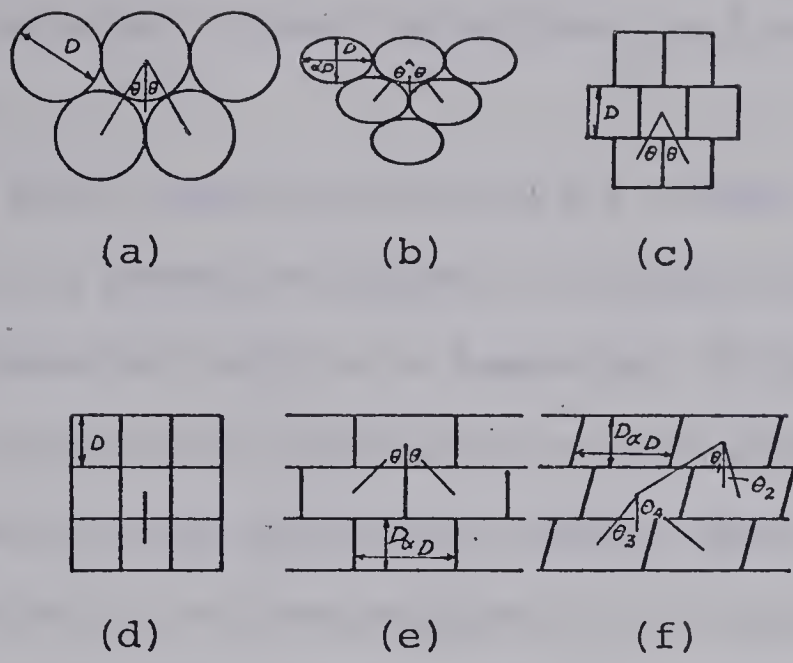


FIG. 3.2 Some Typical Systones

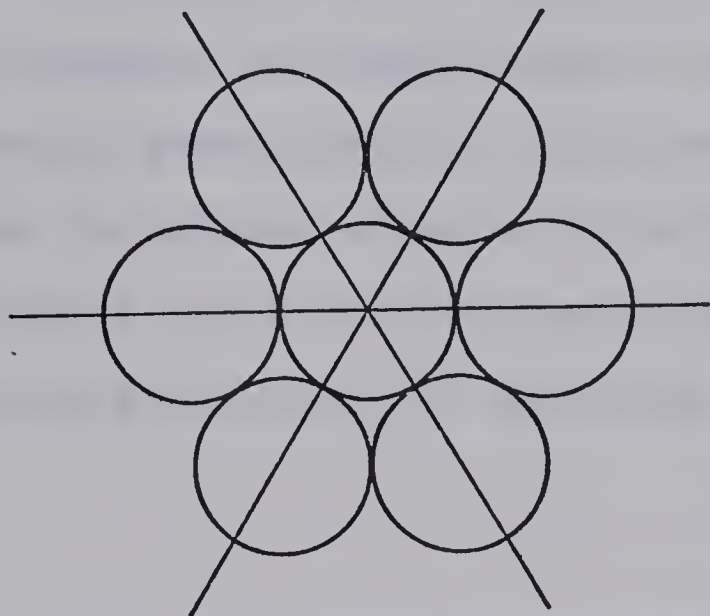


FIG. 3.3a Simple Systone of Disks

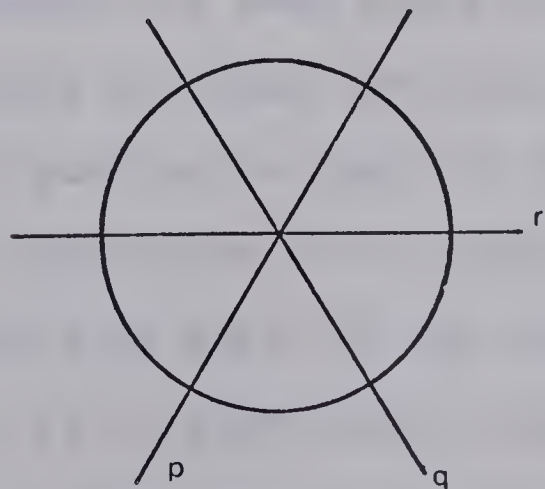


FIG. 3.3b Forces Applied to a Systone Element

no-arching conditions can change very quickly to full-arching (i.e. generate large variations in internal stress distributions).

Hammett (1974) employed Trollope's (1968) systematic arch theory as is presented above for values of $k = 0, 1/2$ and 1 and he compared this to a numerical finite element analysis of a system of imbricated rock blocks under a foundation load. Though Trollope's theory gave an approximate solution to the problem, it is apparent that k is not constant throughout the mass. No technique is currently available to evaluate the k value distribution in such a mass and therefore the usefulness of clastic mechanics is somewhat questionable at this stage.

The technique is failure oriented in an implicit manner similar to that of the limit equilibrium technique but it does not require the selection of a potential slip surface.

3.6. CONCLUSION

A range of analytical approaches has been examined and a number of shortcomings has been noted concerning their use for the study of caving problems. The optimum approach is to examine the specific problem in light of the various techniques that are applicable to the problem.

No technique has much merit if the input data, such as material properties, is of questionable accuracy. In many cases, particularly in the numerical techniques, the accuracy of the techniques outstrips that of the data,

creating a false sense of extreme accuracy in the solution and may give a misleading interpretation.

Currently, the main value of all the techniques lie in the ability to generate a sensitivity analysis of the variations of material parameters on the behavior of structures. This sensitivity analysis coupled with the performance of real structures can greatly aid in identification of the more significant parameters for further investigation and analysis and in development of good design criteria.

The primary value of numerical techniques is in determining the effect of changes in rock mass properties on engineering behavior (i.e. sensitivity analyses). These analyses allow the engineer to identify the most important properties which may require further investigation or measurement and to develop improved design criteria.

CHAPTER 4

A QUALITATIVE PHYSICAL MODEL STUDY OF ROCK MASS CAVING

4.0. INTRODUCTION

During caving in an underground mine, it is physically impossible to enter and visually observe a caving zone because of the difficulty in maintaining access and of the physical danger to man. In order to study the mechanics of caving, only two explicit analytical techniques are currently available; the physical scale model and Cundall's discrete element method (Chapter 3). Due to the specific problems and to the high costs of the discrete element method (See Appendix IV) when run on a large digital computer, such as the Amdahl 470 V/6 at the University of Alberta, the physical modelling technique was used in this study.

Two physical modelling methods are available to study the phenomenological or mechanistic behavior of a failing discontinuum: the vertical caving model and the base friction model. Vertical models employ gravity to generate the loads and deformations leading to stability/instability. Some caving phenomena occur very quickly by this method and are difficult to observe without high-speed photography.

The mechanism of the base friction model is different from the vertical model in that it simulates gravity by

friction and deformations occur at a slow rate. A certain flexibility in scaling can also be incorporated by the proper machine adjustment and critical model material selection.

4.1. BASE FRICTION MODEL TECHNIQUE

4.1.1. MODEL TECHNIQUE

The base friction modelling frame may be considered as an extremely large, slow speed belt sander placed in an inverted position. A large sandpaper belt runs at a very low speed over two rollers placed at either end of a frame. A fixed barrier at one end of the belt creates a restraint to the model material which is uniformly cast and formed upon the belt surface. Thus, when the belt moves towards the end restraint, the friction created by the belt sliding under the restrained model material generates drag forces in the model (fig.4.1).

Prior to the operation of the model, geological discontinuities may be cut into the model material and excavations can be made by the removal of material. During a model run, block movements and deformations can be observed and recorded on film.

4.1.2. MACHINE DESCRIPTION

The equipment has improved since Erguvanli and Goodman (1972) first introduced the technique. They used a

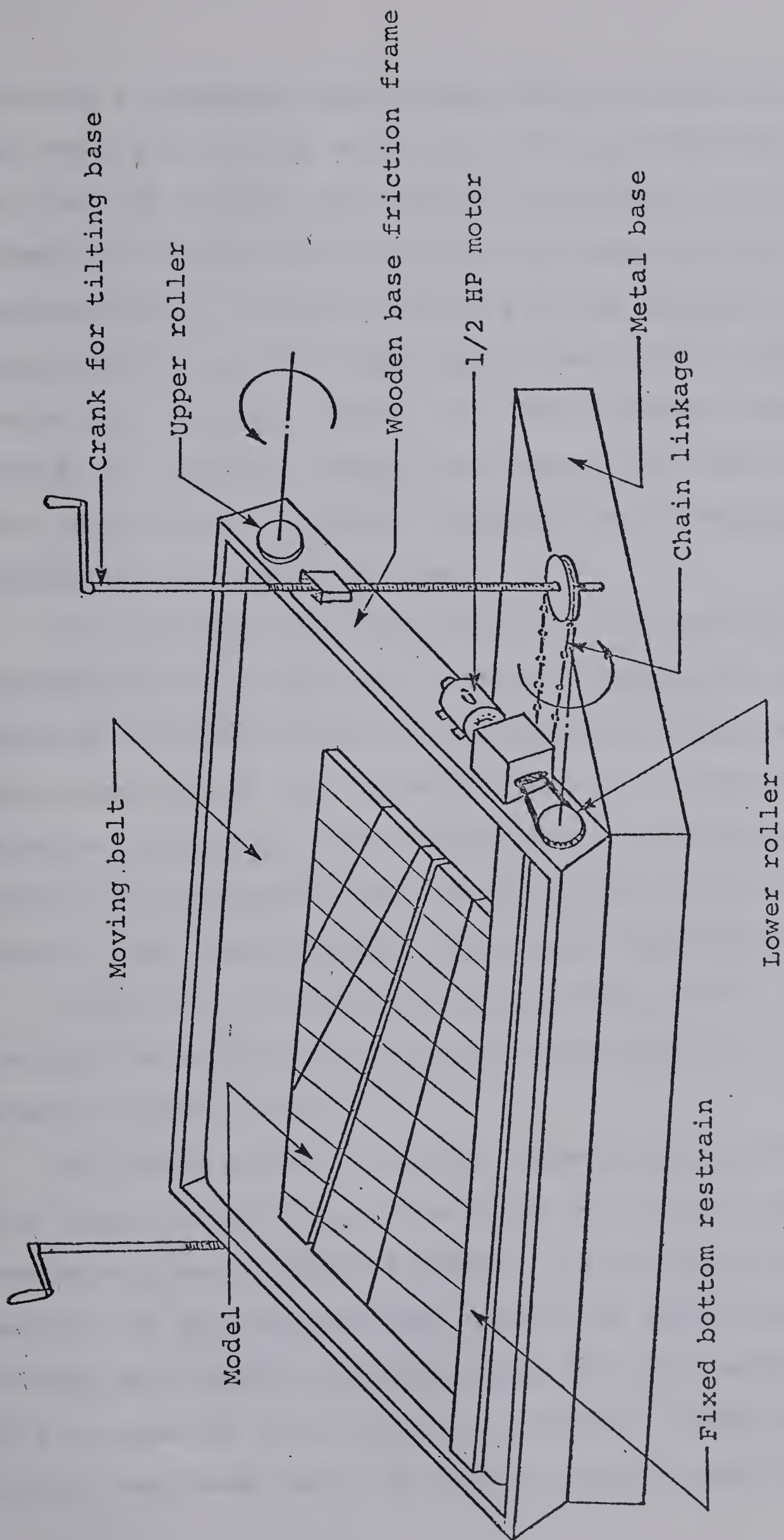


FIG. 4.1 Schematic of a Base Friction Model

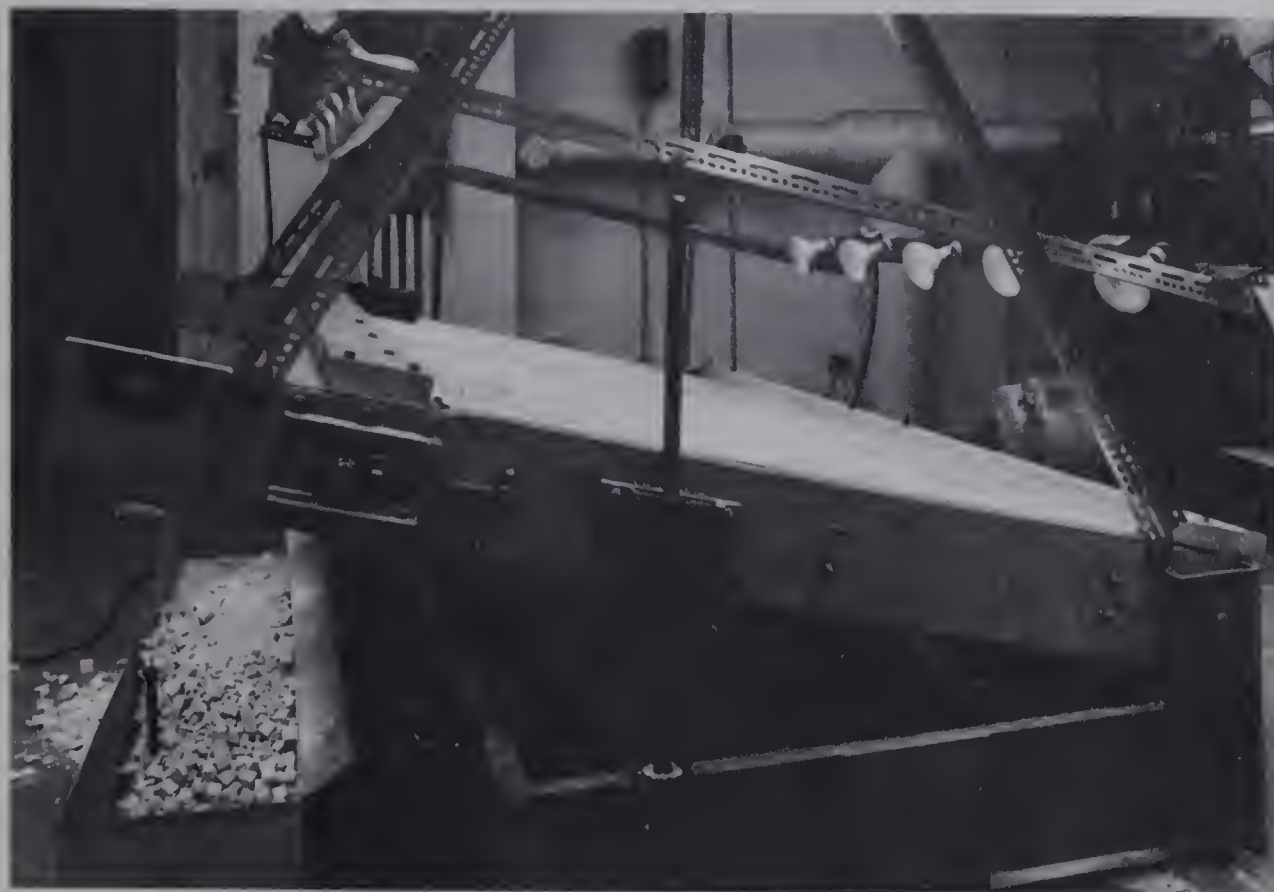
stationary sandpaper sheet across which the model material was pushed. Horizontal machines, which had sandpaper moving as a belt on rollers, were first introduced at Golder, Brawner and Associates Ltd. office in Vancouver and, subsequently, at Imperial College, London (Goodman 1976). Hammett (1974) used the same type of belt model for his tests. All the users claimed that the technique could not provide an accurately scaled two-dimensional model and its main purpose was to examine failures from an exaggerated phenomenological point of view.

In this study, the limitations of the previous equipment were examined and it was determined that some features of scaling could be incorporated. If the machine were tilted out of the horizontal (i.e. in a positive or negative direction), then a component of gravity could be added to or subtracted from the frictional force. On this basis, a very large machine was designed and constructed.

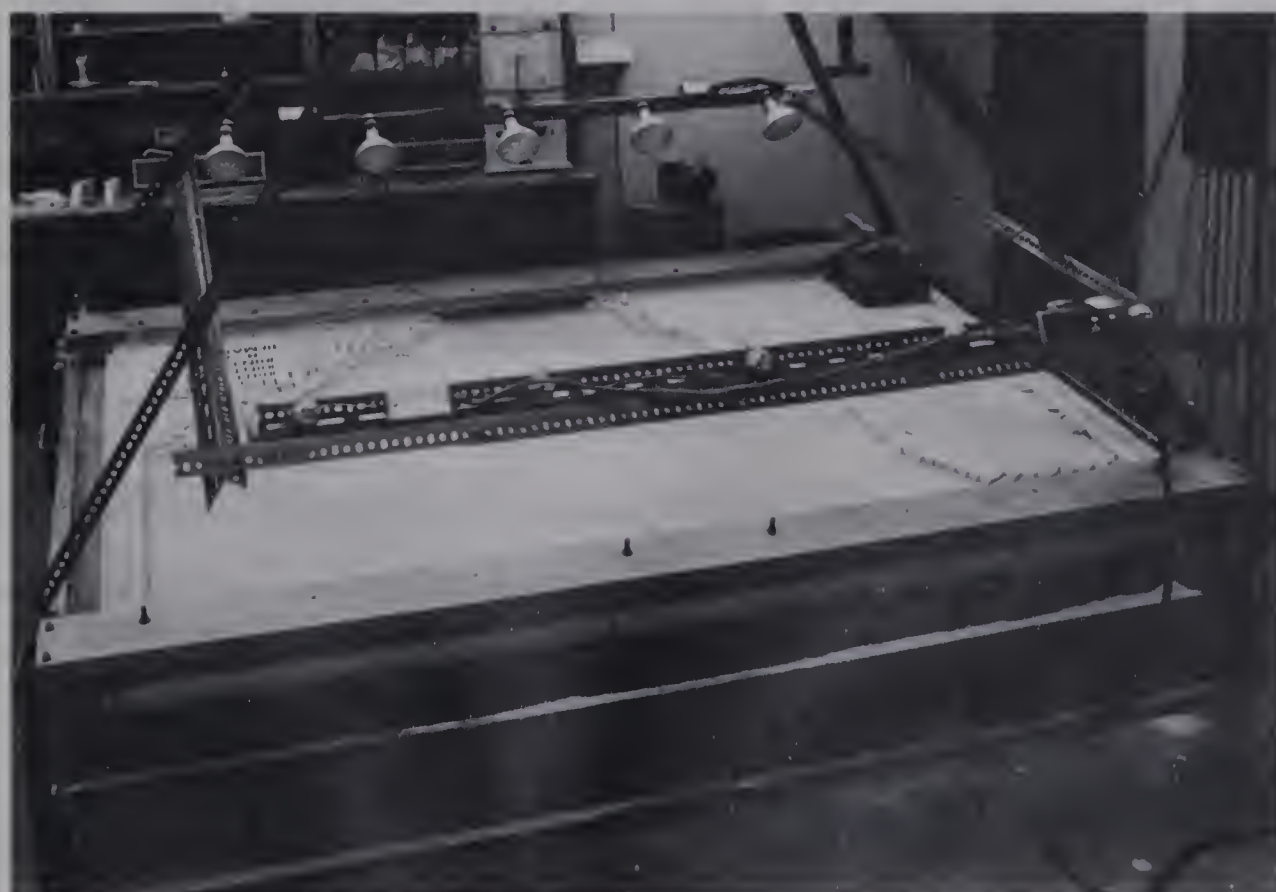
A four feet long and eight feet wide (4'x 8') model surface was selected for the large scale effects to be examined (plate 1a-1b).

The drive and tail rollers, since they were to be eight feet long, needed to be quite rigid so as not to deform excessively under the belt tension and friction loads, and were not to be 'out-of-round' since this would create further belt tension problems. Four inch O.D. steel tubing with one quarter inch walls was selected. Crowning the rollers was found not to be necessary since belt wandering

PLATE 1: BASE FRICTION MACHINE



(A) SIDE VIEW



(B) FRONT VIEW

was slow, but travel limit switches were installed as a precautionary measure to stop the belt should excess wandering occur (plate 2a). No frictional material was needed on the steel rollers.

The belt was custom made by 3M Corp. with a width of eight feet and a circumferential length of ten feet. It is comprised of a #200 grit sandpaper on a resin-reinforced linen cloth base which is unaffected by the methyl alcohol used in the model material. Belt tension is provided by the tail roller tensioning device (plate 2b).

The belt frame pivot is both novel and simple. The outsides of the drive flange bearings were machined round and rotated in a ring yoke firmly attached to the machine base.

The tilt drive mechanism uses two lengths of 1 inch 'all-thread' screws, one on each side of the machine. The lower end is anchored into a self-aligning bearing on the base and the frame support nut pivots on the side of the belt frame assembly. The two screws are coupled together with a link roller chain extending the width of the base (plate 2c). A detachable hand crank placed on the end of one screw, is used to turn the screw and tilt the belt frame uniformly.

The drive system is composed of a 1/2 hp. reversable motor attached to the base. It is connected to a gear reducer which in turn is connected to the drive roller with a link roller chain. By moving the restraint barrier to one

end of the machine or to the other and by advancing or reversing the motor, the addition or subtraction of the gravity component to the frictional force is achieved. The belt speed is approximately five lineal feet per minute. No other belt speeds were examined.

A simple control panel incorporates the power, low voltage travel limit and motor reverse controls (plate 2d).

4.1.3. MODEL MATERIAL

The model materials that have been used in base friction modelling to date have left much to be desired. Axial stress - axial strain curves on various mixtures of the oil, flour and sand materials of Erguvanli and Goodman (1972) showed a prominent non-linear elasto-plastic behavior and these materials were too weak for our purposes (fig.4.2). The rigid materials of cork, wood, plastic and sugar cubes which have been used, proved to be too strong, difficult to handle and costly, since for different joint block geometries they cannot be reused. The model materials surveyed by Stimpson (1970) were also not suitable since they too were difficult to handle and were costly.

Since many strong rocks fail in uniaxial compression at axial strains of less than 0.5%, laboratory investigations were begun to produce a model material with a similar characteristic since the Erguvanli and Goodman mixture did not fit this criterion. A material comprised of flour and methanol was developed, for which, after the alcohol

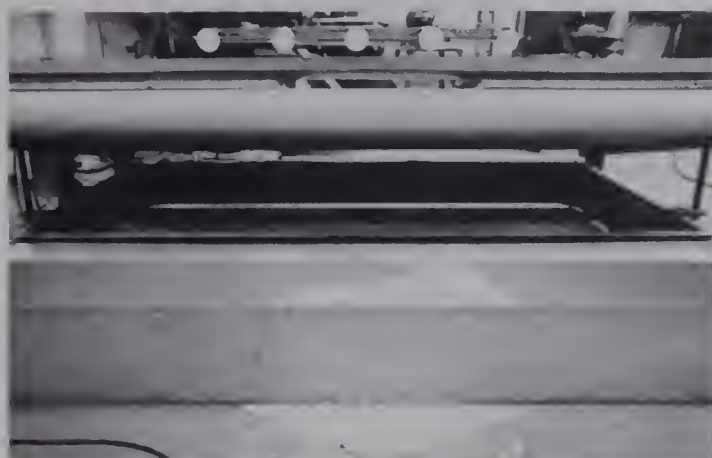
PLATE 2: BASE FRICTION MACHINE DETAILS



(A) BELT TRAVEL LIMIT SWITCH



(B) BELT TENSIONER



(C) FRAME INCLINATION SYNCRONIZING CHAIN



(D) BELT DRIVE SYSTEM

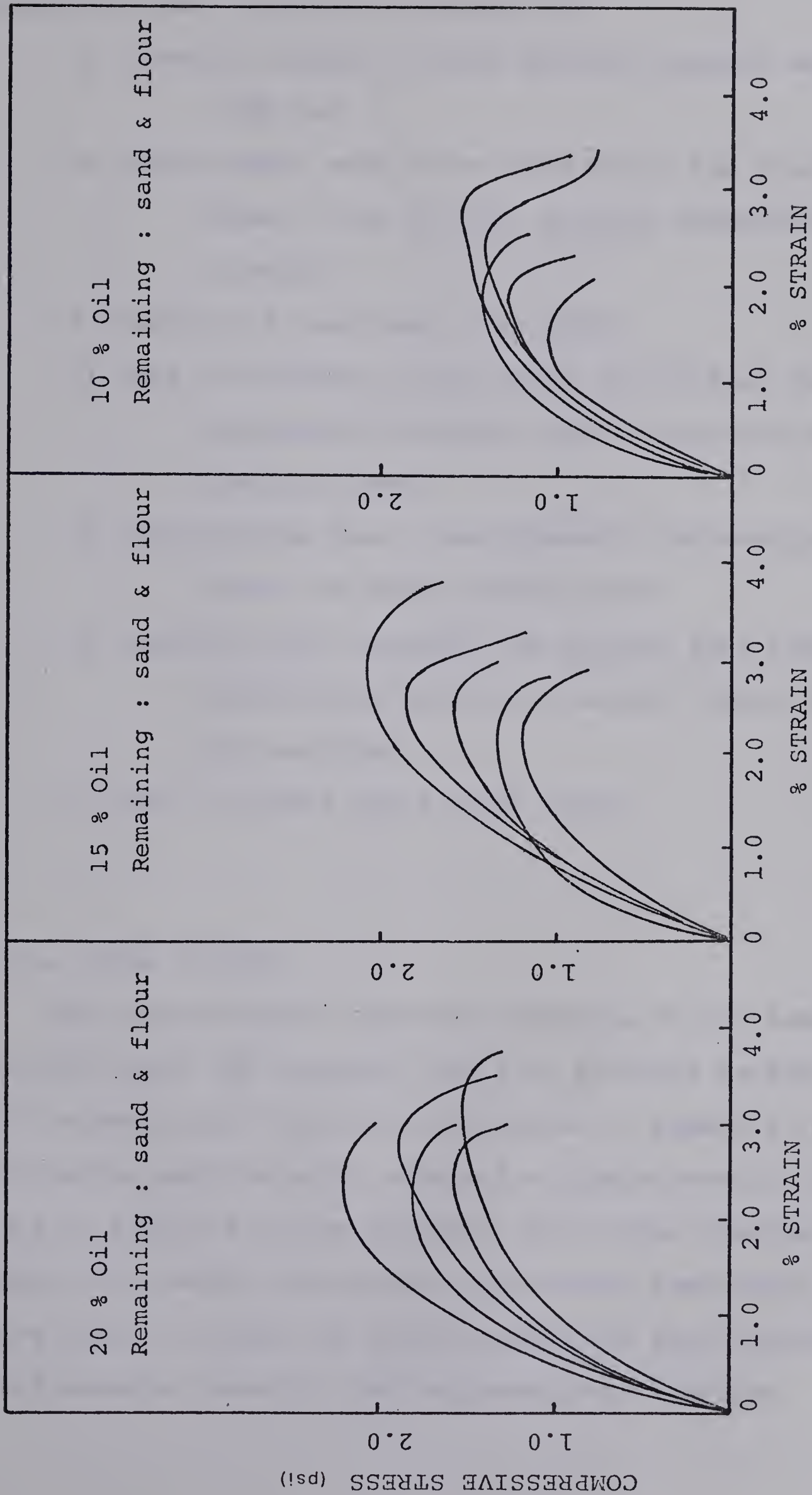


FIGURE 4.2

Uniaxial Load - Deformation Curves of Oil, Flour, and Sand Model Materials

evaporated, the material was (fig.4.3):

- 1) linearly elastic to near failure (tangent modulus = 2,500 psi.)
- 2) sufficiently weak to be utilized in the friction frame (10 to 25 psi. uniaxial compressive strength)
- 3) failing at less than 1.5% strain
- 4) weak in tension, in the order of 8-12% of its compressive strength (0.9 to 2.6 psi. by Brazilian test)
- 5) non-creeping (i.e. time-dependent deformation) during the base friction test
- 6) reusable after crushing the initial hard blocks and remobilizing with more alcohol (about 10 runs are possible)
- 7) easy to handle while still moist.

4.1.4. MODEL SCALING

The characteristic operating equation of the machine is dependant upon the kinematic angle of friction between the model material and the belt (derivation in Appendix I). By tilting the machine until material slippage occurs, this angle of friction can be measured. This value provides a single point which identifies a particular 'vertical' stress curve from the family of stress curves for that particular model material density. The characteristic equation

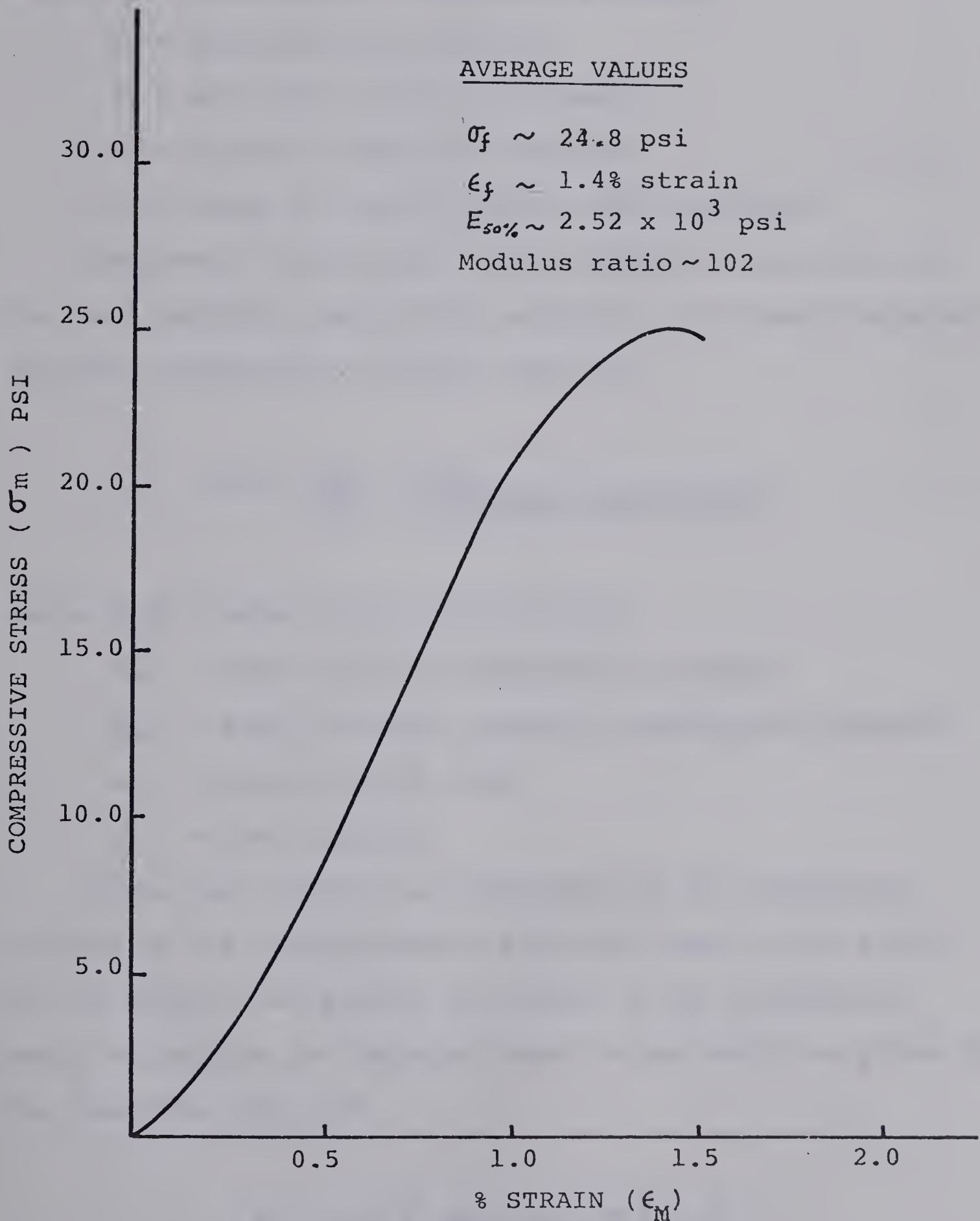


FIG. 4.3

Uniaxial Stress-Strain Curve of Flour and Methanol Model Material

(fig.4.4) is:

$$\sigma_{\theta} = \gamma_m h_m (\cos \theta \tan \phi + \sin \theta)$$

where σ_{θ} = longitudinal ('vertical') stress

γ_m = model material density

θ = belt angle (from horizontal)

ϕ = angle of kinematic friction

h_m = depth of superincumbent model material.

The model stress scale factor (MSSF) is the ratio of the rock uniaxial compressive strength to the model material uniaxial compressive strength. That is:

$$\text{MSSF} = \frac{\sigma_{cr}}{\sigma_{cm}} = \frac{\gamma_r h_r}{\gamma_m h_m (\cos \theta \tan \phi + \sin \theta)}$$

where MSSF = model stress scale factor

σ_{cr} = rock uniaxial compressive strength

σ_{cm} = model material uniaxial compressive strength

h_r = depth in rock mass

γ_r = rock density.

Since the stresses are developed by the cumulative loading of the superincumbent material, both in the model and in nature, the machine is tilted to the appropriate angle to provide the required model stress scale as given by the relation (fig.4.5)

$$\theta = \sin^{-1} \left(\frac{\sigma_{cm} \gamma_r h_r \cos \phi}{\sigma_{cr} \gamma_m h_m} \right) - \phi$$

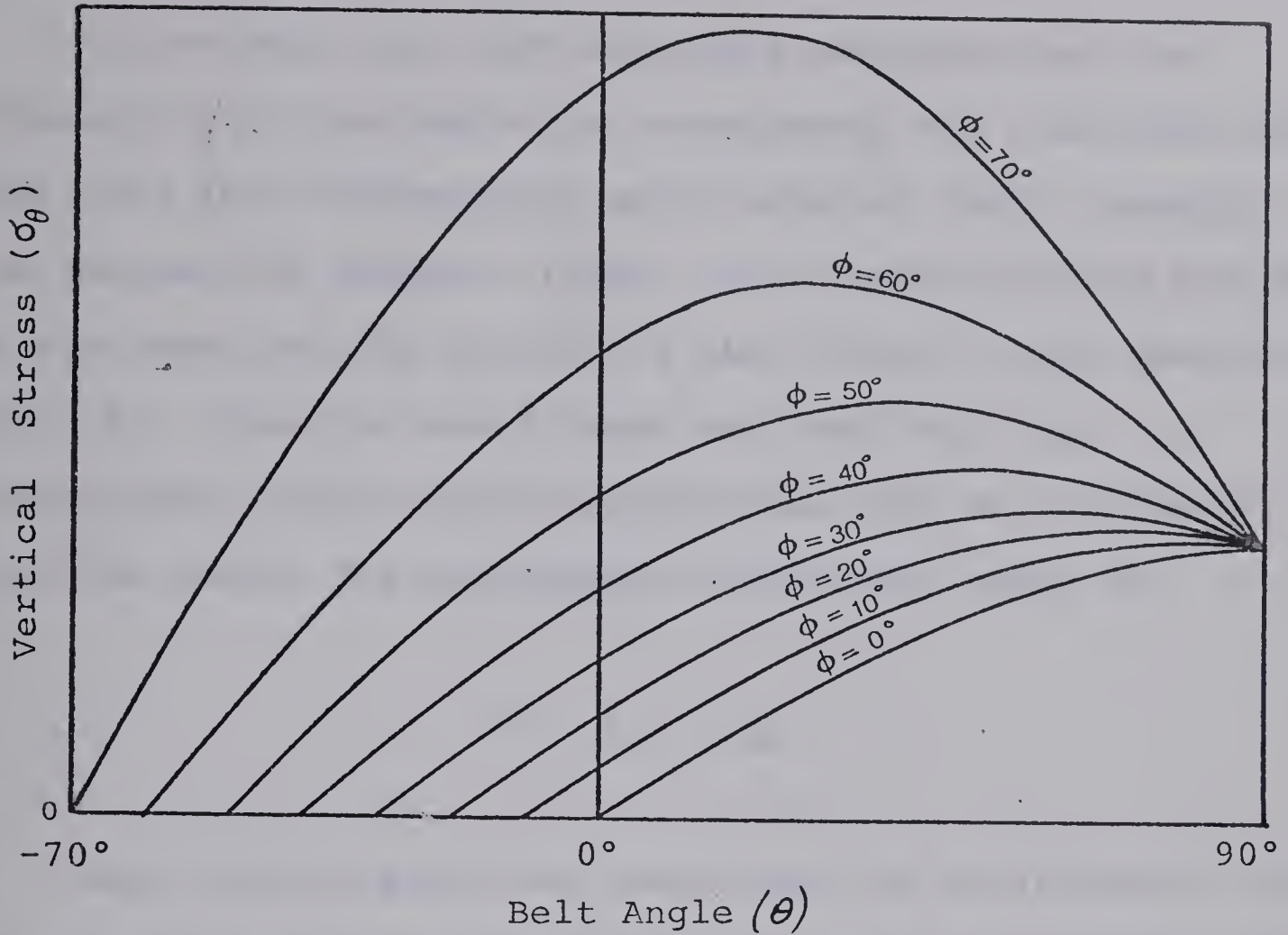


Fig. 4.4 Base Friction Vertical Stress as a Function of Machine Rotation θ and Kinematic Angle of Friction ϕ

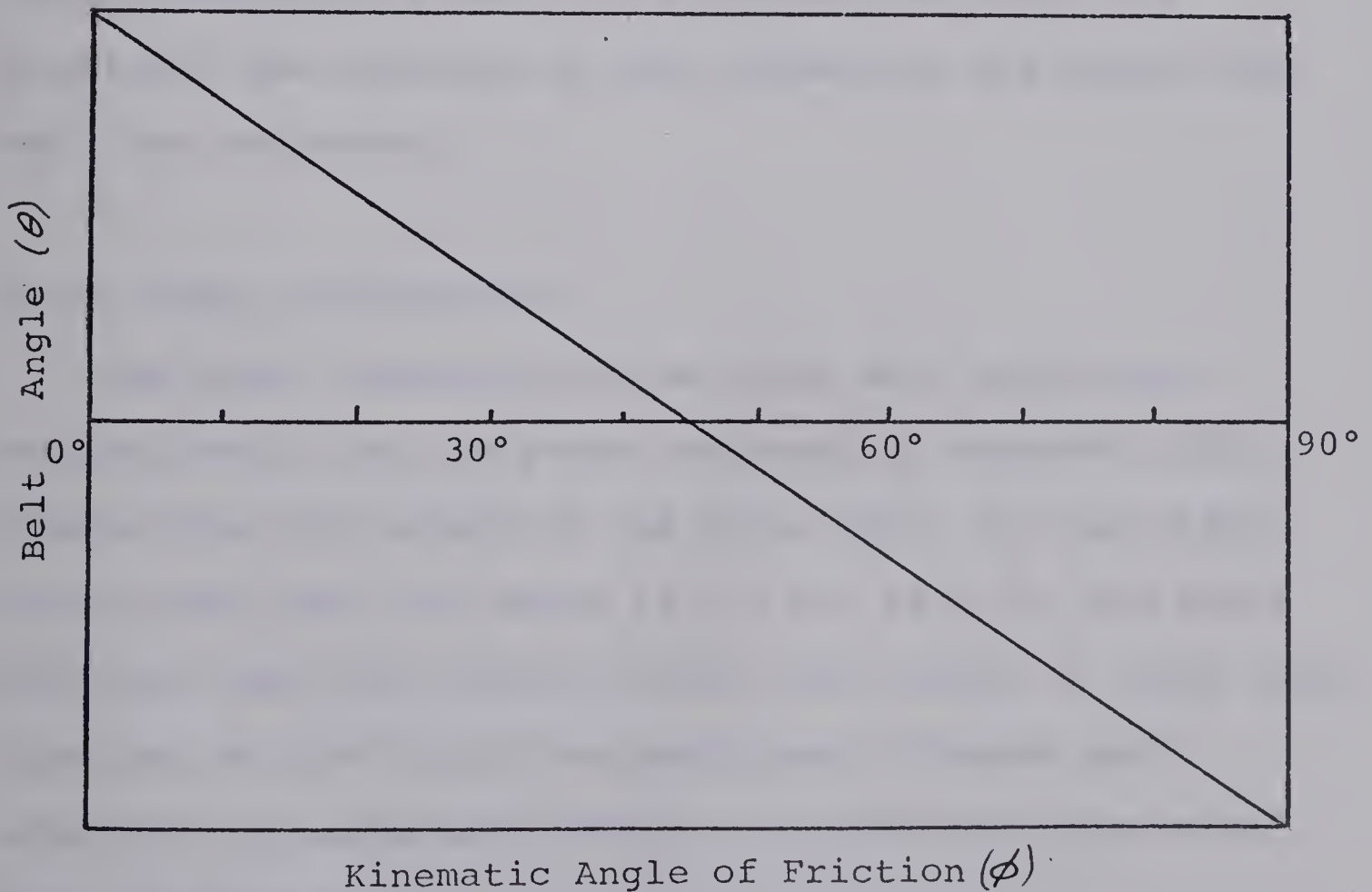


Fig. 4.5 Base Friction Machine Rotation θ as a function of The Kinematic Angle of Friction ϕ

If the MSSF, the rock and model densities and the kinematic friction angle are established, the simulated rock depth and the corresponding model material depth (usually the maximum the machine allows) are automatically determined by the equation. The machine is then tilted to the specified angle θ . Once the model depth and rock depth are established, scaled joint spacings can then be introduced into the model. The appropriate dimensional scale is:

$$h^* = h_r / h_m$$

Once all the modelling parameters are established, the mixed model material (Appendix II) is cast and formed on the frame. While the material is still moist, the discontinuities are cut to the appropriate scale and direction. The material is then allowed to dry before the tests are conducted.

4.1.5. MODEL PREPARATION

The model material must be mixed with sufficient methanol such that the proper strength is acquired. This depends upon the nature of the flour used. In this study, Purity cake flour was mixed in a 2 ft. by 2 ft. lab scale ball mill with 100 lbs. of 2 inch steel balls. A large dough mixer may be used if it has sufficient strength and capacity. Approximately 100 lbs. of flour was mixed with 5 gals. of methanol.

The resultant single batch mixture was removed from the ball mill and the steel balls were separated. The mixture was then evenly distributed on the level machine and packed down by foot, paying particular attention to the material against the machine frame. The packed mixture was then shaved to the proper 1 inch thickness with a sharp edged 2 in. by 6 in. by 8 ft. piece of lumber.

A 2 ft. by 2 ft. cutting jig was made to simplify the cutting of uniform joints. Care must be taken in cutting the material since the moist mixture is friable and subject to damage. Speed is essential in preparing the model since it dries fairly rapidly.

Good ventilation is imperative. A safety hazard exists with the methanol fumes and the diluted fumes must be exhausted to the outdoors.

Tests were conducted every second day which allowed about 40 hours of drying.

Once the material is dry, the model material must be compacted by running it against the end restraint and by adjusting the side boards inward such that the expansion effects of joint cutting and the shrinkage effects of the material are compensated.

4.2. BASE FRICTION MODEL STUDY

The effect of joint geometry and spacing on the caving of a rock mass was studied by the base friction modelling method. The rock mass, as scaled on the machine, was

composed of two continuous, intersecting joint sets.

In the first series of tests, the joints were uniformly spaced at one inch intervals, forming one inch by one inch blocks. The second series of tests had one joint set spacing twice that of the other set. The blocks thus formed were one inch by two inches in size.

For each of the two series of tests, the joints intersect at different angles. In the first group of tests, the joints were orthogonal to one another, in the second group at fifteen degrees from the orthogonal, and in the third group at thirty degrees from the orthogonal.

The joint orientations were also rotated relative to the reference frame formed by the machine boundaries. In the case of the one inch by one inch orthogonal jointed material, the joint set geometries were rotated at fifteen degree intervals to the machine restraint barrier (i.e. 0-90, 15-105, 30-120, 45-135 degrees). Other orientations such as 60-150 degrees were unnecessary due to the symmetry of the joint systems and, in this case, was duplicated by the 30-120 degree orientation.

The two-to-one joint space ratio test program was similar. The orthogonal joint patterns were rotated in fifteen degree steps through an arc of 180 degrees; the joints at fifteen degrees from the orthogonal were rotated in thirty degree steps. Tests with joints at thirty degrees from the orthogonal were omitted.

For all tests, the machine was tilted -15 degrees as

shown in the worked example in Appendix I. An arbitrary caving span was chosen that permitted failure in most test cases and the end conditions on the frame were fixed. Table 4.1. presents the joint geometries measured from the horizontal and joint spacings for the tests that were conducted.

4.1. GEOMETRY OF BASE FRICTION MODEL TESTS

Section	Test	Plates	Joint 1	Joint 2	Aspect Ratio
4.2.1	001	3 & 4	0	90	1:1
4.2.2	002	5 & 6	15	105	1:1
4.2.3	003	7 & 8	30	120	1:1
4.2.4	004	9 & 10	45	135	1:1
4.2.5	009	11 & 12	0	105	1:1
4.2.6	013	13 & 14	15	120	1:1
4.2.7	014	15 & 16	30	135	1:1
4.2.8	015	17 & 18	-15	90	1:1
4.2.9	016	19 & 20	0	120	1:1
4.2.10	017	21 & 22	15	135	1:1
4.2.11	018	23 & 24	30	150	1:1
4.2.12	019	25 & 26	-15	105	1:1
4.2.13	020	27 & 28	-30	90	1:1
4.2.14	005	29	0	90	1:2
4.2.15	006	30	15	105	1:2
4.2.16	008	31	30	120	1:2
4.2.17	010	32	45	135	1:2
4.2.18	007	33	30	120	2:1
4.2.19	012	34	15	105	2:1
4.2.20	011	35	0	90	2:1
4.2.21	024	36	0	105	1:2
4.2.22	021	37	30	135	1:2
4.2.23	025	38	120	45	1:2
4.2.24	023	39	120	15	1:2
4.2.25	022	40	90	15	1:2
4.2.26	026	41	30	105	1:2

4.2.1. TEST #001 (PLATES 3 & 4)

Test #001 with 1:1 ratio orthogonal jointing shows the

PLATE 3: TEST #001



(A)



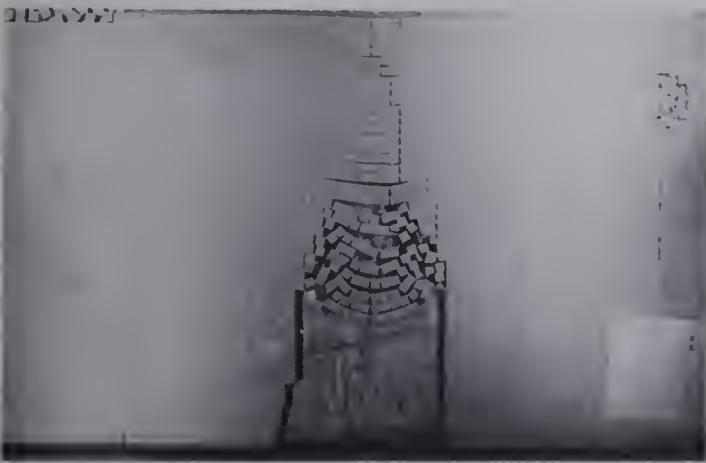
(B)



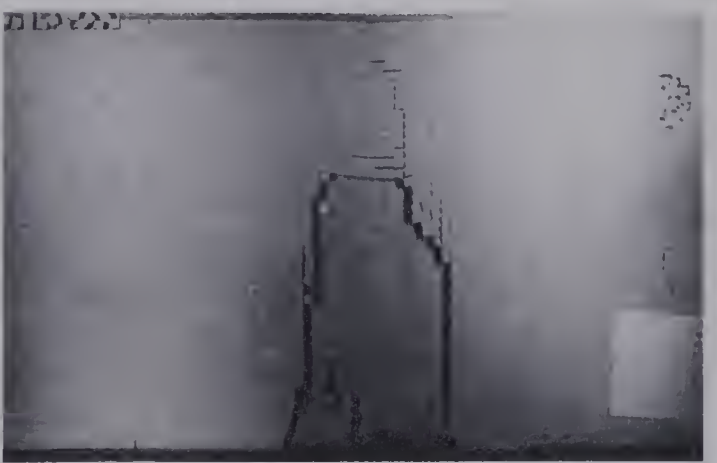
(C)



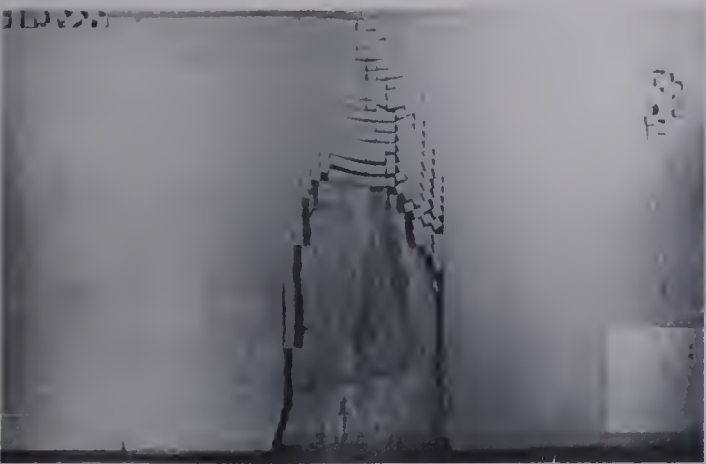
(D)



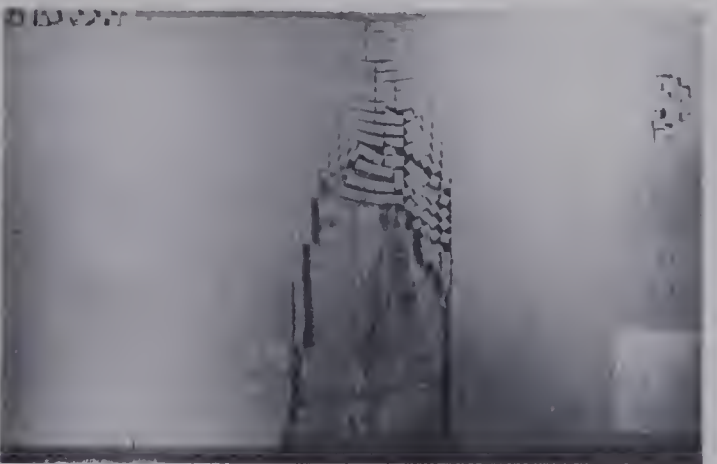
(E)



(F)

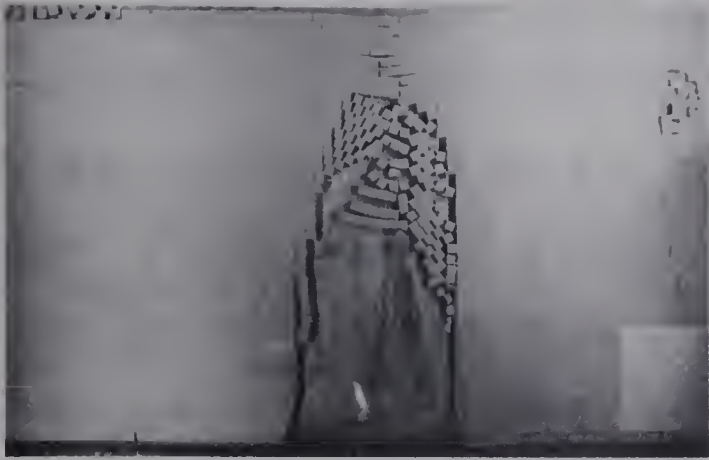


(G)



(H)

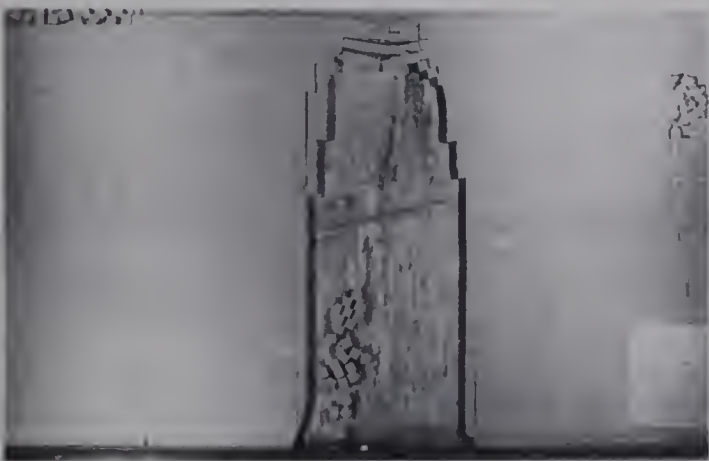
PLATE 4: TEST #001 (CON'T)



(I)



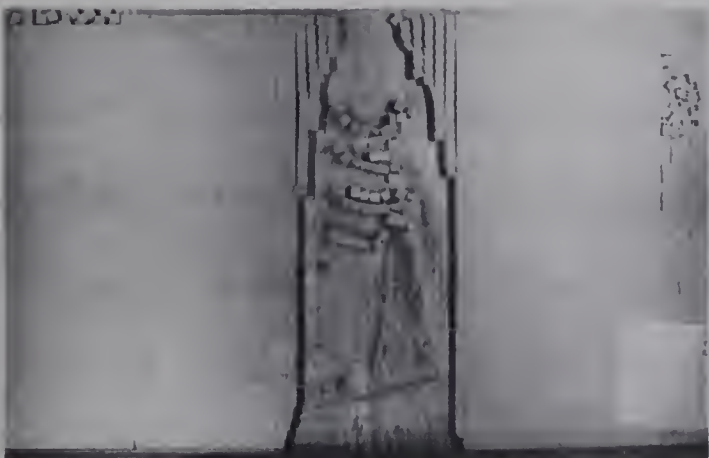
(J)



(K)



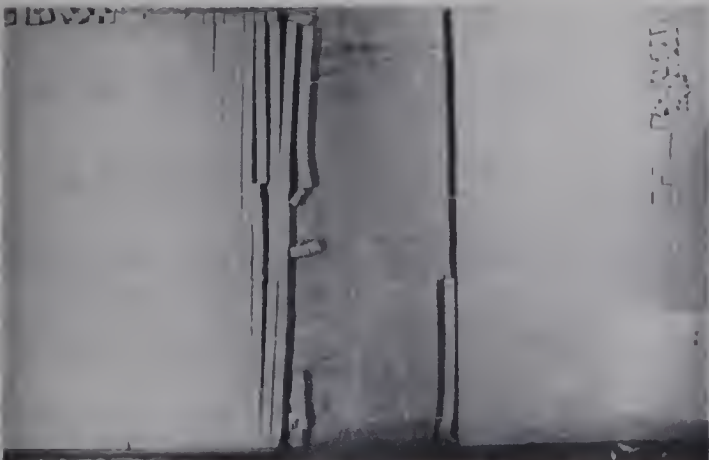
(L)



(M)



(N)



(O)



(P)

sequential flexure and failure of individual horizontal beam-columns. A void opens between each beam-column, indicating that each member is not loaded by the overlying member. However, it is not clear what boundary conditions occur at the ends of these members.

The beam-column ends are not rigidly clamped as block rotations are evident in the immediate abutments. The overall member deflection is therefore increased. Major shearing along joint surfaces is not evident other than along individual blocks 'hung-up' on block corner protrusions initially caused by the abutment block rotations.

The failure zone progresses vertically upward, gradually narrowing and forming an unstable arch. This narrowing is caused by individual blocks being held by block corner protrusions and arching between the beam-column and abutments (fig.4.6). The arching effect transmits lateral forces and delays abutment column buckling failure. Once the arch is destroyed, toppling and buckling of the abutment columns occurs.

4.2.2. TEST #002 (PLATE 5 & 6)

In this test, the 1:1 ratio orthogonal blocks are rotated fifteen degrees from the restraint barrier. Beam-column flexure continues to occur as in Test #001, not vertically, but in the direction perpendicular to the fifteen degree joint set. The beam-columns deflect

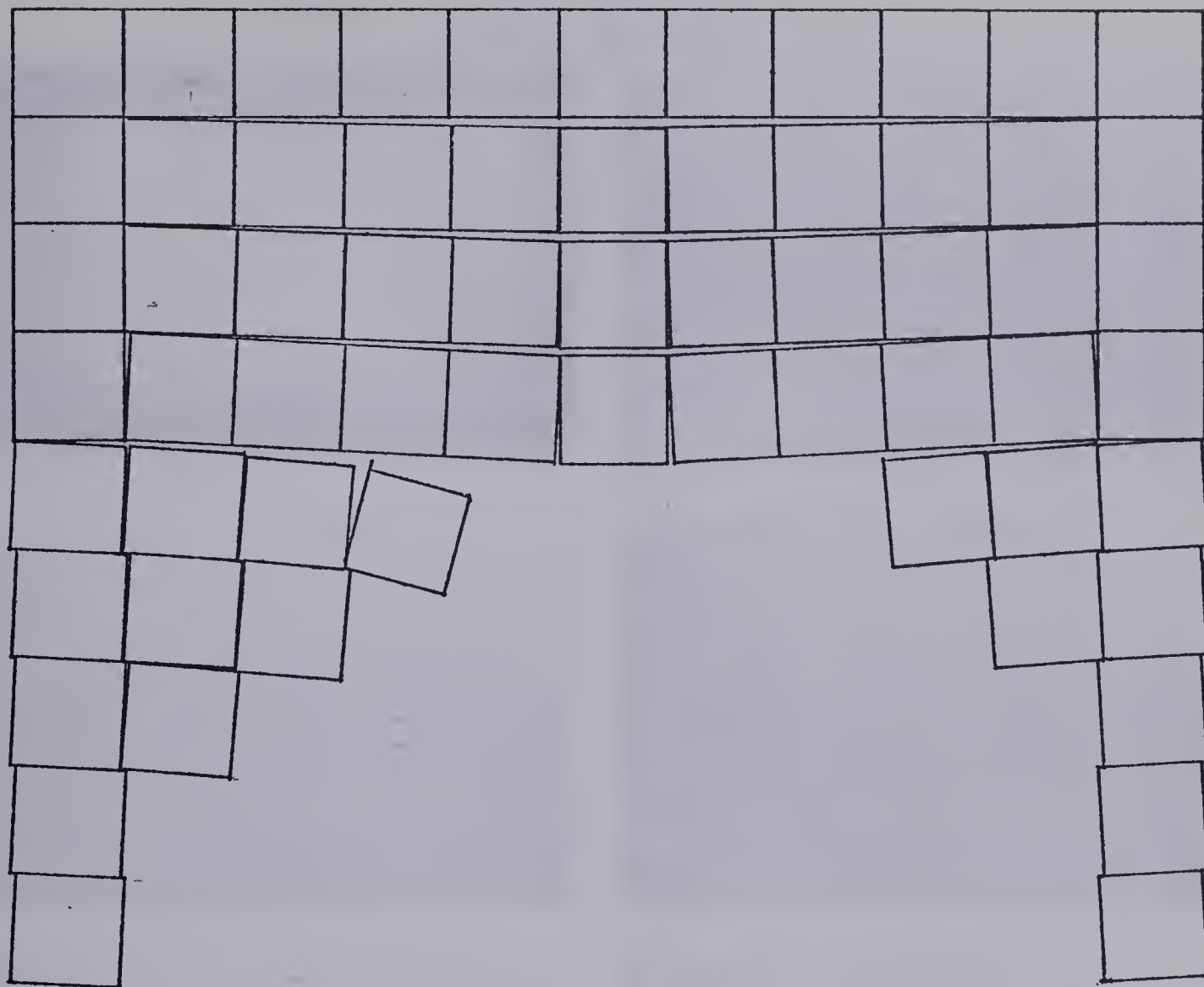
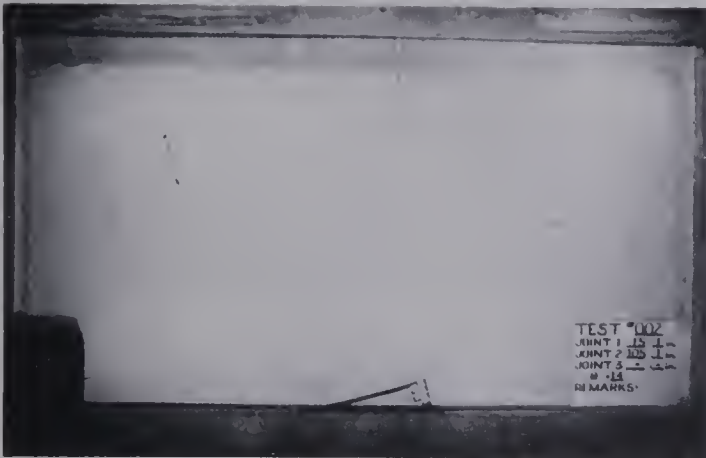


FIG. 4.6 Arching Supported by Block Protrusions

PLATE 5: TEST #002



(A)



(B)



(C)



(D)



(E)



(F)



(G)

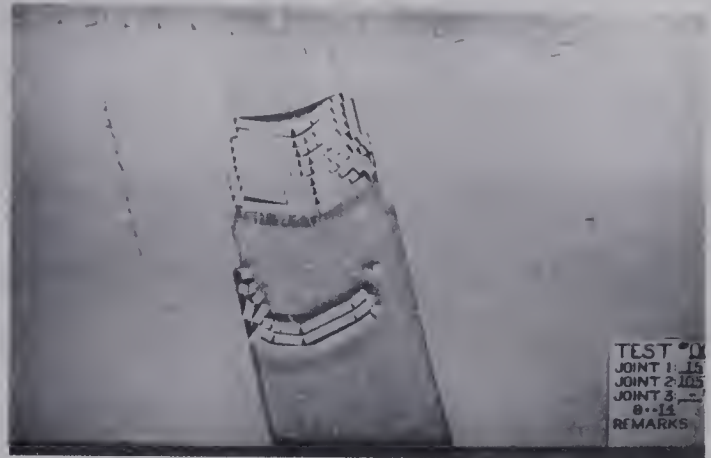


(H)

PLATE 6: TEST #002 (CON'T)



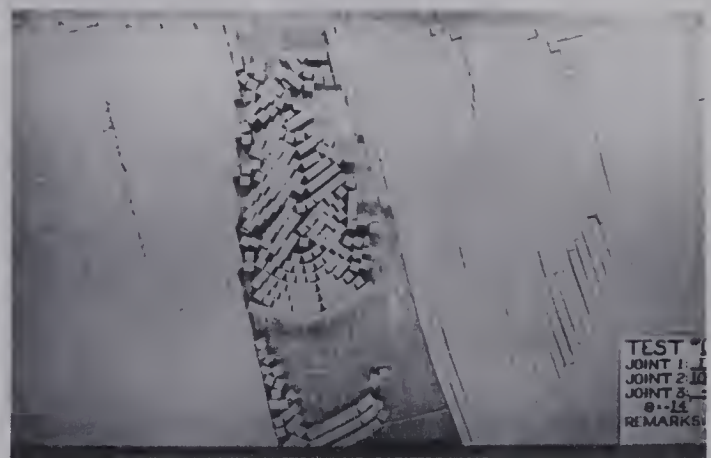
(I)



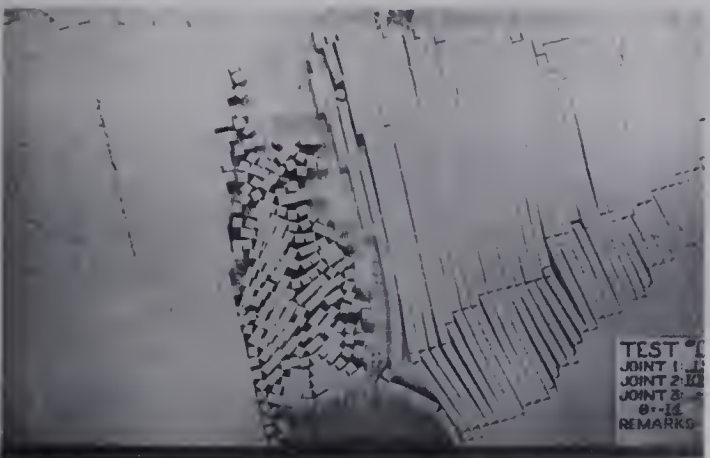
(J)



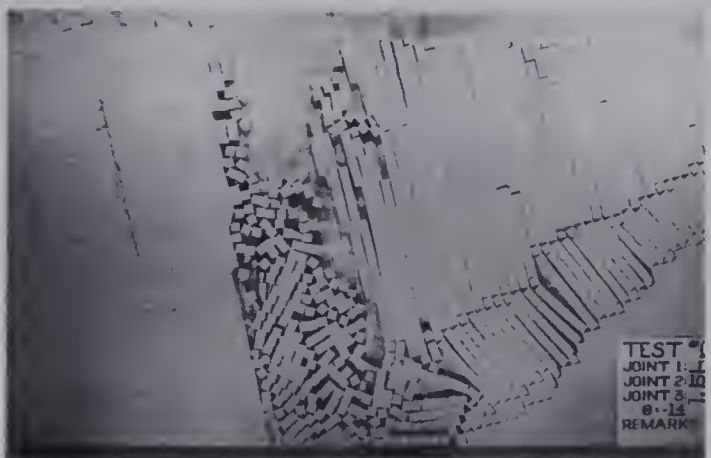
(K)



(L)



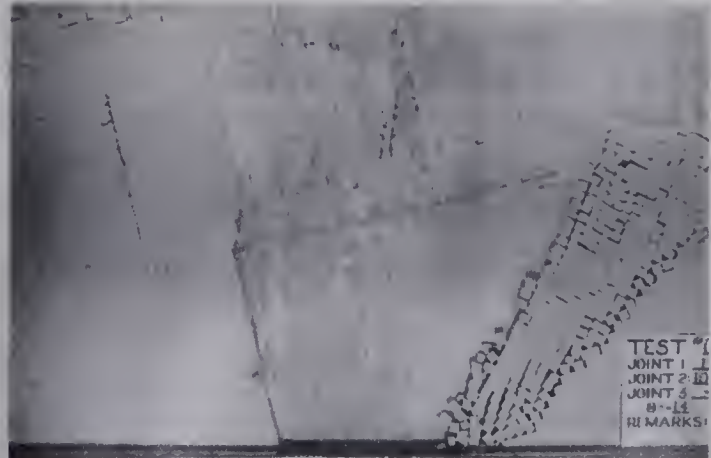
(M)



(N)



(O)



(P)

independently and small abutment rotations are observed.

Minor amounts of hangingwall beam-column buckling occurs and an unstable arch is formed. Once the arch fails, the lateral force is no longer resisted and the hangingwall fails catastrophically by buckling. A kink-band is formed obliquely to the joint directions. The kink-band is not as regular as that portrayed in Section 2.1.2 but it does verify the interpretation of the failure mechanism.

4.2.3. TEST #003 (PLATES 7 & 8)

The beam-columns rotated at thirty degrees from the restraint show the same behavior as the previous test since the beam-column failure progresses perpendicular to the thirty degree joint set. That is, the long, low angle beam column is less stable than the high angle abutment beam-column. When the unstable arch has reached mid-point, the hangingwall begins to buckle since the slenderness ratio of the abutment beam-columns has increased beyond its stable length at that orientation. An irregular kink-band begins to form with the bottom hinge forming at an oblique angle to the joint sets. The top hinge is experiencing some sliding since the axial normal force component is insufficient to mobilize the shear strength. The flexure of the initial arch prevents further sliding. The top hinge of the kink-band then continues to rotate. In effect two kink-bands are formed, both converging to a point (fig.4.7).

The entire structure collapses when the void volume

PLATE 7: TEST #003



(A)



(B)



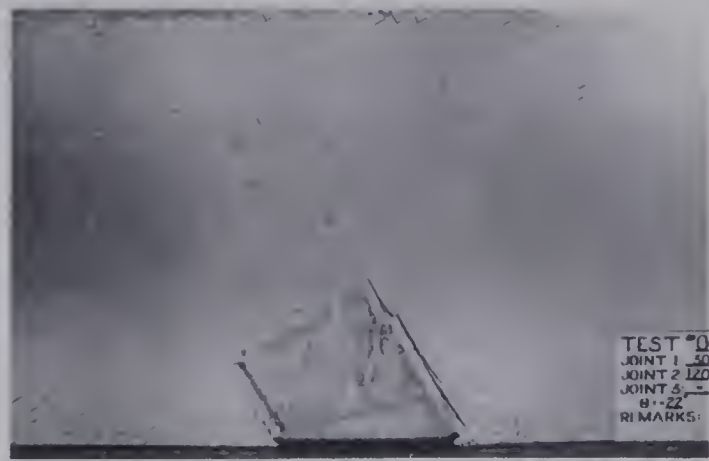
(C)



(D)



(E)



(F)



(G)

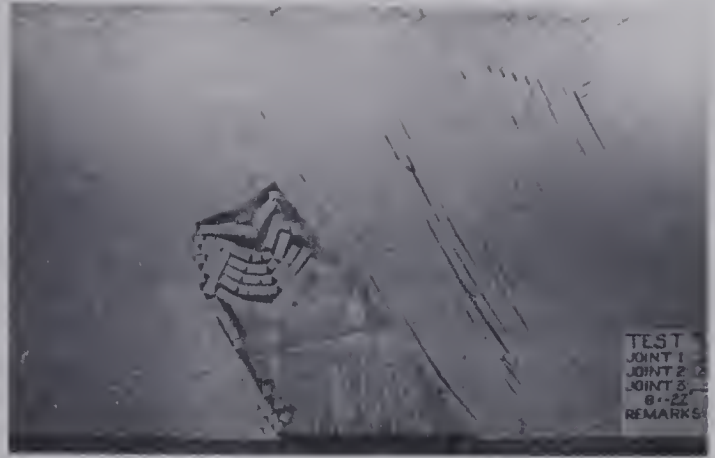


(H)

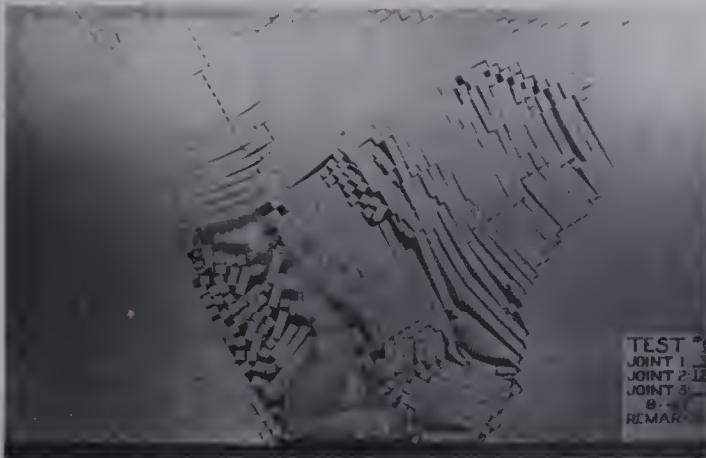
PLATE 8: TEST #003 (CON'T)



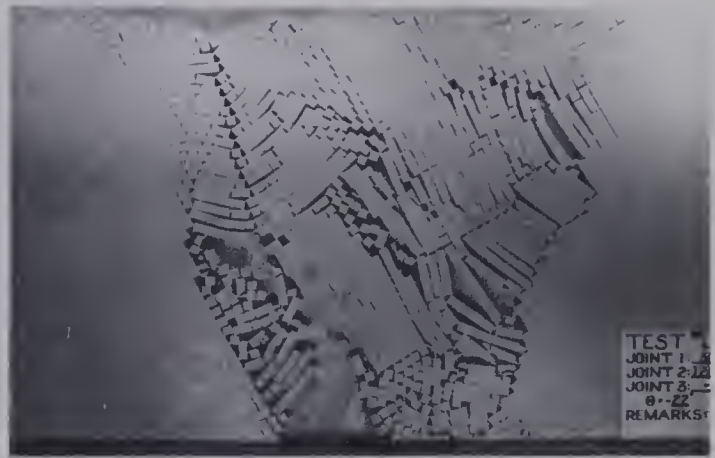
(I)



(J)



(K)



(L)



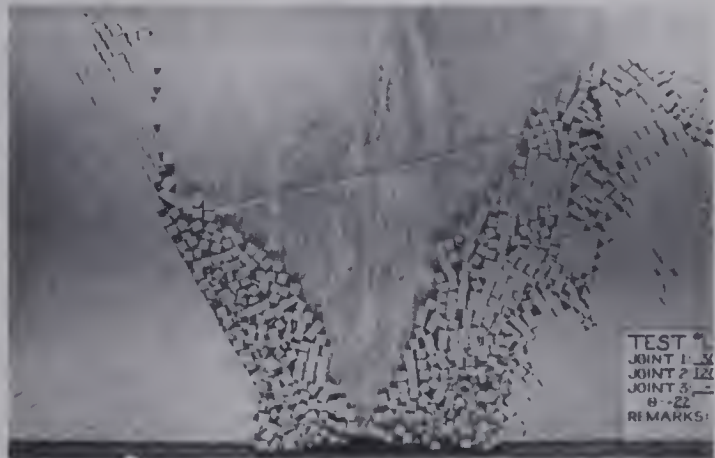
(M)



(N)



(O)



(P)

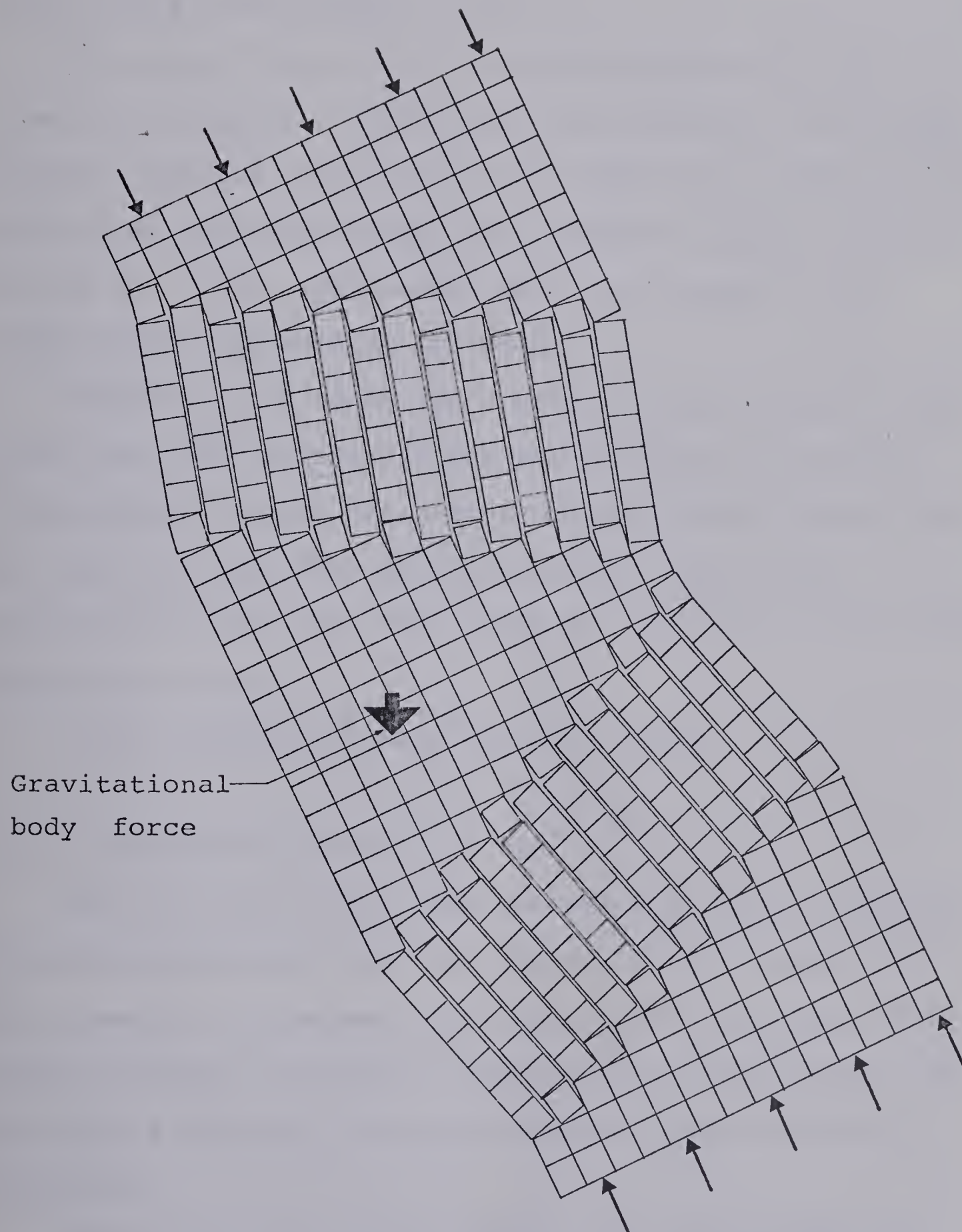


Fig. 4.7
Converging Kink Bands

increases and bin flow of angular material then begins.

4.2.4. TEST #004 (PLATES 9 & 10)

The joint sets are at forty-five degrees to the restraint barrier. A stable arch was formed and no further failure occurred, since each beam-column was stable for that particular span. The author then manually failed one beam-column at a time, alternating from one abutment to the other, until instability occurred.

Beam-column failure again occurs perpendicular to one joint set. The hangingwall becomes a series of unstable beam-columns forming the same modified double kink-band as in fig. 4.7. Some film was lost but the loss is not significant since Test #003 gives an indication of the final massive failure.

After massive failure, bin flow occurs.

4.2.5. TEST #009 (PLATES 11 & 12)

The 1:1 ratio joint sets intersect at fifteen degrees from the orthogonal. That is, one set is at 0 degrees and the other at 105 degrees from the restraint barrier. Beam-column flexure occurs as in the previous tests but the end conditions affecting block rotations is quite different (fig. 4.8).

The right ends of the members can rotate freely and loose contact with the abutment. The left ends are restrained from rotating due to the interference of the

PLATE 9: TEST #004



(A)



(B)



(C)



(D)



(E)



(F)

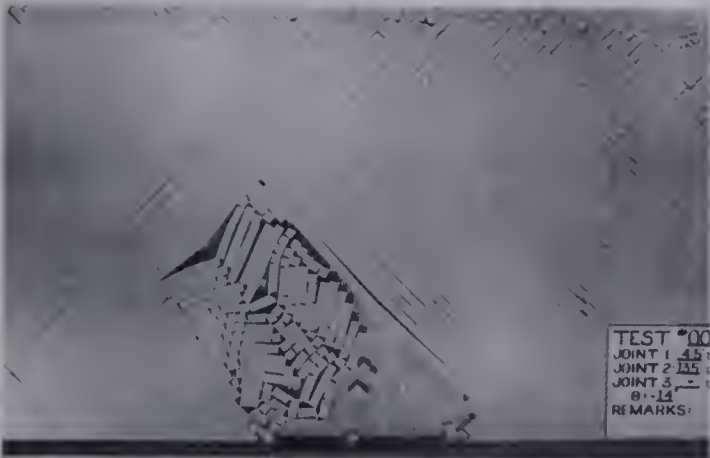


(G)



(H)

PLATE 10: TEST #004 (CON'T)



(I)



(J)



(K)

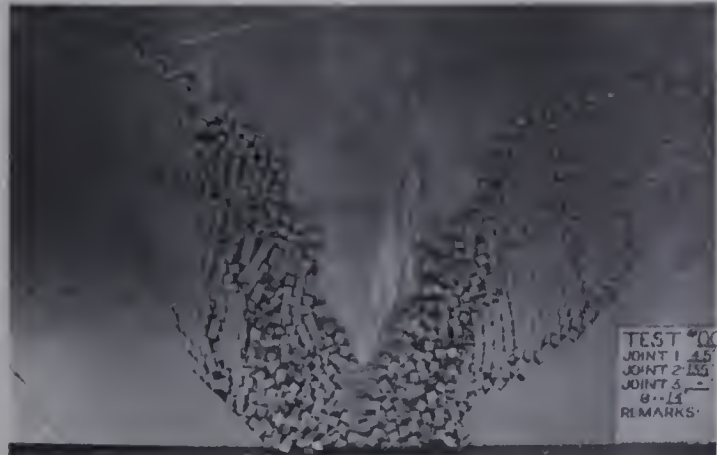


(L)

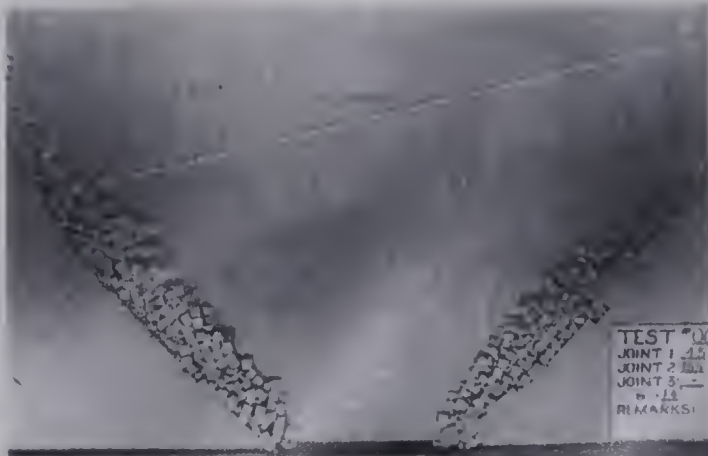
MISSING
PHOTOGRAPHS



(N)



(O)



(P)

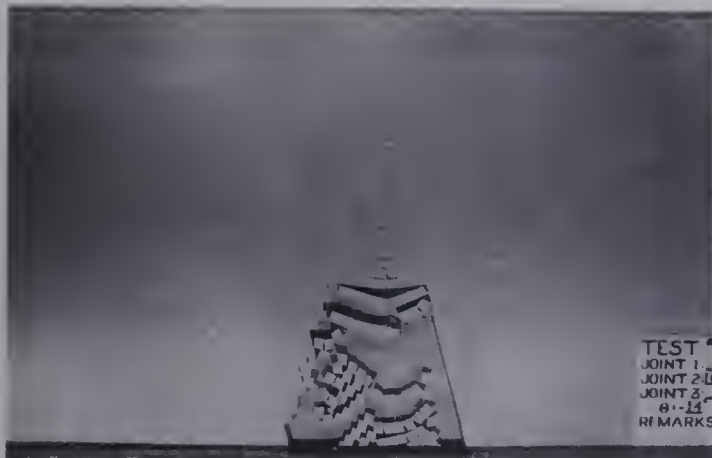
PLATE 11: TEST #009



(A)



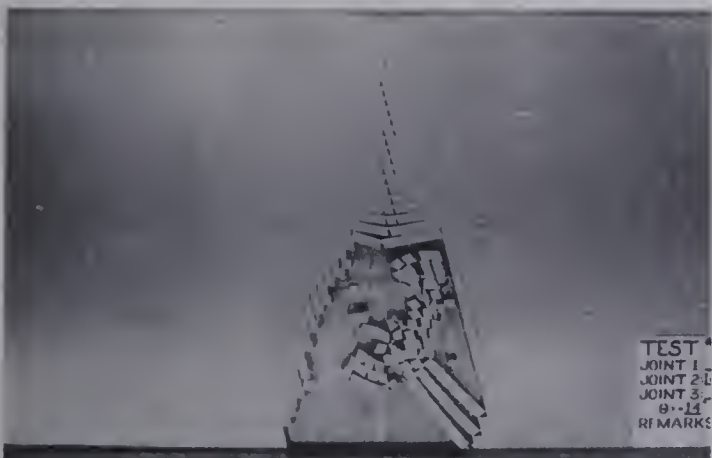
(B)



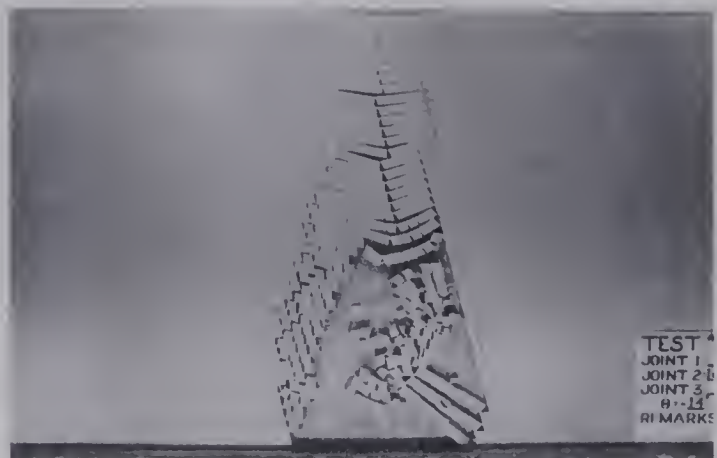
(C)



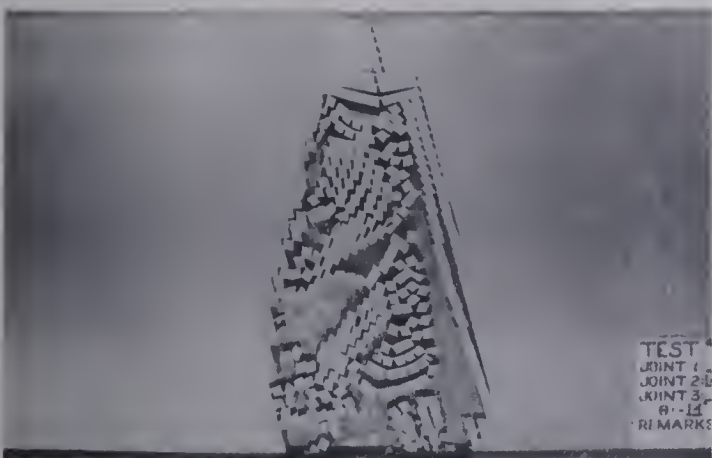
(D)



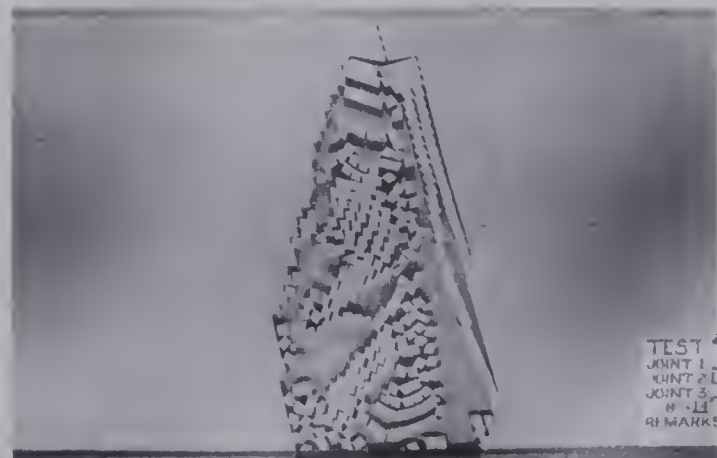
(E)



(F)

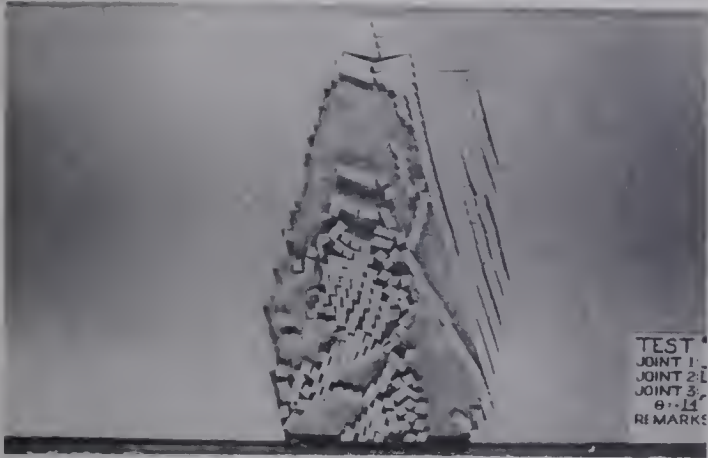


(G)



(H)

PLATE 12: TEST #003 (CON'T)



(I)



(J)



(K)



(L)



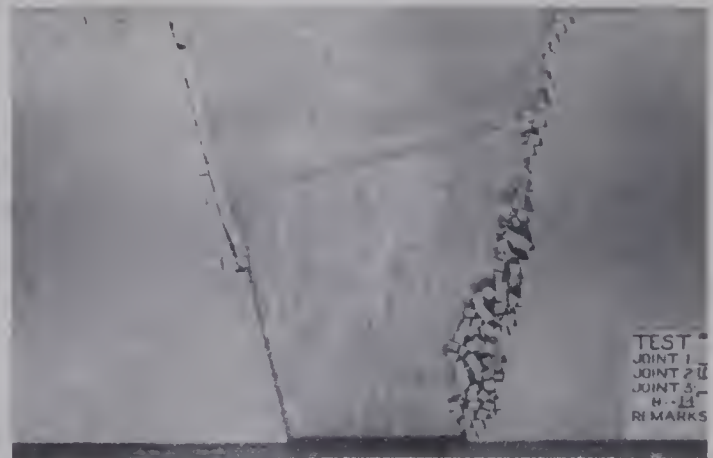
(M)



(N)



(O)



(P)

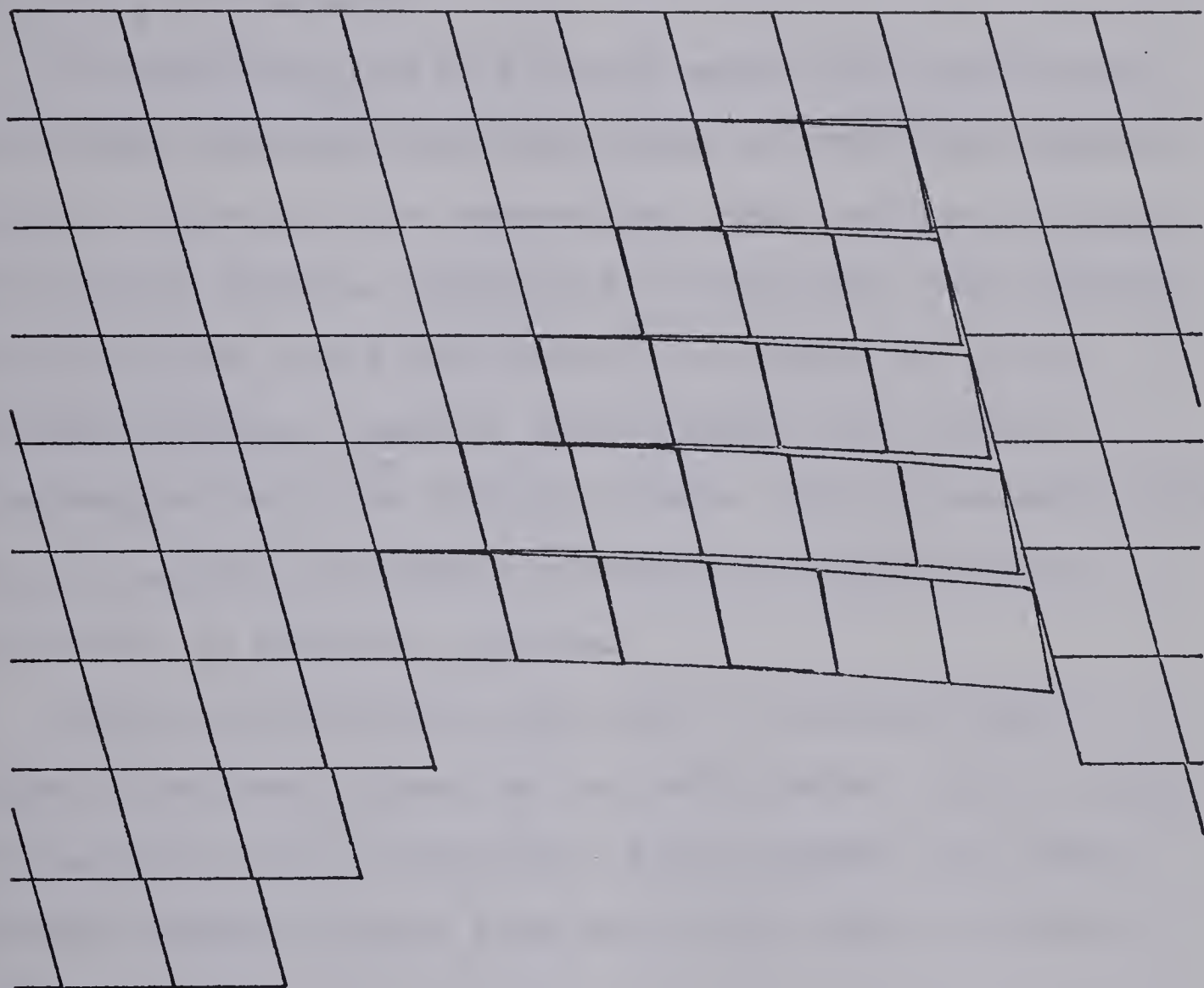


FIG. 4.8 End Conditions affecting
Beam - Column Stability

block acute angle apex with the overlying beam-column. The left side blocks do rotate a limited amount forming a rough shear surface tending to prevent downward block sliding. The left abutment then converges with the right abutment tending to form a stable arch.

If sufficient driving forces exist, the stabilizing block edge asperities are overridden and the left abutment shears, increasing the beam-column span. Failure continues in the same fashion, generating a converging left abutment with the right until roof stability occurs. The right abutment columns, however, buckle since the critical slenderness ratio for that particular load is exceeded. This column failure increases the beam-column span leading ultimately to buckling failure.

When the arch fails, the lack of lateral support reduces the normal force on the left abutment and it fails by shearing along a continuous joint surface. The right abutment members topple also due to the lack of lateral support.

4.2.6. TEST #013 (PLATES 13 & 14)

Initial failure in this test is similar to the previous test. Beam-column failure occurs since little deflection and rotation is required to detach the member from the right abutment. Once the right end separates the cantilevered beam-column has no strength and quickly collapses. The right abutment columns or high-angled beam-columns lose stability

PLATE 13: TEST #013



(A)



(B)



(C)



(D)



(E)



(F)

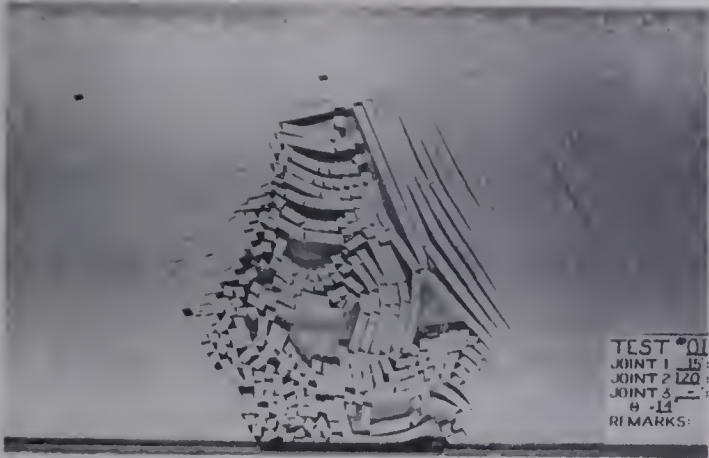


(G)



(H)

PLATE 14: TEST #013 (CON'T)



(I)



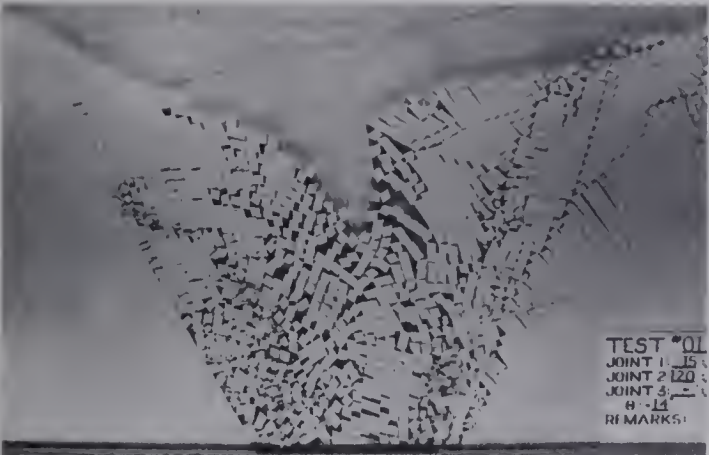
(J)



(K)



(L)



(M)



(N)



(O)



(P)

and effectively increase the roof span.

Little lateral force is transmitted through the overlying arch and the resulting low normal force on the left abutment allows shear failure to occur. The right abutment fails by buckling as observed by the kink-band. The caving span fails catastrophically and bin flow begins.

4.2.7. TEST #014 (PLATES 15 & 16)

A relatively stable configuration is developed in Test #014. Beam-column buckling along both abutments occurs in a time-dependent, progressive fashion. Very little downward movement is required to detach the right end of the beam-column from the right abutment and this becomes a major failure mechanism. If the axial load through the beam-column is low, shear failure along the right abutment becomes preferred.

Once the free spans become large, the converging double kink-bands are again formed. The angle of obliquity of the kink-band appears steep at the constrained bottom hinge and is zero along a joint plane at the top hinge.

The overlying strata then fails as a massive composite beam with much internal sliding and rotation of individual blocks. Bin flow follows.

4.2.8. TEST #015 (PLATES 17 & 18)

The left ends of the beam-columns readily rotate away from the abutment due to the favorable rotational geometry

PLATE 15: TEST #014



(A)



(B)



(C)



(D)



(E)



(F)



(G)

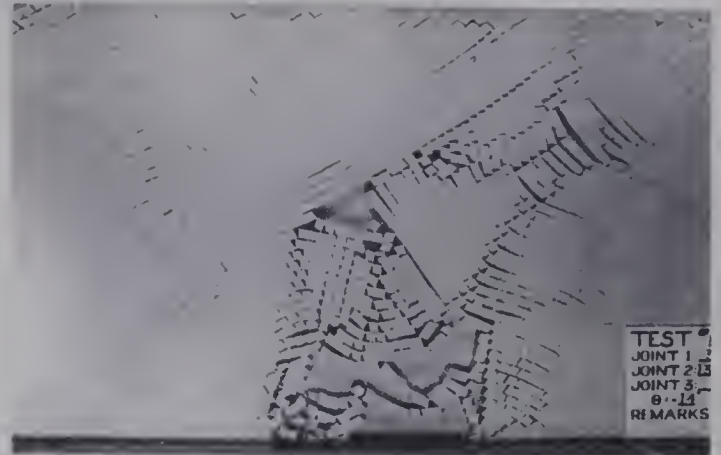


(H)

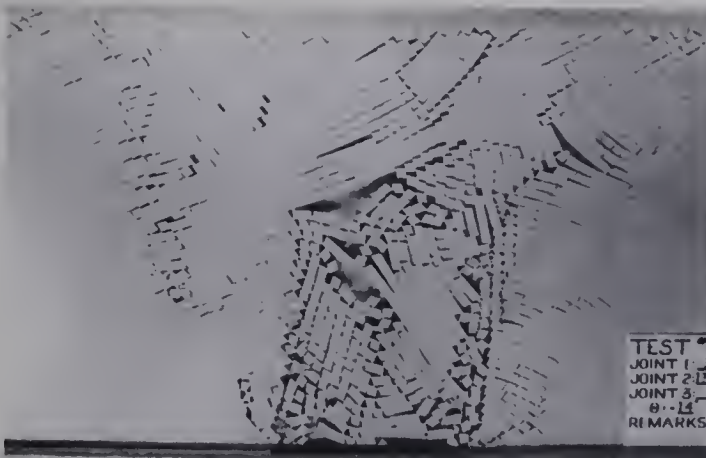
PLATE 16: TEST #014 (CON'T)



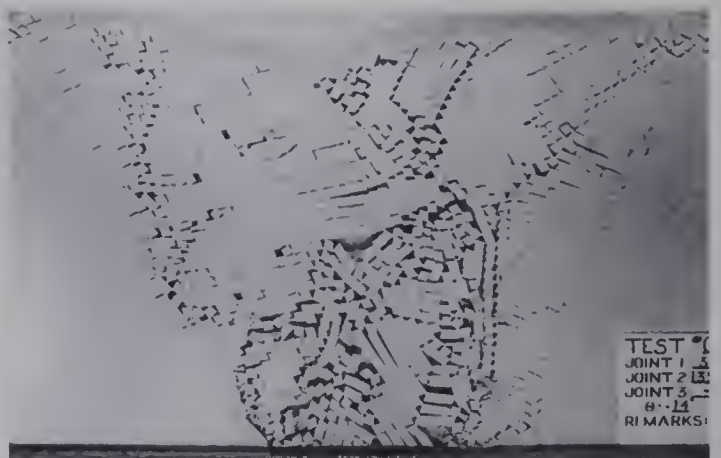
(I)



(J)



(K)



(L)



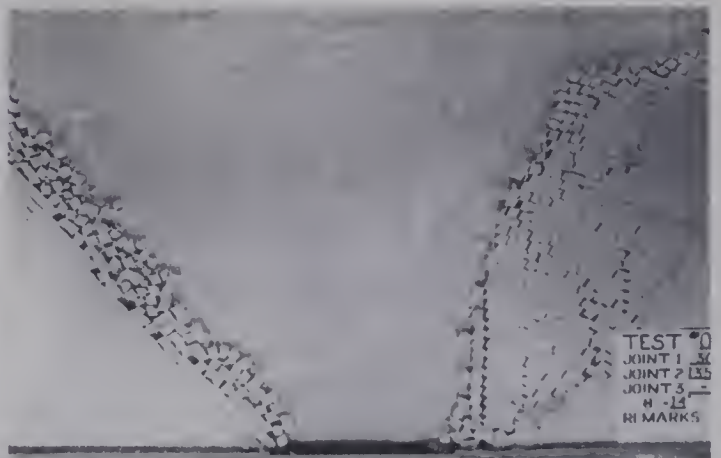
(M)



(N)



(O)

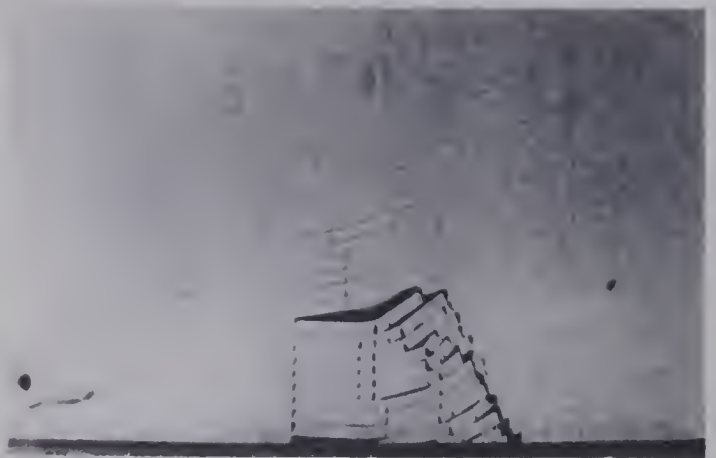


(P)

PLATE 17: TEST #015



(A)



(B)



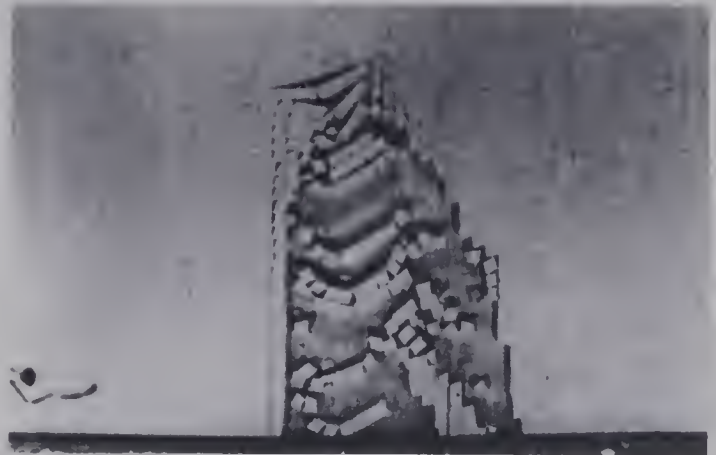
(C)



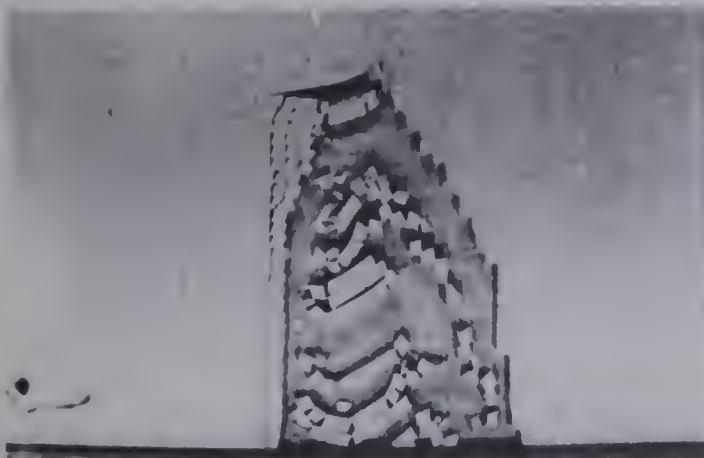
(D)



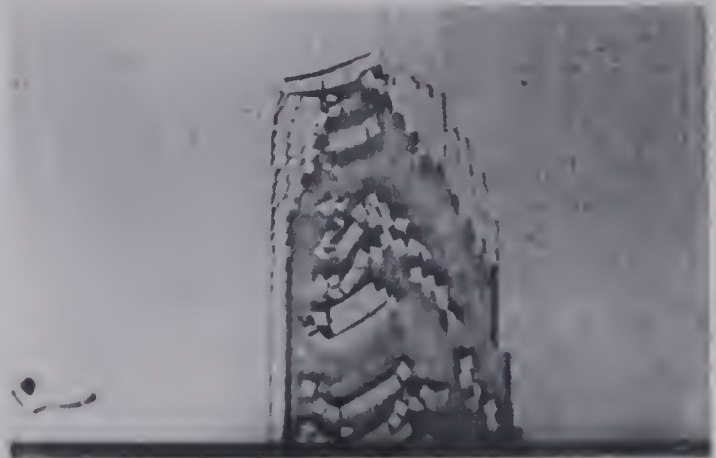
(E)



(F)

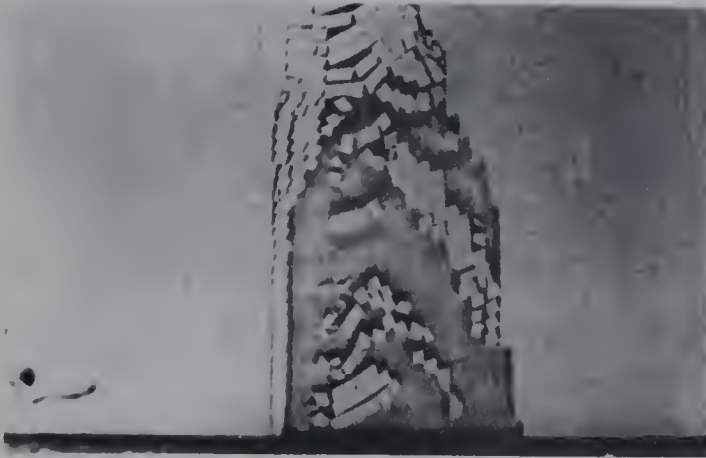


(G)

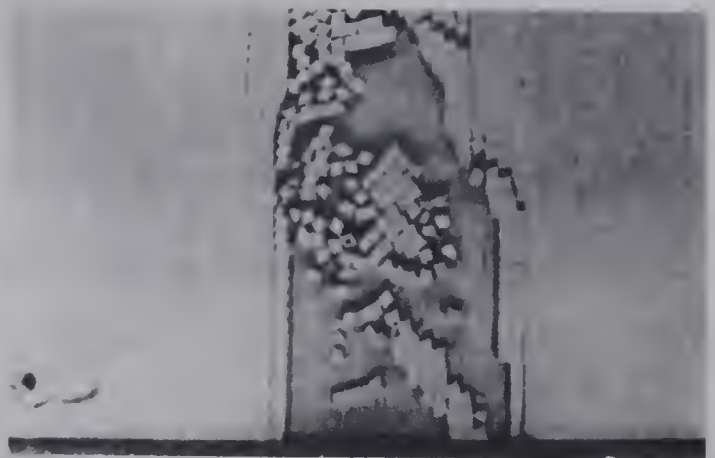


(H)

PLATE 18: TEST #015 (CON'T)



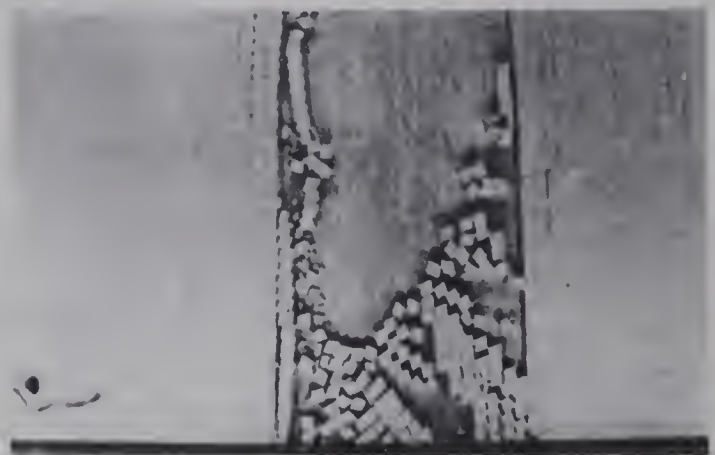
(I)



(J)



(K)



(L)



(M)



(N)



(O)



(P)

along the vertical abutment. This is not the case along the right abutment. As a result, the right abutment converges to the left abutment, forming an arch.

Due to the progressive caving, the increasing weight of the overhanging arch exceeds the shear strength along the vertical discontinuities. As a result, the excessive weight portion of the overhanging arch shears and detaches away from the arch. The resulting increase of the beam-column span promotes further flexural failure and the sequence begins anew until it reaches surface. The arch is then broken and the right abutment arch components shear to a vertical wall. The walls then buckle and topple.

4.2.9. TEST #016 (PLATES 19 & 20)

These 1:1 ratio blocks formed by the joint intersections at thirty degrees from the orthogonal show a tendency to fail internally. The rhombohedral blocks with one inch edges and diagonal dimensions of 1.00 inch by 1.73 inches, experience both bending and point load forces which often exceeds the block material strength. This is mainly due to the change of the cross-sectional area along the block. The acute angle apexes are particularly prone to failure.

Shear failure along the block faces is also common since the shear resisting forces are insufficient to prevent movement. Where shear failure is restrained by the interference of surrounding blocks, kink-band formation with

PLATE 19: TEST #016



(A)



(B)



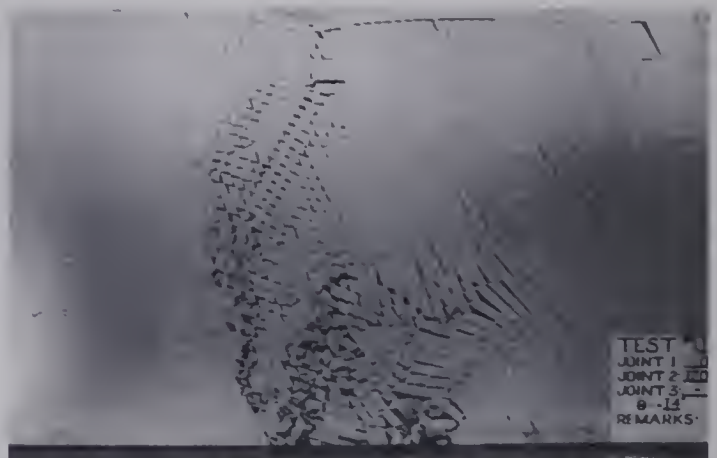
(C)



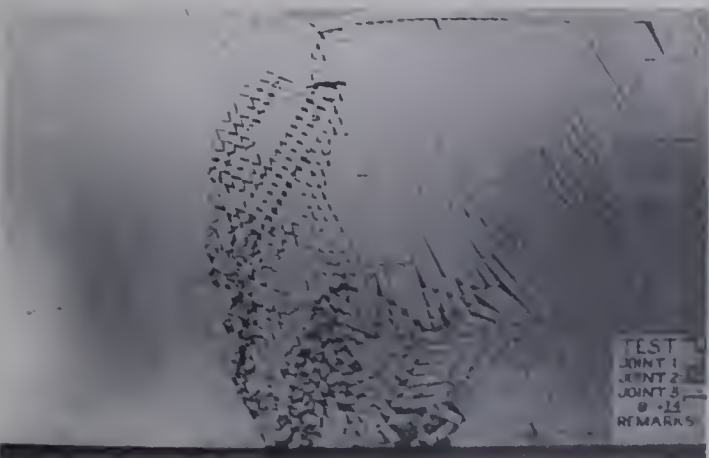
(D)



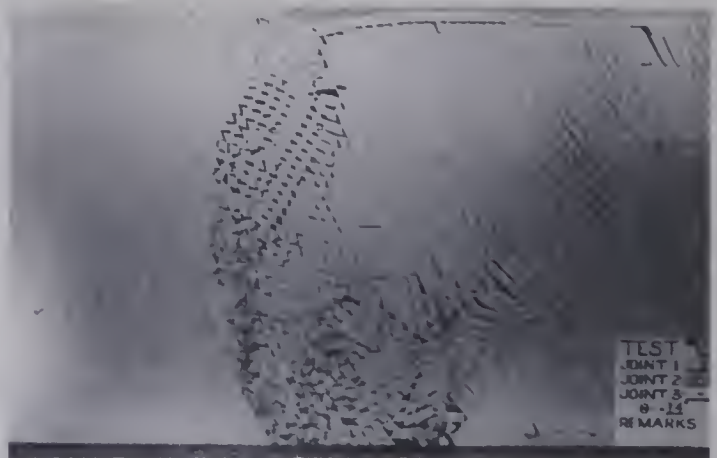
(E)



(F)

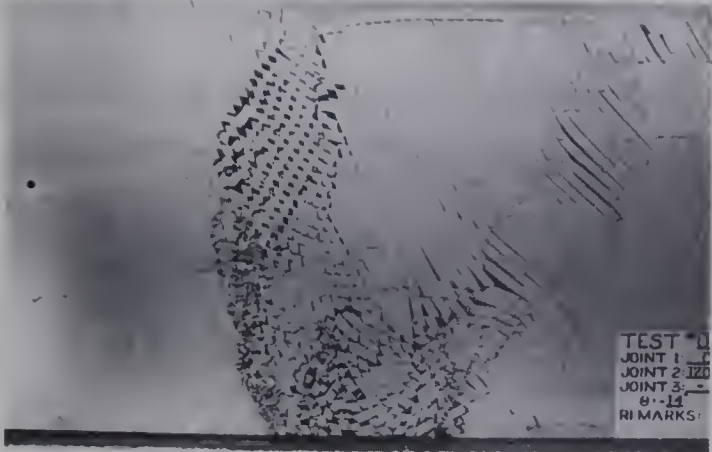


(G)

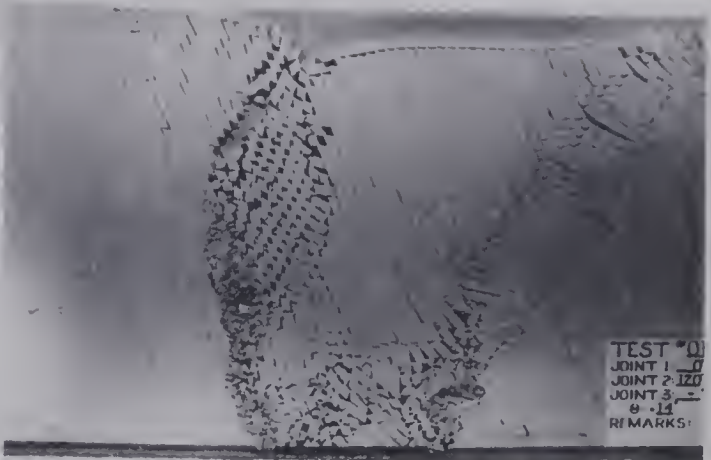


(H)

PLATE 20: TEST #016 (CON'T)



(I)



(J)



(K)



(L)



(M)



(N)



(O)



(P)

the associated destruction of block apexes along the hinges, occurs. This failure in terms of block caving is quite undesirable since the caved rock is failing as a relatively intact mass creating great crushing forces and the plug chokes the draw point. Thus bin flow is greatly modified and reduced in volume.

4.2.10 TEST #017 (PLATES 21 & 22)

Test #017 shows the same effects as Test #016 in that beam-columns readily detach from the right abutment, the blocks shear along the discontinuities and intact rock failure occurs. Where shear failure is restrained by the surrounding interference, beam-column flexure and kink-band formation occurs. The boundary kink-band structures rotate allowing the central rock mass to drop downward into the excavation, reducing the chance of incomplete rock mass dissociation as in the previous test. Bin flow begins and when the toe load on the surrounding steep slopes is reduced, the slopes slide into the opening.

4.2.11 TEST #018 (PLATES 23 & 24)

The debris of the initial beam-column shear failure hinders the shear failure of the right abutment and a nearly vertical double kink-band forms. With the deformation of the right abutment beam-columns, the left abutment beam-columns again slide along their underside, promoting still further kink-band development in the right abutment. This failure

PLATE 21: TEST #017



(A)



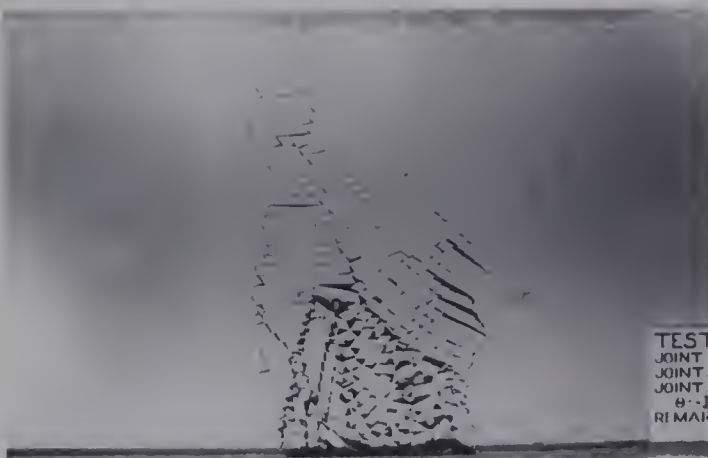
(B)



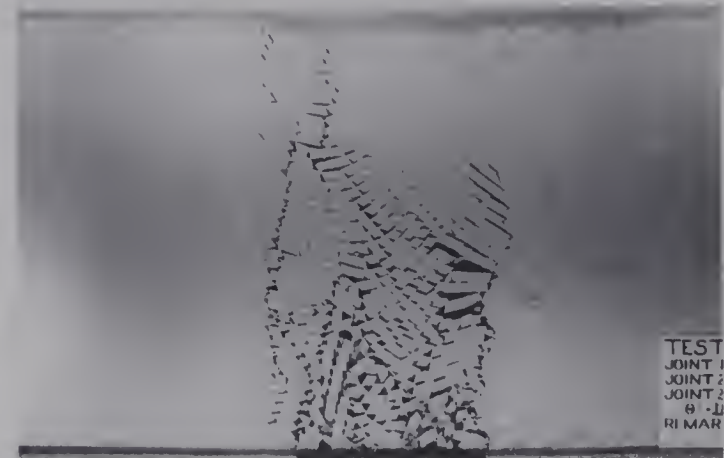
(C)



(D)



(E)



(F)



(G)

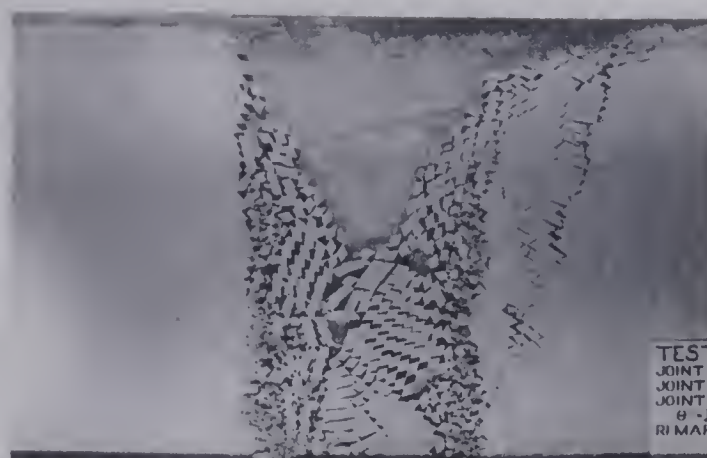


(H)

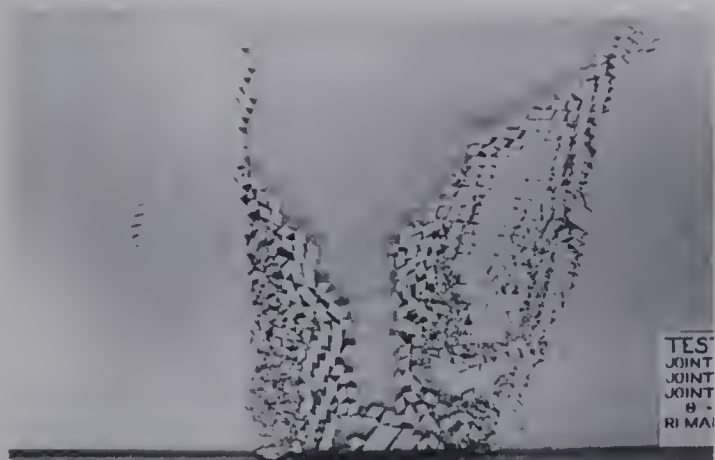
PLATE 22: TEST #017 (CON'T)



(I)



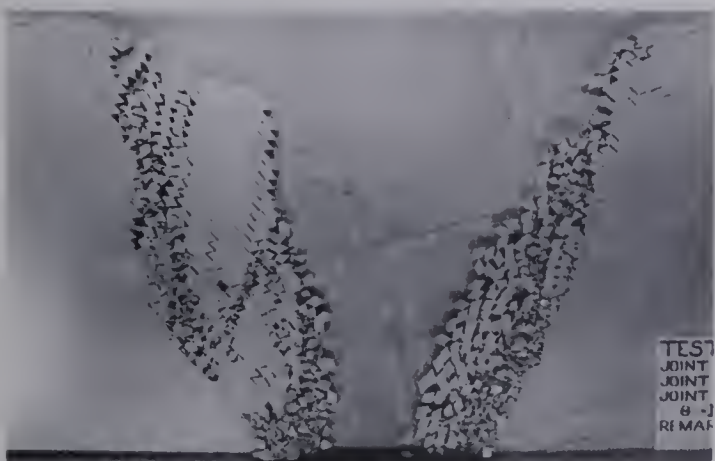
(J)



(K)



(L)



(M)



(N)



(O)

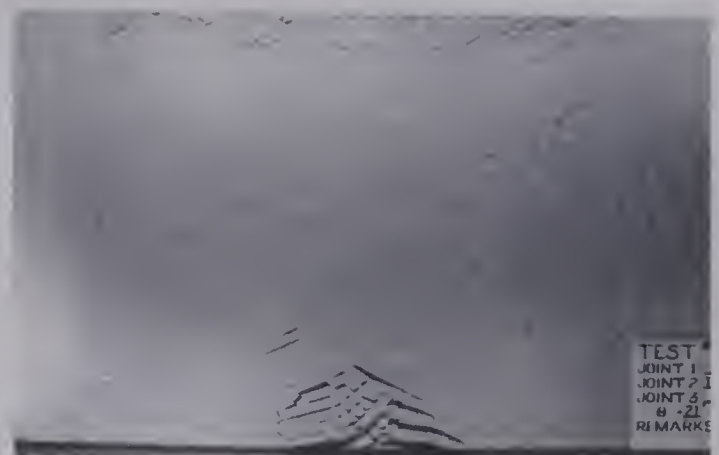


(P)

PLATE 23: TEST #018



(A)



(B)



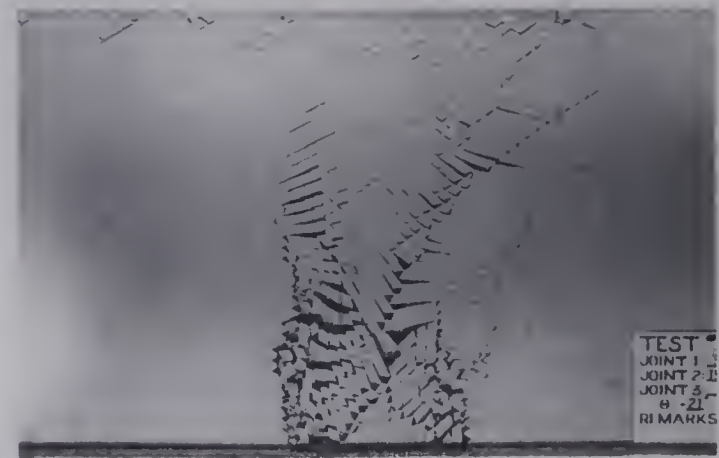
(C)



(D)



(E)



(F)



(G)



(H)

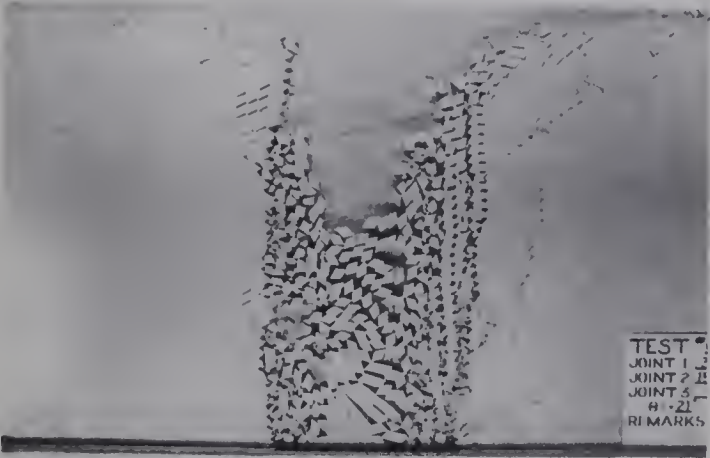
PLATE 24: TEST #018 (CON'T)



(I)



(J)



(K)



(L)



(M)



(N)



(O)



(P)

continues to 'zig-zag' upwards through the mass.

A narrow caving 'chimney' is formed and the steep slopes ultimately fail along the joint shear planes.

4.2.12. TEST #019 (PLATES 25 & 26)

With one joint set at a low angle of fifteen degrees and the other at a 75 degree angle, the beam-columns cannot detach by downward sliding from the right abutment. Sufficient member deflection must first occur before shear failure along the beam-column axes can occur.

Beam-column flexure is predominant as kink-band formation. When the caving has broken through to surface, the overhanging right abutment forms a kink-band and fails by toppling. The reduced normal load on the left abutment results in the steep wall failing along a joint surface. Note the disruption of the left abutment caused by the load of the steep wall and lack of shear resistance of the columns. It appears that a circular arc failure is imminent.

4.2.13. TEST #020 (PLATES 27 & 28)

Shear failure is predominant in Test #020. The beam-columns apparently have a low axial load and, therefore, the low shear resistance along the vertical fractures allows the members to slide down.

Kink-band formation occurs but shear failure rapidly prevents large kink-band deformations.

The vertical chimney walls rapidly fail by the combined

PLATE 25: TEST #019



(A)



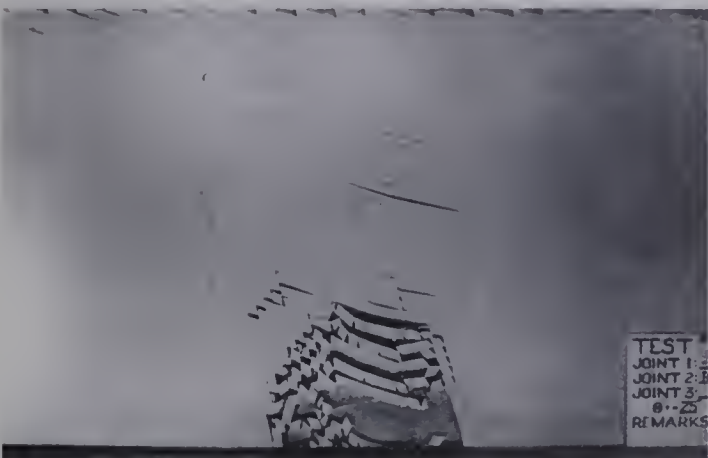
(B)



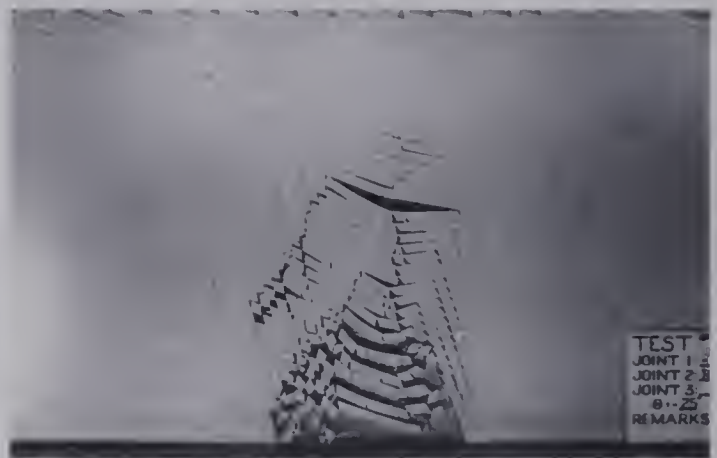
(C)



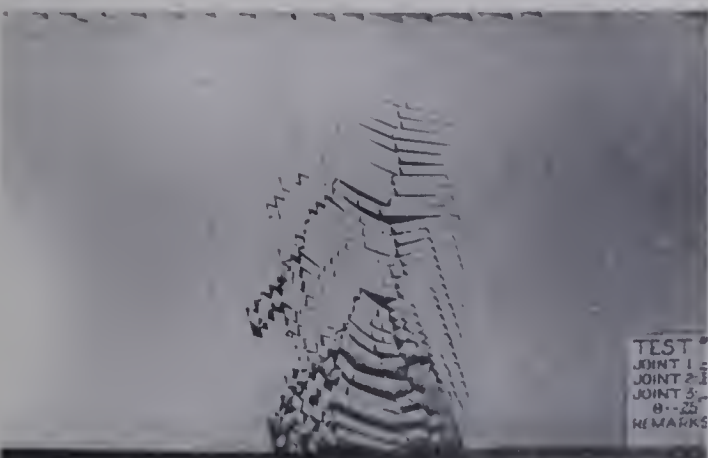
(D)



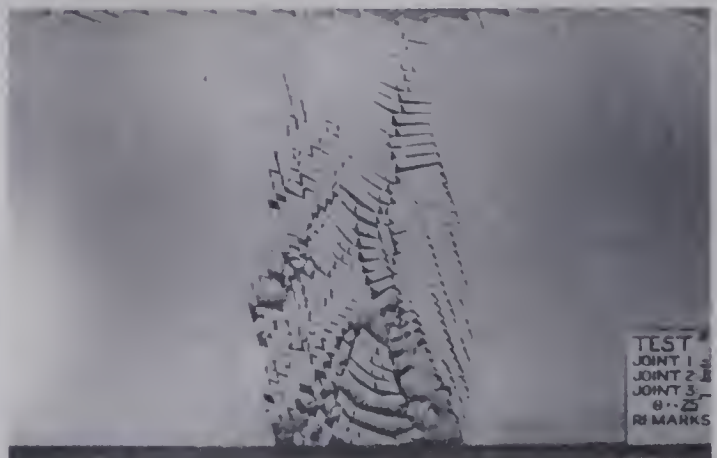
(E)



(F)

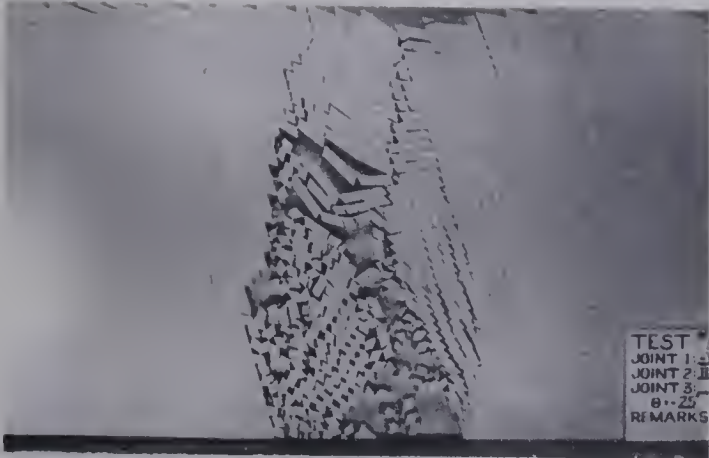


(G)

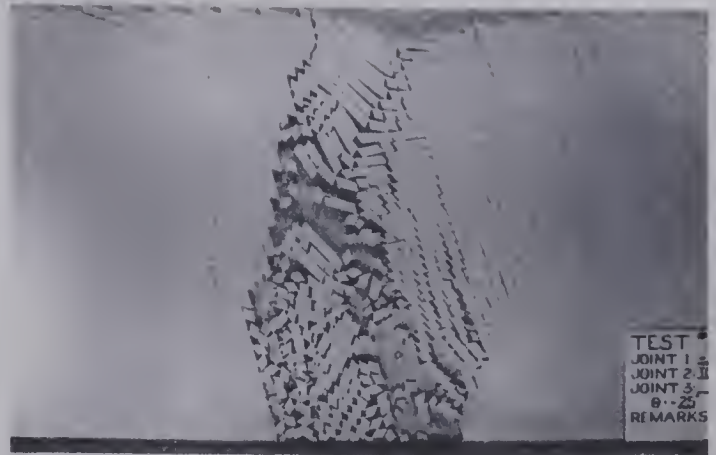


(H)

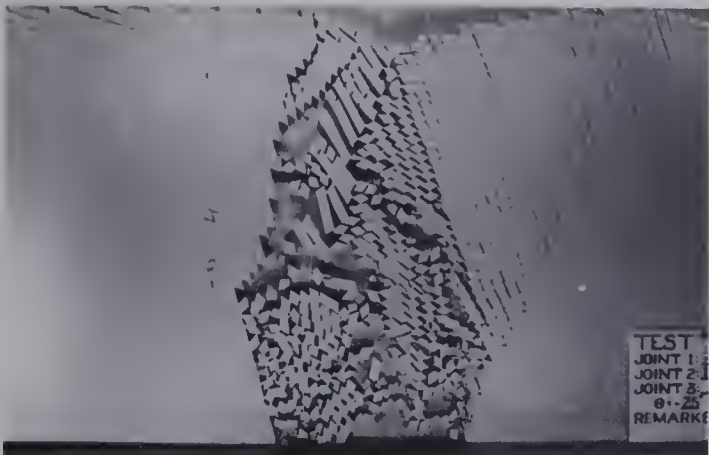
PLATE 26: TEST #019 (CON'T)



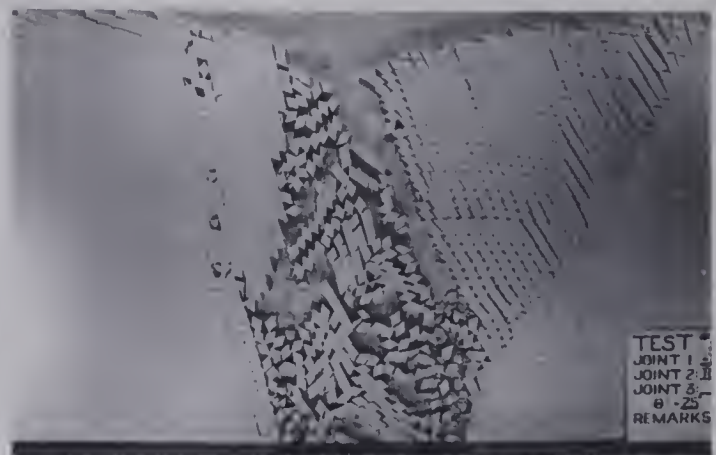
(I)



(J)



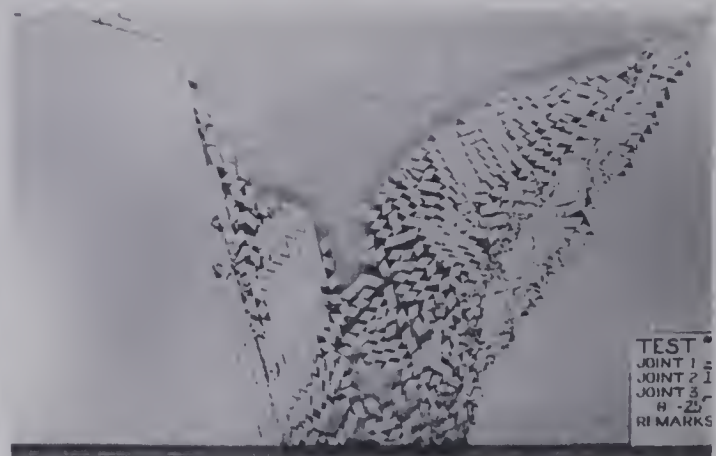
(K)



(L)



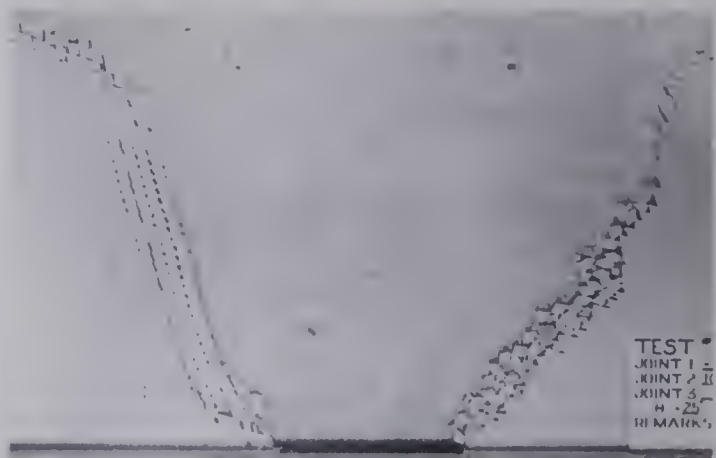
(M)



(N)



(O)



(P)

PLATE 27: TEST #020



(A)



(B)



(C)



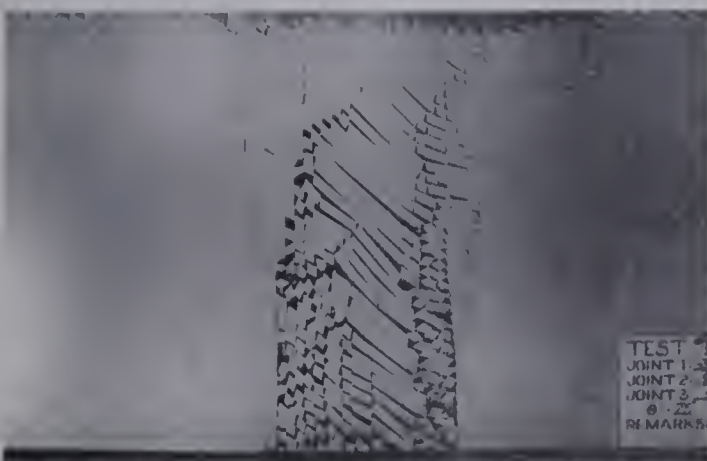
(D)



(E)



(F)



(G)



(H)

PLATE 28: TEST #020 (CON'T)



(I)



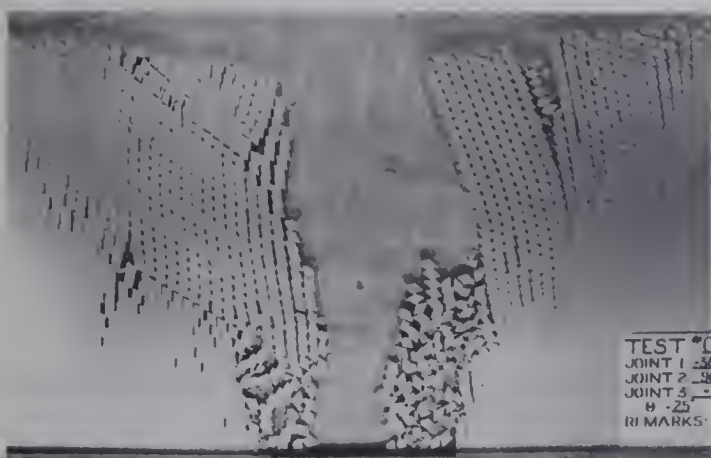
(J)



(K)



(L)



(M)



(N)



(O)



(P)

action of shearing and buckling.

4.2.14. TEST #005 (PLATE 29)

This test begins the 2:1 joint space ratio tests. The joint sets are orthogonal with one another and the blocks derived are one inch by two inches.

As in Test #001, beam-column flexure is the primary failure mode. Since the beam depth is also one inch and failure occurs as readily as Test #001, the number of vertical fractures has little influence on the failure mode.

After caving has broken through to surface, the chimney walls buckle and topple.

4.2.15. TEST #006 (PLATE 30)

The closely spaced joint set is rotated fifteen degrees from the horizontal. Beam-column flexural failure is the primary mode of caving, continuing through to surface.

Once the lateral support of the arch is eliminated, the hangingwall columns buckle forming a very wide and very oblique kink-band as compared to Test #002.

4.2.16. TEST #008 (PLATE 31)

At thirty degrees, the one inch depth beam-columns fail as their 1:1 counterpart in Test #004. Prior to the caving surface break through, the two inch depth hangingwall beam-columns begin to buckle. Sliding is also quite noticeable. Apparently, the axial force is insufficient in terms of the

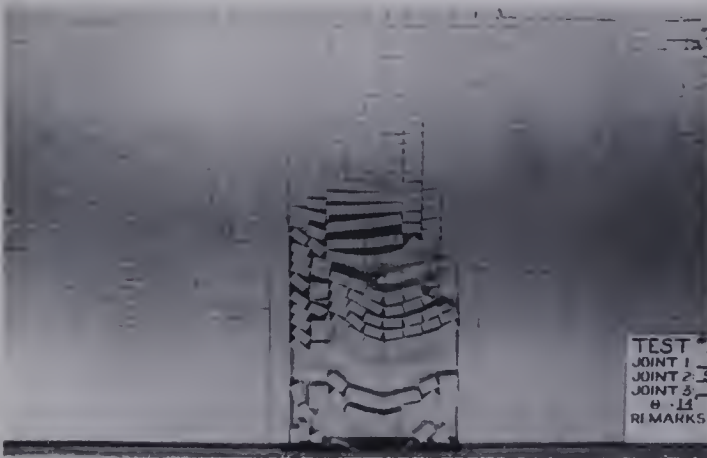
PLATE 29: TEST #005



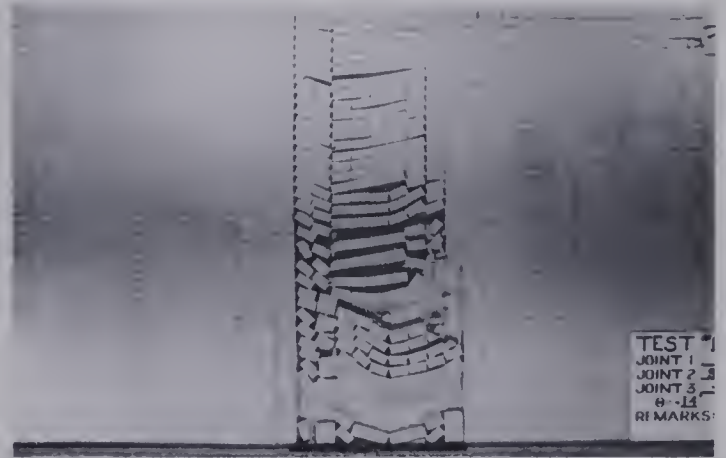
(A)



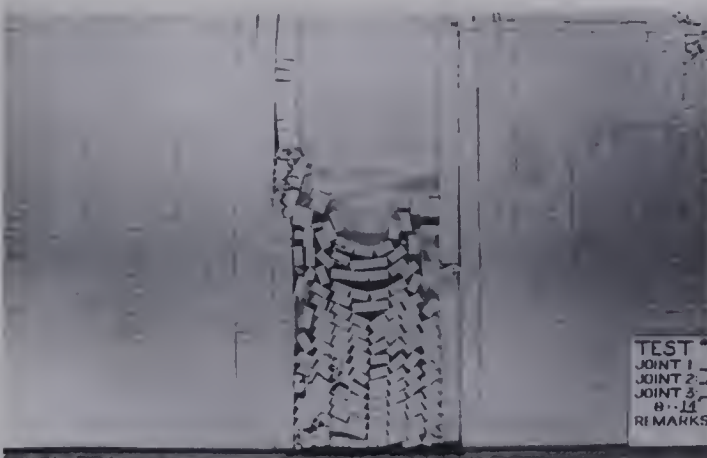
(B)



(C)



(D)



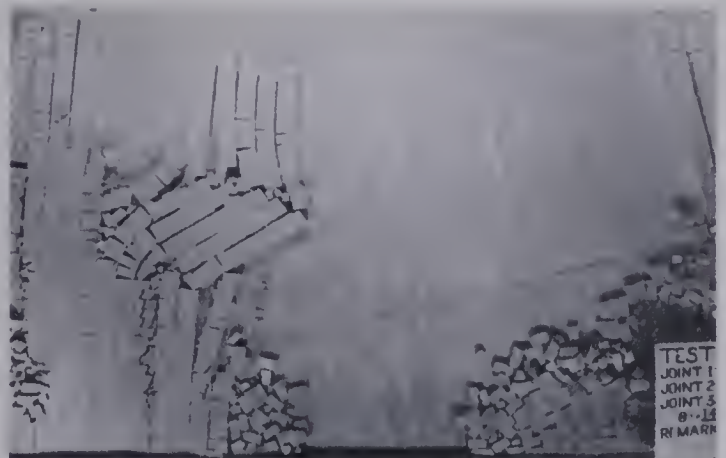
(E)



(F)



(G)



(H)

PLATE 30: TEST #006



(A)



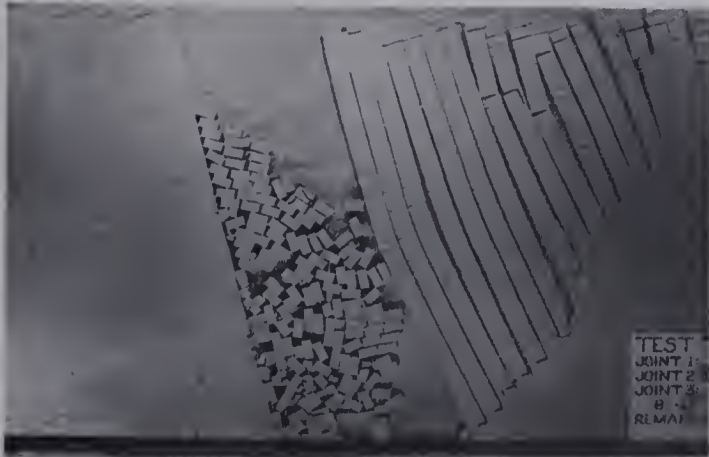
(B)



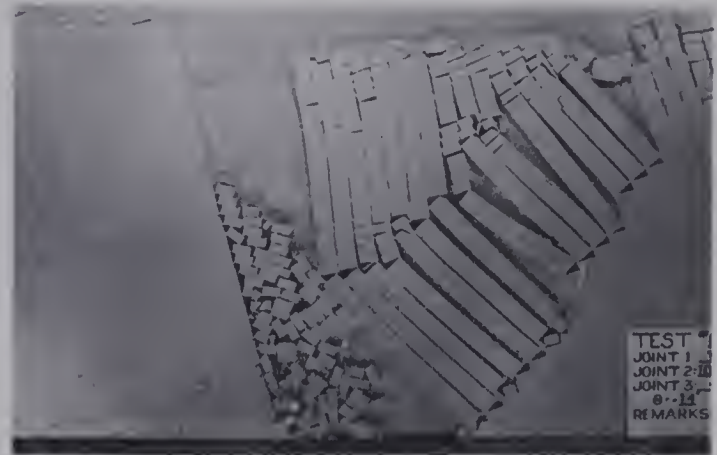
(C)



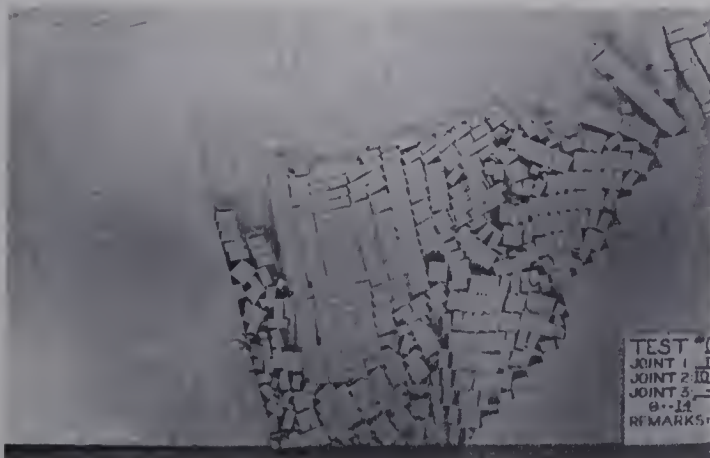
(D)



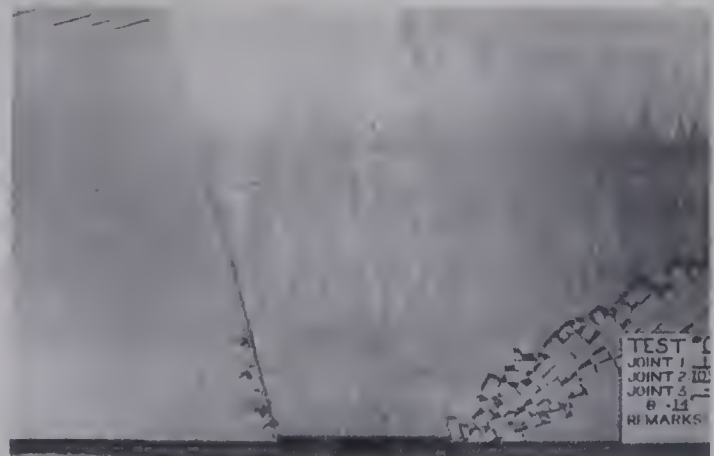
(E)



(F)



(G)



(H)

PLATE 31: TEST #008



(A)



(B)



(C)



(D)



(E)



(F)



(G)



(H)

joint normal force to actuate the shear resistance. However, the sliding stabilizes and a poorly-defined double kink-band is formed resulting in the eventual ultimate failure and bin flow.

4.2.17. TEST #010 (PLATE 32)

Initially, a stable arch is generated. The author slowly failed one thin beam-column at a time until failure progressed on its own. Beam-column failure of the thin members continued until the thick hangingwall beam-columns began to buckle. Kink-band formation within the hangingwall began but the top hinge began to slide due to a low normal force on the top hinge surface. Ultimately, the structure collapsed and bin flow takes over.

4.2.18. TEST #007 (PLATE 33)

The two inch thick beam-columns are now at thirty degrees and form a stable opening. The right and left beam-columns are successively failed manually until an unstable condition is reached. The right abutment beam-columns then begin to buckle and form a double kink-band. The top hinge shows some sliding since the axial force on the beam-columns synonymous with the normal force on the hinge surface is insufficient to totally mobilize the shear resistance forces. As the left abutment fails, the overhead roof span is increased and the thick beam-columns fail by flexural buckling.

PLATE 32: TEST #010



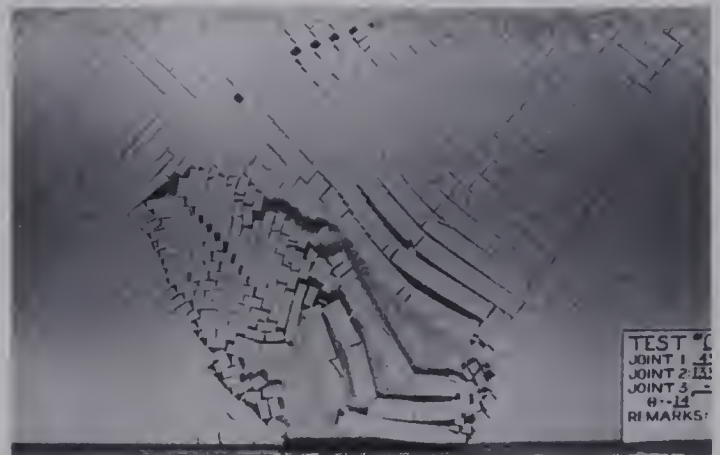
(A)



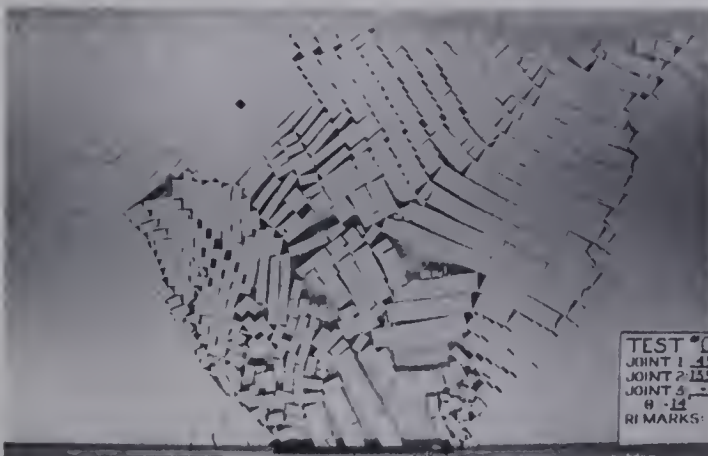
(B)



(C)



(D)



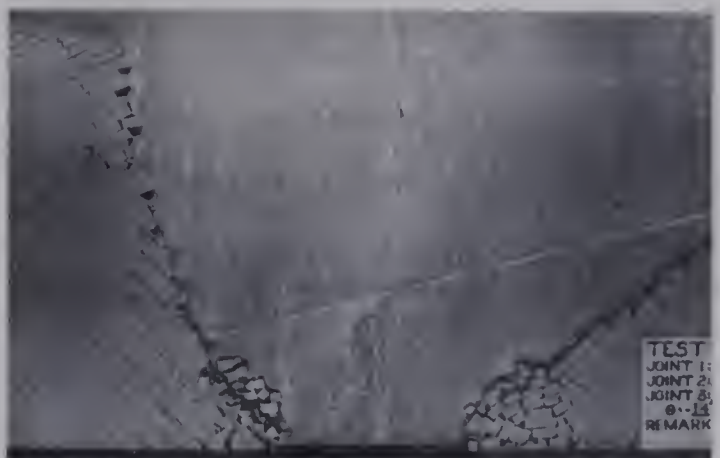
(E)



(F)



(G)



(H)

PLATE 33: TEST #007



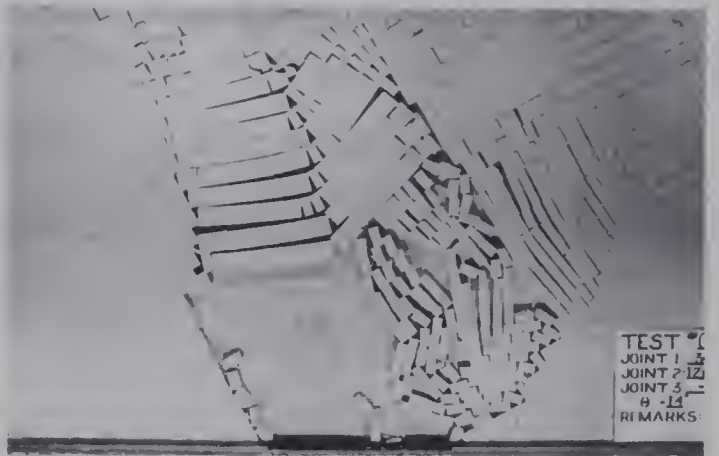
(A)



(B)



(C)



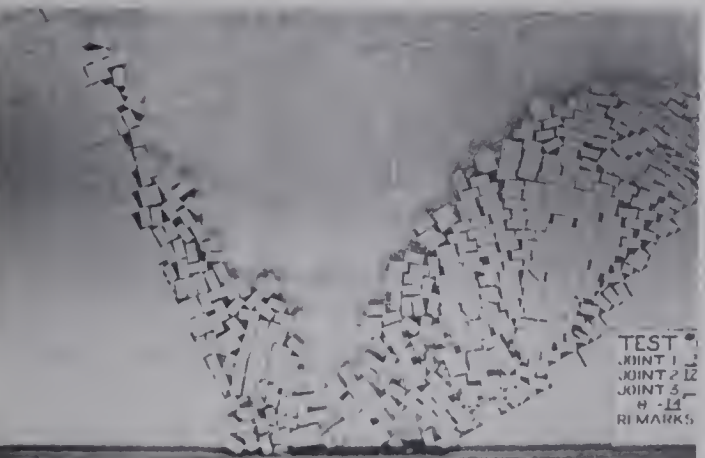
(D)



(E)



(F)



(G)



(H)

Once the horizontal restraint on the top surface is removed, the right abutment topples and bin flow begins.

4.2.19. TEST #012 (PLATE 34)

At fifteen degrees, the two inch thick beam-columns form a stable roof, though flexure is observed. The author manually failed one member at a time until an unstable condition was reached. This occurred when the roof span approached surface. The right abutment experiences a lateral force by the overhang of the hangingwall, producing a lateral thrust through the excavation roof span. This excess thrust allows block corner deformation and a double kink-band forms.

When surface break through occurs, the hangingwall then topples.

4.2.20. TEST #011 (PLATE 35)

The thick horizontal beam-columns in this test prove to be unstable. A low axial load allows the members to shear along the vertical discontinuities rather than buckle. Sidewall toppling takes over after the caving arch surfaces.

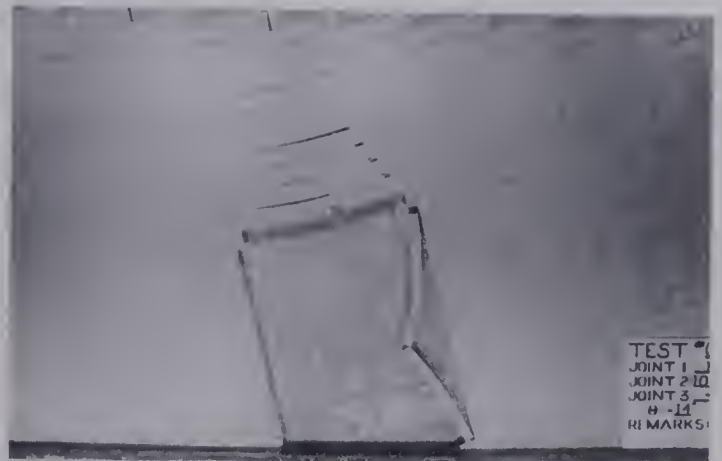
4.2.21. TEST #024 (PLATE 36)

The last series of tests are composed of 2:1 spaced joint sets intersecting at fifteen degrees from the orthogonal; the joint sets being rotated at thirty degree intervals.

PLATE 34: TEST #012



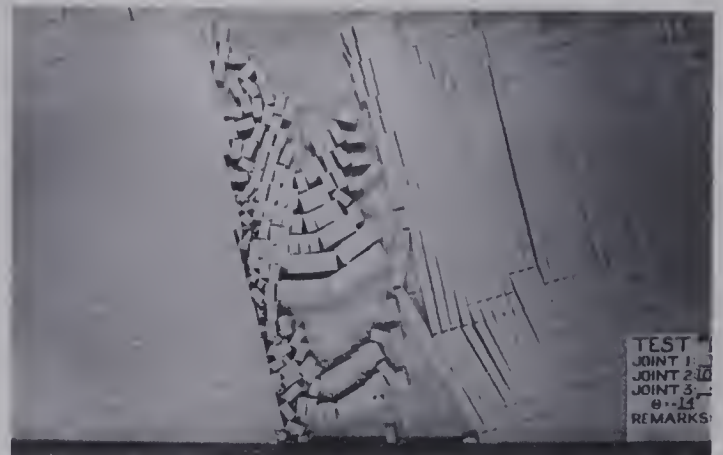
(A)



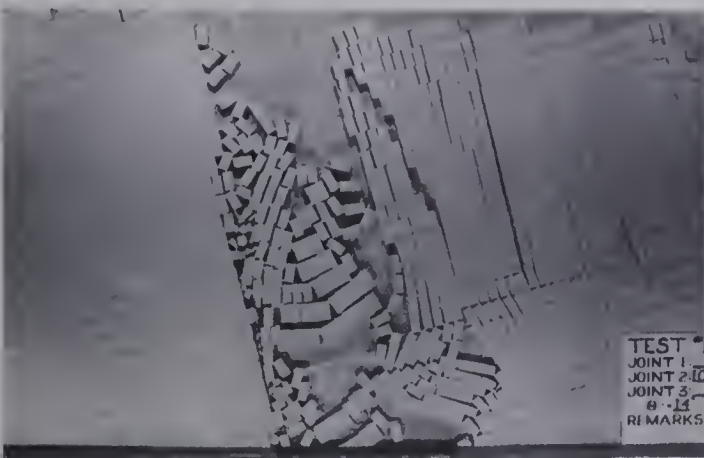
(B)



(C)



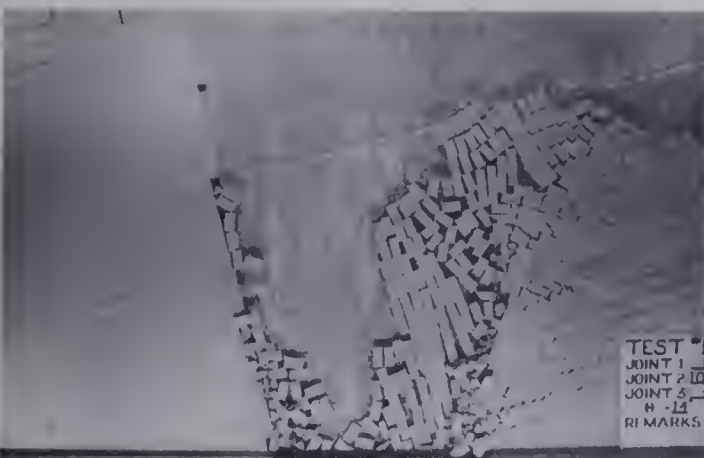
(D)



(E)



(F)



(G)



(H)

PLATE 35: TEST #011



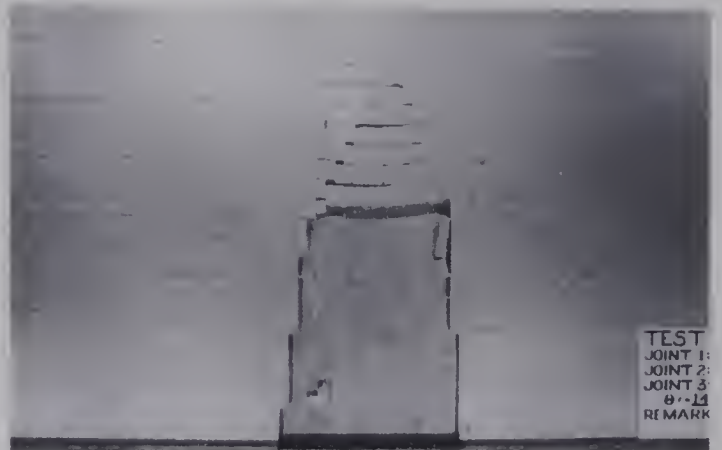
(A)



(B)



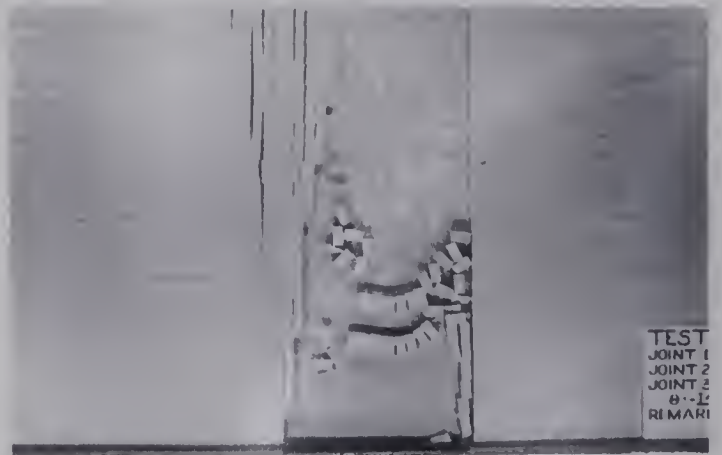
(C)



(D)



(E)



(F)



(G)



(H)

PLATE 36: TEST #024



(A)



(B)



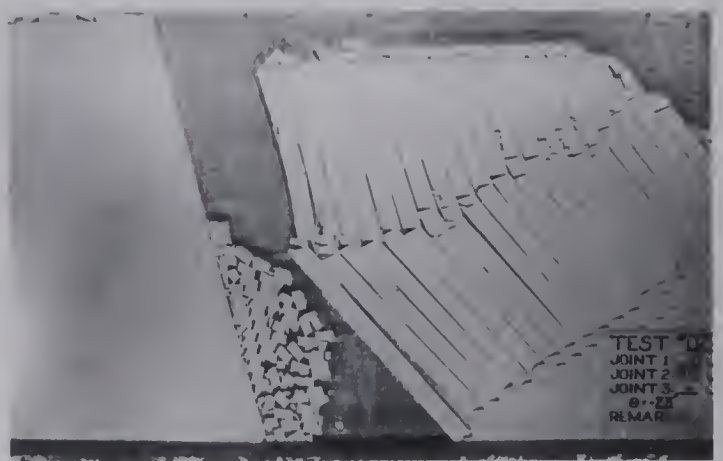
(C)



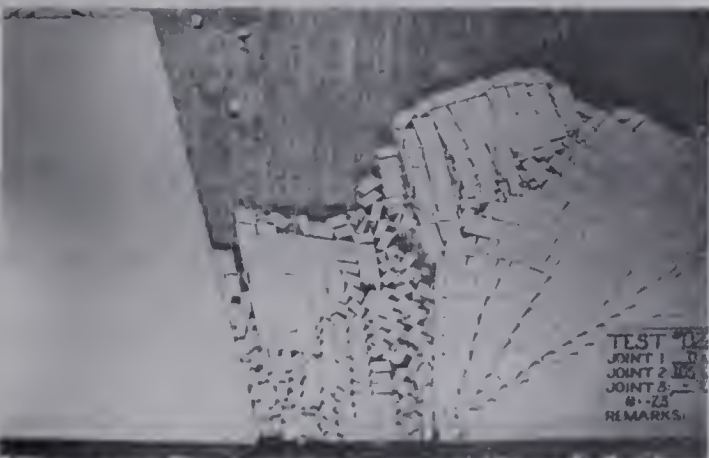
(D)



(E)



(F)



(G)



(H)

Test #024 is composed of one inch beam-columns in the horizontal position. The members require very little deflection to detach from the right abutment. Failure occurs rapidly. Toppling of the hangingwall forms kink-bands and bin flow then occurs.

4.2.22. TEST #021 (PLATE 37)

Both sliding and buckling is important in this test. Minor amounts of sliding reduces the effective thickness of the beam-columns and greatly reduces the buckling stability.

The thin members of the left abutment fail initially. When sufficient hangingwall span is generated, the right abutment slips and buckles, increasing the overhead span. This span continues to shear and buckle slowly. The right abutment span becomes too great and a double kink-band forms. The top hinge shows rotation along a joint plane mainly due to the block obtuse angle apex not interfering with the next block. Total collapse of the span occurs leading to bin flow.

4.2.23. TEST #025 (PLATE 38)

Again the thin beam-columns, though they are at a steep sixty degree angle, are the first to fail. The shear failure mode is predominant as well as when the thick beam-columns fail. The shear displacements reduce the effective depth of the members and further flexure and shearing occurs.

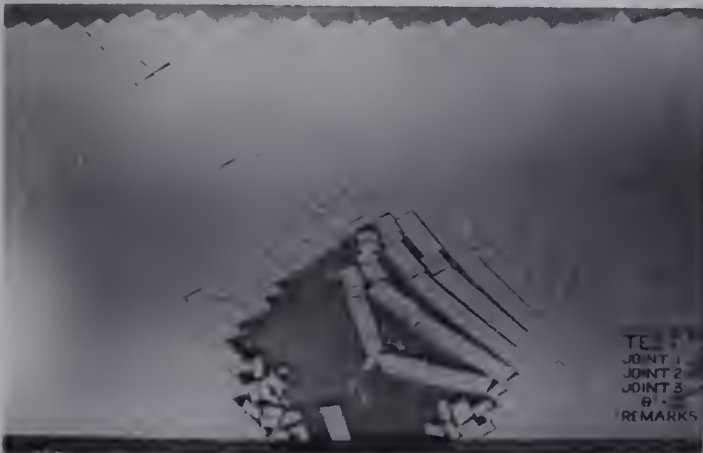
PLATE 37: TEST #021



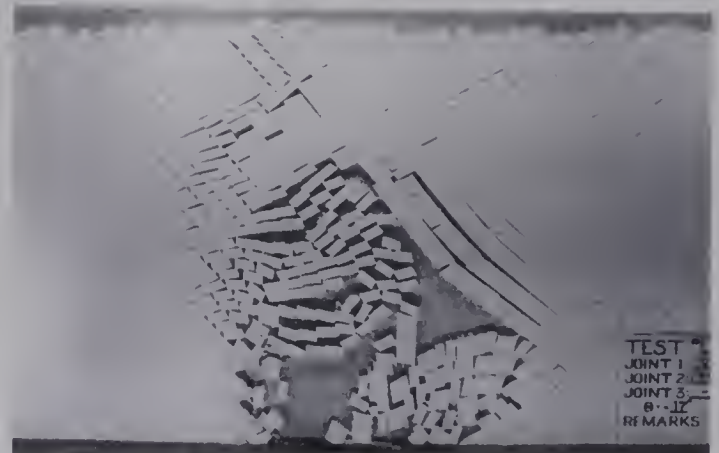
(A)



(B)



(C)



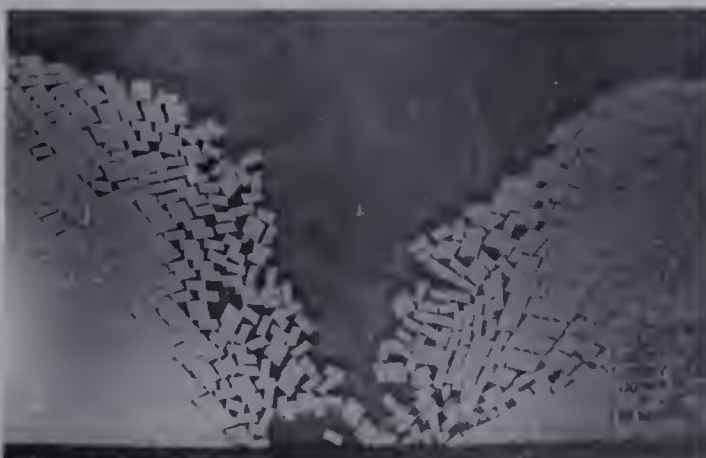
(D)



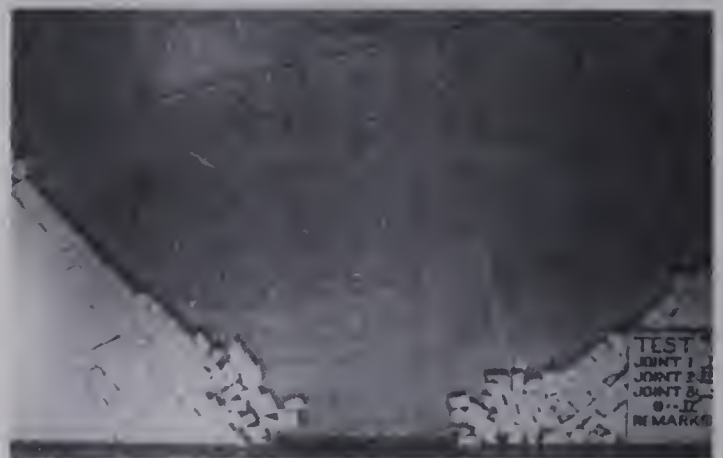
(E)



(F)



(G)



(H)

PLATE 38: TEST #025



(A)



(B)



(C)



(D)



(E)



(F)



(G)



(H)

Double kink-bands form in both the thin and thick beam-columns resulting ultimately, in the collapse of the entire structure and bin flow.

4.2.24. TEST #023 (PLATE 39)

The thick beam-columns readily detach from the right abutment when downward flexure occurs.

The right abutment beam-columns require a greater free span at 75 degrees than at 60 degrees as in the previous test, to buckle and shear. The thick roof beam-columns then form a double kink-band, collapsing and allowing the hangingwall to buckle and fail.

4.2.25. TEST #022 (PLATE 40)

The thick beam columns simply shear along the vertical discontinuities since they cannot flex sufficiently to form an axial load.

4.2.26. TEST #026 (PLATE 41)

An initial, small shear displacement along the thin beam-columns reduces the apparent thickness of the members. The member flexure cannot exert a high lateral force to the abutments and, therefore, continues to rotate and slide. Failure rapidly propagates to surface at constant span. The hangingwall then buckles and topples, forming a kink-band leading to bin flow.

PLATE 39: TEST #023



(A)



(B)



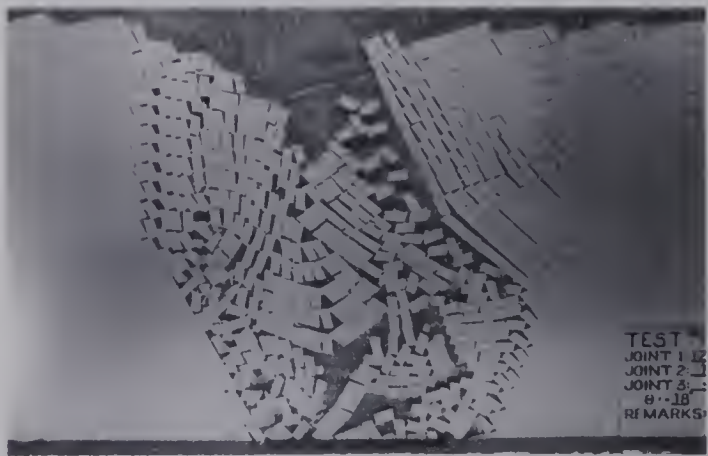
(C)



(D)



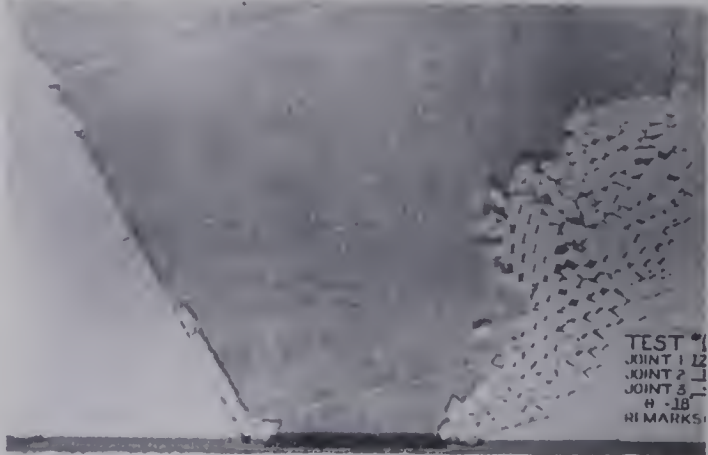
(E)



(F)



(G)



(H)

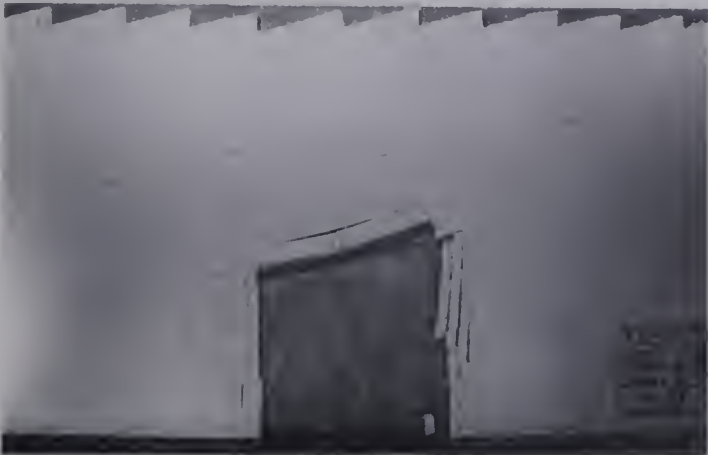
PLATE 40: TEST #022



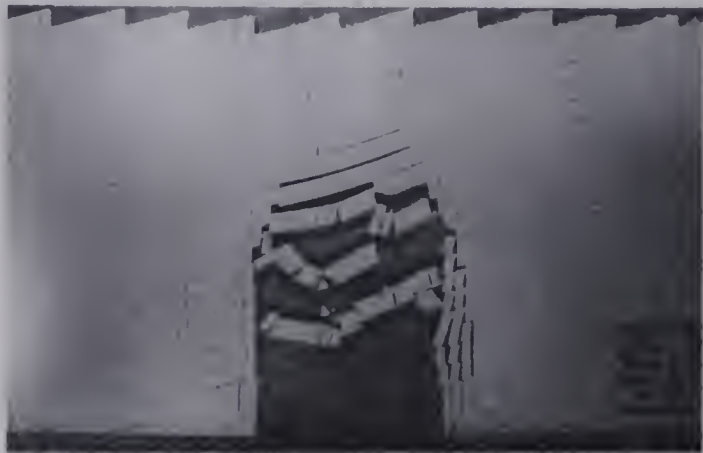
(A)



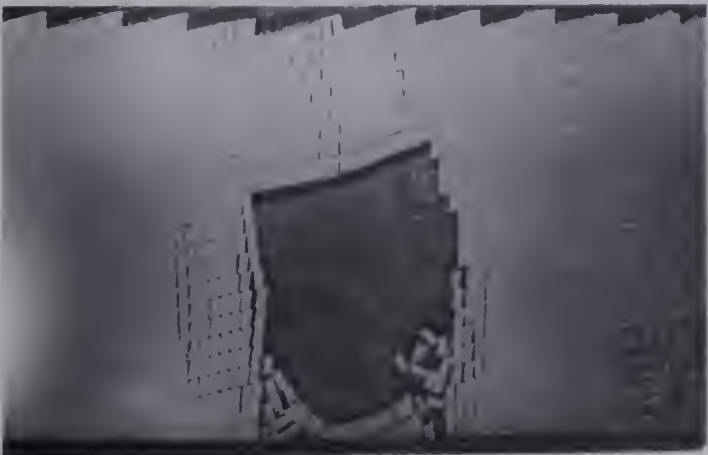
(B)



(C)



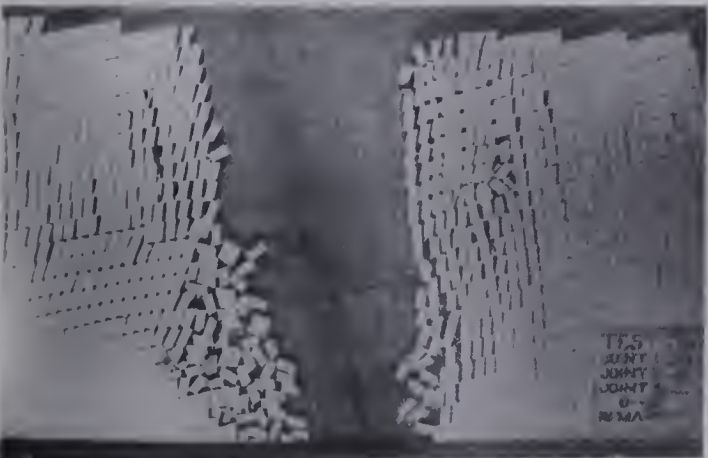
(D)



(E)



(F)



(G)



(H)

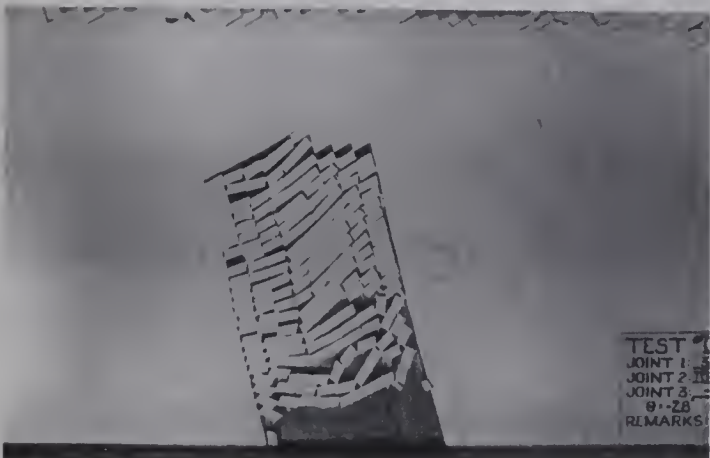
PLATE 41: TEST #026



(A)



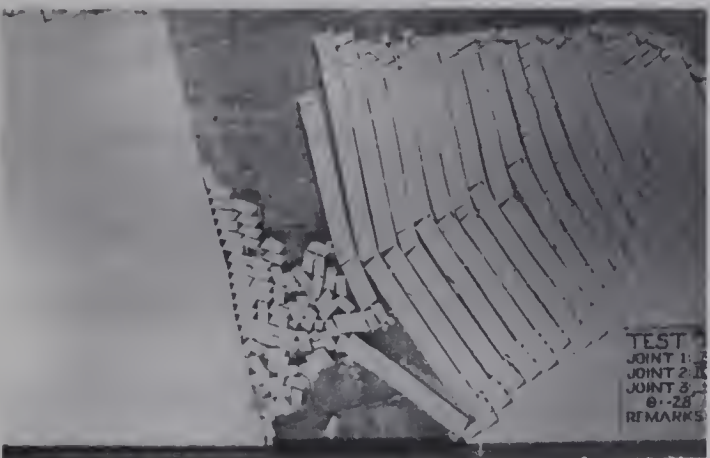
(B)



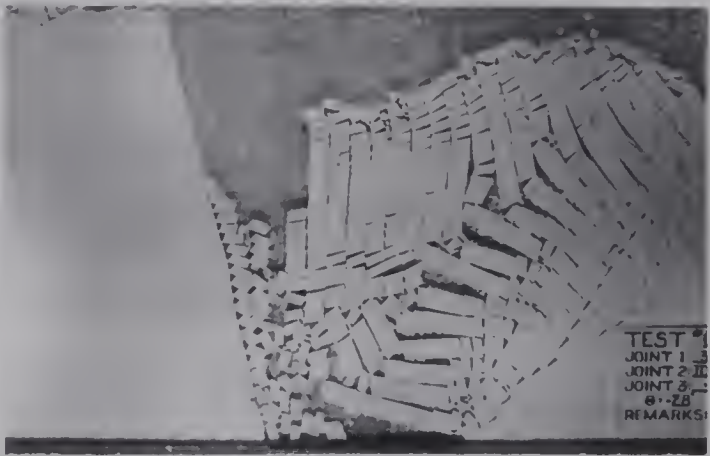
(C)



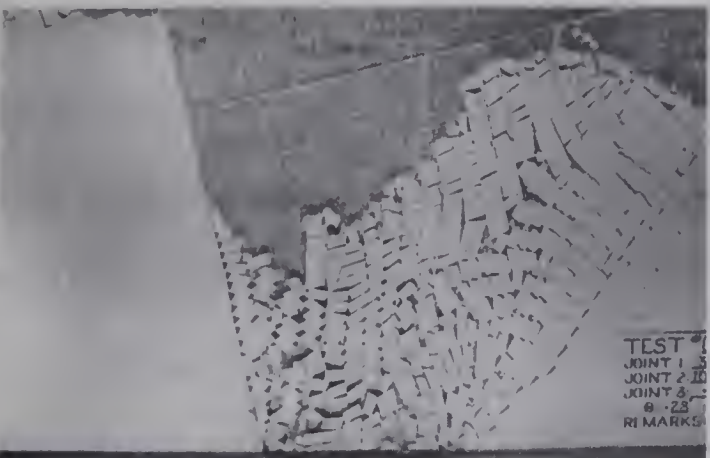
(D)



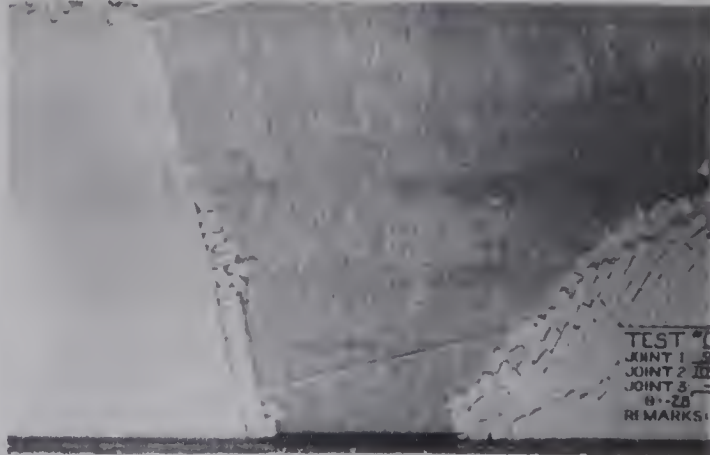
(E)



(F)



(G)



(H)

CHAPTER 5

CONCLUSION AND RECOMMENDATIONS

Two sets of continuous joints delineate an assemblage of rock blocks in a 2-D model as do three or more joint sets, generally, define a 3-D rock block assemblage.

In creating a large excavation in an assemblage of rock blocks, stresses are re-distributed. Deformation takes place and can lead to instability around this opening. Three inter-related failure modes can occur. First, inter-block sliding takes place when normal forces are low relative to tangential driving forces. Second, inter-block rotations can occur under two conditions: one, when the normal forces are high, relative to tangential driving forces, as in buckling of beam-columns and kink-bands, and two, when the driving forces on a block are highly eccentric with respect to the centroid. Third, yielding of intact material may occur if the compressive and tensile strengths are exceeded by point load crushing and tension, and by flexural tension.

All three failure modes occur simultaneously when instability does occur. Usually one mode is predominant at any one stage of failure, but the other modes significantly modify the progression of collapse.

The quantification of stability/instability parameters is difficult at this stage since these parameters are functions of:

rock block geometry

aspect ratio

position and orientation in space

intact material properties

inter-block friction

ambient stress fields

excavation size and orientation.

The testing has demonstrated, in a qualitative sense, how the three failure modes are affected by only three variables; the rock block geometry, aspect ratio and position and orientation in space. All the remaining parameters remained constant in this model. However, no simple trend can be evaluated since the failure modes are interactive, not discrete, and the predominant failure mode does change during the failure process.

Complexity of these failure modes requires complex analytical models for their evaluation. The current promising models are the discrete element method (requiring a rock failure algorithm) and the physical model, both base friction and vertical caving. Both models require increased refinement.

With improvements, the base friction modelling technique could be used to study the effects of subsidence, lateral pressures and stability of various mining methods and support systems (e.g. room and pillar or longwall mining).

Subsidence profile measurements may be conducted by

applying dial gages to the top surface of the model or by enhancing photographic techniques in conjunction with reference markings. Care in cutting the material is necessary since detrital material will slip between the belt and the model, creating adverse model behavior. It is not recommended that, with the present model material, joint spacings be less than one inch.

Lateral pressures might be provided by placing a mercury bag and standpipe against both side boards. When the machine is stationary, the belt friction would prevent the lateral transfer of this load. However, when the belt is moving, the belt vibration would probably allow this load transfer. The magnitude of the lateral pressure must be carefully monitored since, at some point, the lateral load may be sufficient to lift and buckle the model material.

Similarly, surload pressures may be applied to the top of the model by placing lead block weights against the top end of the belt. Here too, care must be taken so as not to overload the model or the material may lift and buckle.

Almost any two-dimensional excavation model may be examined by this method. The effects of sequenced excavation can be incorporated since, under low angle conditions, the belt can be stopped to allow manual block extraction.

More definitive examinations of beam-column and kink-band mechanisms should be conducted to quantify their behaviors.

Due to the difficulty in evaluating every condition

that may exist in a rock mass, no general behavior model can yet be outlined. Therefore, each specific rock mass problem requires a specific analytical model. At this stage, some combination of both numerical and physical modelling is required. For example, in order to evaluate an undercut size for a block cave mining system, a site specific rock mass model must be created by both numerical and physical methods from which, different undercut spans can be compared and evaluated.

BIBLIOGRAPHY

- BUCKY, P.B. (1956), "Fundamental considerations in block caving," Quart. Colo. School of Mines, Vol. 51, No. 3, pp. 128-146.
- CHAPMAN, J.C. and SLATFORD, J. (1956), "The elastic buckling of brittle columns," Proc. of I.C.E. , pp. 107-125.
- COATES, D.F. (1970), " Rock Mechanics Principles ," Canadian Dept. of Energy, Mines and Resources, Monograph 874 (revised 1970).
- CUNDALL, P.A. (1971), "A computer model for simulating progressive large scale movements in blocky rock systems," Proc. Int. Symp. on Rock Fracture , (ISRM), Nancy, France, paper II-8.
- CUNDALL, P.A. (1974), "A Computer Model for Rock-mass Behavior Using Interactive Graphics for the Input and Output of Geometrical Data," U.S. Corp. of Engineers, Technical Report MRD-2-74.
- EVANS, W.H. (1941), "The strength of undermined strata," Trans. I.M.M. , Vol. L, pp. 475-500, Discussion pp. 500-532.

- ERGUVANLI, K.A. and GOODMAN, R.E. (1972), "Application of models to engineering geology for rock excavations," Bull. A.E.G. , Vol. 9, No. 2, pp.89-104.
- FUMAGALLI, (1968), ", " Chap. 11 in Rock Mechanics in Engineering Practice , Ed. K.G. Stagg and O.C. Zienkiewicz, pp. , (John Wiley and Sons).
- GOODMAN, R.E. (1976), " Methods of Geological Engineering in Discontinuous Rocks ," (West Publishing Co.).
- HAMMETT, R.D. (1974), "A Study of the Behavior of Discontinuous Rock Masses," Ph.D. Thesis, James Cook University of North Queensland, Australia.
- LADANYI, B. and ARCHAMBAULT, G. (1972), "Evaluation de la resistance au cisaillement d'un massif rocheux fragmente," Proc. 24th Int. Geol. Cong. , Montreal, Canada, Section 13, p249.
- LEKHNITSKII, S.G. (1963), " Theory of Elasticity of an Anisotropic Elastic Body ," (Holden-Day, Inc.).
- MORGENSTERN, N.R. (1968), "Ultimate behavior of rock structures," Chap. 10 in Rock Mechanics in Engineering Practice , Ed. K.G. Stagg and O.C. Zienkiewicz, pp.321-351, (John Wiley and Sons).

- NASCIMENTO, U. and TEIXEIRA, H. (1971), "Mechanisms of internal friction in soils and rocks," Proc. Symp. on Rock Fracture , (ISRM), Nancy, France, paper II-3.
- OBERT, L. and DUVALL, W.I. (1967), " Rock Mechanics and the Design of Structures in Rock ," (John Wiley and Sons).
- PATTON, F.D. (1966), "Multiple modes of shear failure in rock," Proc. 1st Cong. I.S.R.M. , Lisbon, Portugal, Vol. 1, pp.509-513.
- PRICE, N.J. (1966), " Fault and Joint Development in Brittle and Semi-brittle Rock ," (Pergamon Press).
- STIMPSON, B. (1970), "Modelling materials for engineering rock mechanics," Int. J. Rock Mech. Min. Sci. , Vol. 7, pp.77-121.
- TIMOSHENKO, S.P. and GERE, J.M. (1961), " Theory of Elastic Stability ," (2nd edition), (McGraw-Hill).
- TROLLOPE, D.H. (1968), "The mechanics of discontinua or clastic mechanics in rock problems," Chap. 9 in Rock Mechanics in Engineering Practice , Ed. K.G. Stagg and O.C. Zienkiewicz, pp.275-320, (John Wiley and Sons).
- WHITTAKER, B.N. (1974), "An appraisal of strata control

practice," The Mining Engineer , No. 166, Vol. 134,
pp.9-24.

WOODRUFF, S.D. (1966), " Methods of Working Coal and Metal
Mines ," Vol. 1, (Pergamon Press).

ZIENKIEWICZ, O.C. (1971), " The Finite Element Method in
Engineering ," (McGraw-Hill).

APPENDIX I

ANALYSIS OF A BASE FRICTION MODEL AND THE MODEL SCALE LAW DERIVATIONS

Consider a small slice of model material (fig.6.1) of length Δx , thickness h , bulk density γ and belt width b , subjected to both the induced friction force due to belt motion and the gravitational body force.

For equilibrium in the direction of belt motion at angle θ :

$$\sum F_{\theta} = \sigma_{\theta} bh - (\sigma_{\theta} + \Delta\sigma_{\theta}) bh + \tau_{\phi} \Delta x b + \tau_{\theta} \Delta x b = 0 \quad /$$

where σ_{θ} = superincumbent strata stress

τ_{ϕ} = belt shear stress

τ_{θ} = gravitational shear stress component

therefore:

$$\tau_{\theta} = \frac{\Delta W \sin \theta}{\Delta x b} \quad 2$$

where ΔW = weight of section Δx .

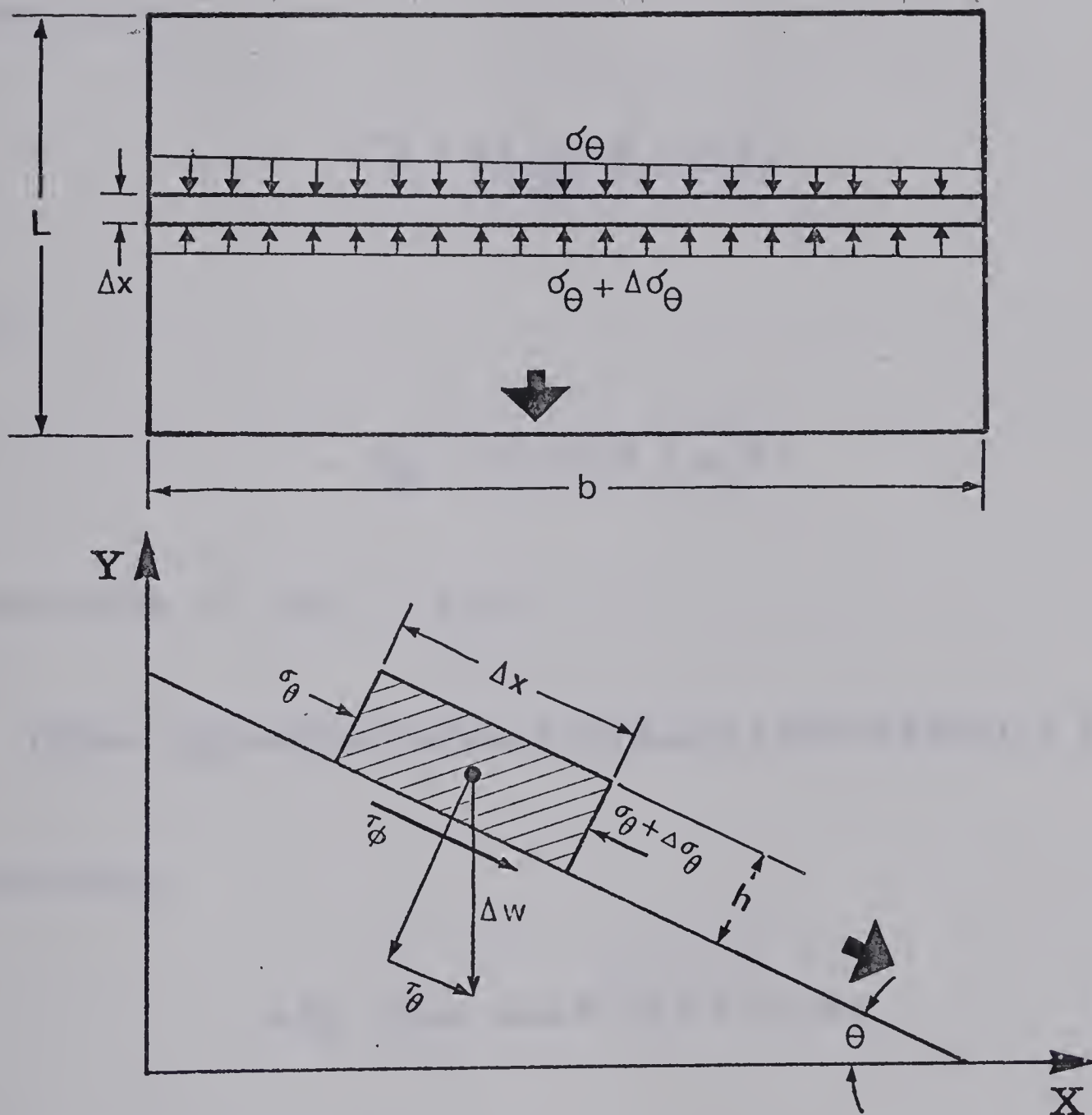


FIG. 6.1
Base Friction Stress Analysis

alternatively:

$$\tau_{\theta} = \gamma h \sin \theta \quad 3$$

similarly:

$$\tau_{\phi} = \frac{\Delta W \cos \theta \tan \phi}{\Delta x b} \quad 4$$

or:

$$\tau_{\phi} = \gamma h \cos \theta \tan \phi \quad 5$$

Substitute 3 and 5 into 1 :

$$(\sigma_{\theta} b h) - (\sigma_{\theta} + \Delta \sigma_{\theta}) b h + (h \gamma \cos \theta \tan \phi \Delta x b) + (h \gamma \sin \theta \Delta x b) = 0$$

therefore:

$$\Delta \sigma_{\theta} = \gamma \Delta x (\cos \theta \tan \phi + \sin \theta) \quad 6$$

integration results in:

$$\sigma_{\theta} = \gamma h (\cos \theta \tan \phi + \sin \theta) \quad 7$$

From equation 7 , the scaling laws can be developed, comparing the belt friction model to gravity-loaded rock.

Let the subscript r denote rock and m denote model material. The vertical stress developed in a rock mass is:

$$\sigma_r = \gamma_r h_r \quad 8$$

and the frictional stress developed in the model is:

$$\sigma_m = \gamma_m h_m (\cos \theta \tan \phi + \sin \theta) \quad 9$$

Therefore, for stress comparisons, the model stress scale factor (MSSF) is the ratio between the two equations 8 and 9 :

$$\text{MSSF} = \frac{\gamma_r h_r}{\gamma_m h_m (\cos \theta \tan \phi + \sin \theta)} \quad 10a$$

solving for θ :

$$\sin(\phi + \theta) = \frac{\sigma_m \gamma_r h_r \cos \phi}{\sigma_r \gamma_m h_m}$$

or:

$$\theta = \sin^{-1} \left(\frac{\sigma_m \gamma_r h_r \cos \phi}{\sigma_r \gamma_m h} \right) - \phi \quad 10b$$

or:

$$\theta = \sin^{-1} \left(\frac{\gamma^* h^* \cos \phi}{\sigma^*} \right) - \phi \quad 10c$$

where $\gamma^* = \gamma_r / \gamma_m$

$h^* = h_r / h_m$

$\sigma^* = \sigma_r / \sigma_m$

The simplest criterion for determining the value of the model stress scale factor is by comparing the rock and model material compressive strengths. That is:

$$\text{MSSF} = \frac{\sigma_{cr}}{\sigma_{cm}} \quad //$$

Therefore, for test purposes, the model must be tilted to:

$$\theta = \sin^{-1} \left(\frac{\sigma_{cm} \gamma_r h_r \cos \phi}{\sigma_{cr} \gamma_m h_m} \right) - \phi \quad 12$$

or:

$$\theta = \sin^{-1} \left(\frac{\gamma^* h^* \cos \phi}{\text{MSSF}} \right) - \phi$$

The appropriate rotation, θ , of the frame can be made and the initial stress distribution on the belt friction

model is directly proportional to that in a rock mass.

For example, the values used in this study are:

$$\gamma_m = 60 \text{ pcf}$$

$$\gamma_r = 165 \text{ pcf}$$

$$h_m = 48 \text{ inches}$$

$$h_r = 96 \text{ feet}$$

$$\sigma_{cm} = 25 \text{ psi}$$

$$\sigma_{cr} = 12,000 \text{ psi}$$

$$\phi = 22 \text{ degrees}$$

from equation 10b:

$$\theta = -15 \text{ degrees}$$

that is, the model material must be dragged upwards, towards the fixed restraint

The model stress scale factor from equation 10a is:

$$\text{MSSF} = 480$$

and the stress at the fixed restraint from equation 7 is:

$$\sigma_\theta = 0.23 \text{ psi}$$

In order to represent 24 inch joint spacings on the model, where:

$$h^* = 24$$

therefore:

$$h_m = 1 \text{ inch}$$

Therefore, the base friction model was tilted -15 degrees, the model material was 48 inches deep and the joints were cut at 1 inch spacings to represent a 96 foot rock depth and a 24 inch rock joint spacing.

APPENDIX II

MODEL MATERIAL PROPERTIES

An examination of different model materials was made. The material that appeared suitable for base friction modelling was a mixture of wheat flour and methanol. The following are some of the properties of this mixture (fig.7.1):

- a) tangential modulus of elasticity = 2,500 psi.
- b) compressive failure strength = 10 to 25 psi.
- c) failure strain = 1.4 %
- d) Brazilian tensile strength = 0.9 to 2.6 psi.
- e) density = 60 pcf.
- f) non-creeping

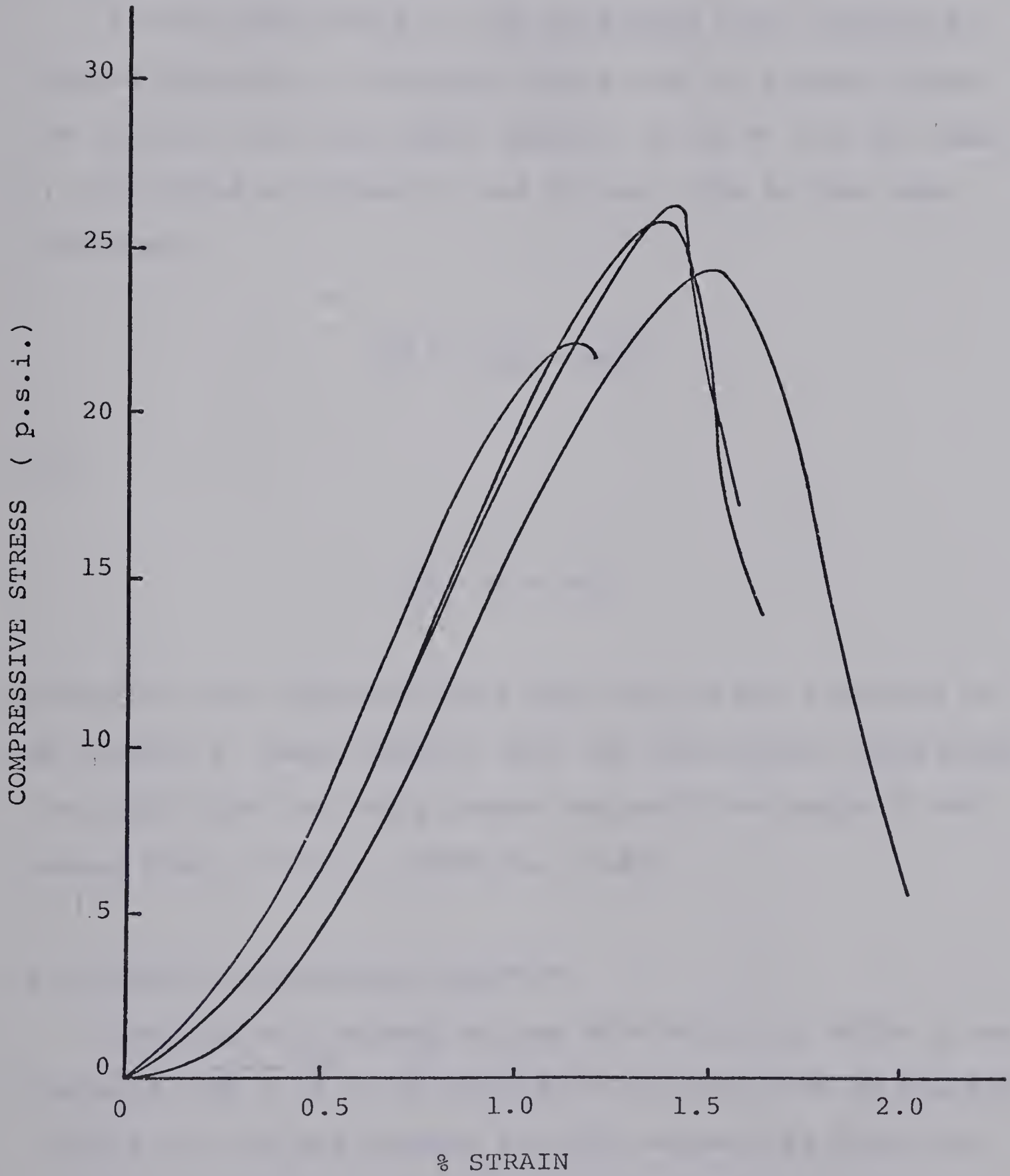


FIG. 7.1

Model Material Properties

APPENDIX III

KINK-BAND DETAILS

8.1 KINK-BAND HINGE ROTATIONS

As the first block in the kink-band hinge rotates α -degrees (fig.8.1), triangular space ABB' is formed. Since the initial and final sides opposite B and B' are the same, the angles at corners B and B' must also be the same. Therefore:

$$\beta = (180 - \alpha) / 2$$

or:

$$\beta = 90 - \alpha / 2$$

Therefore, the adjacent block can only rotate a maximum of $\alpha/2$ before it makes contact with the first block. Similarly, the third block can only rotate one half the angle of the second block, that is, $(\alpha/2)/2$, or $\alpha/4$.

8.2 VERTICAL MECHANICAL DILATION

Consider a kink-band column with height a , width b and diagonal $\sqrt{a^2 + b^2}$ at an angle γ , all rotated by an angle α (fig.8.2). For the maximum vertical mechanical dilation:

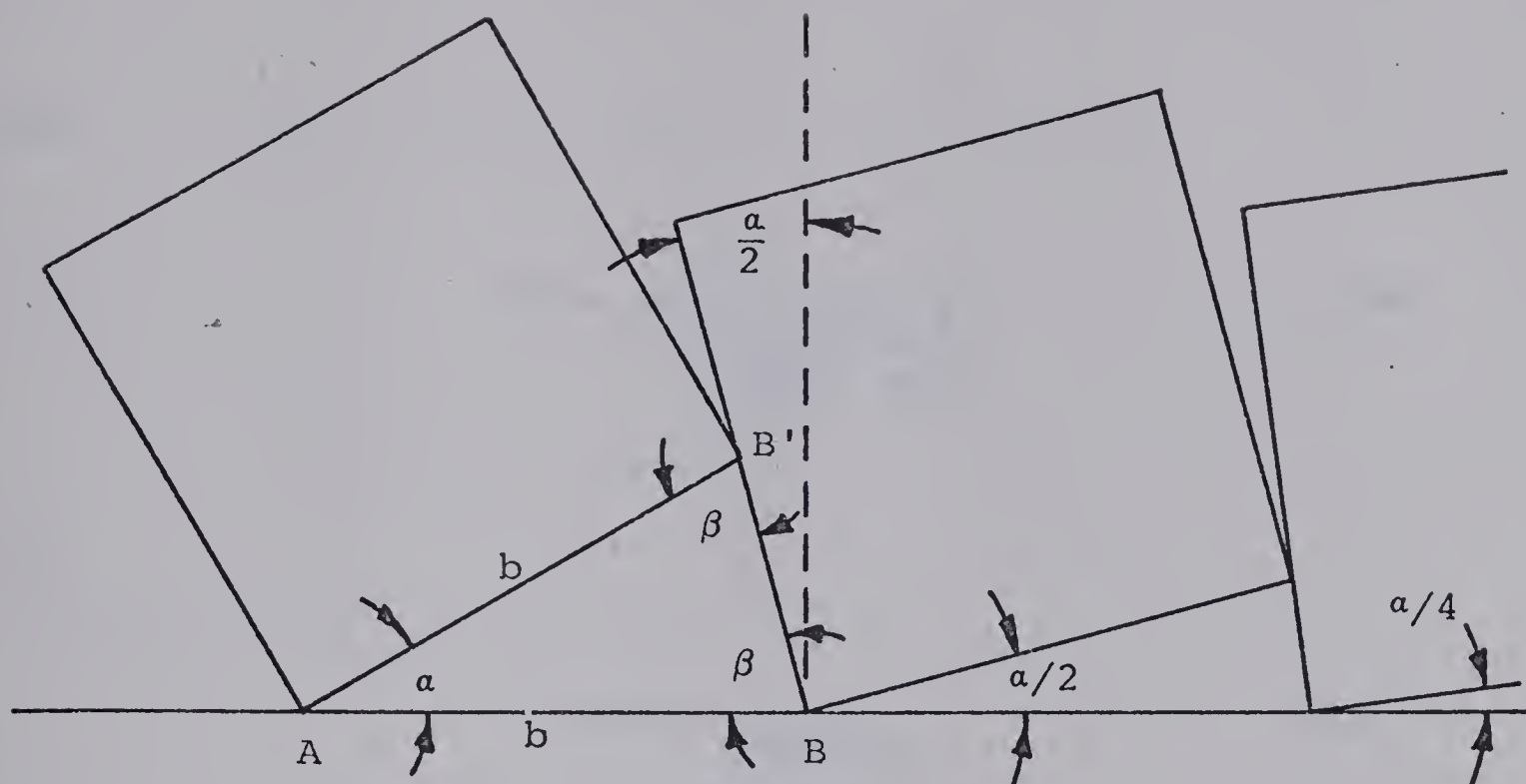


Fig. 8.1 Kink-Band Hinge Rotations

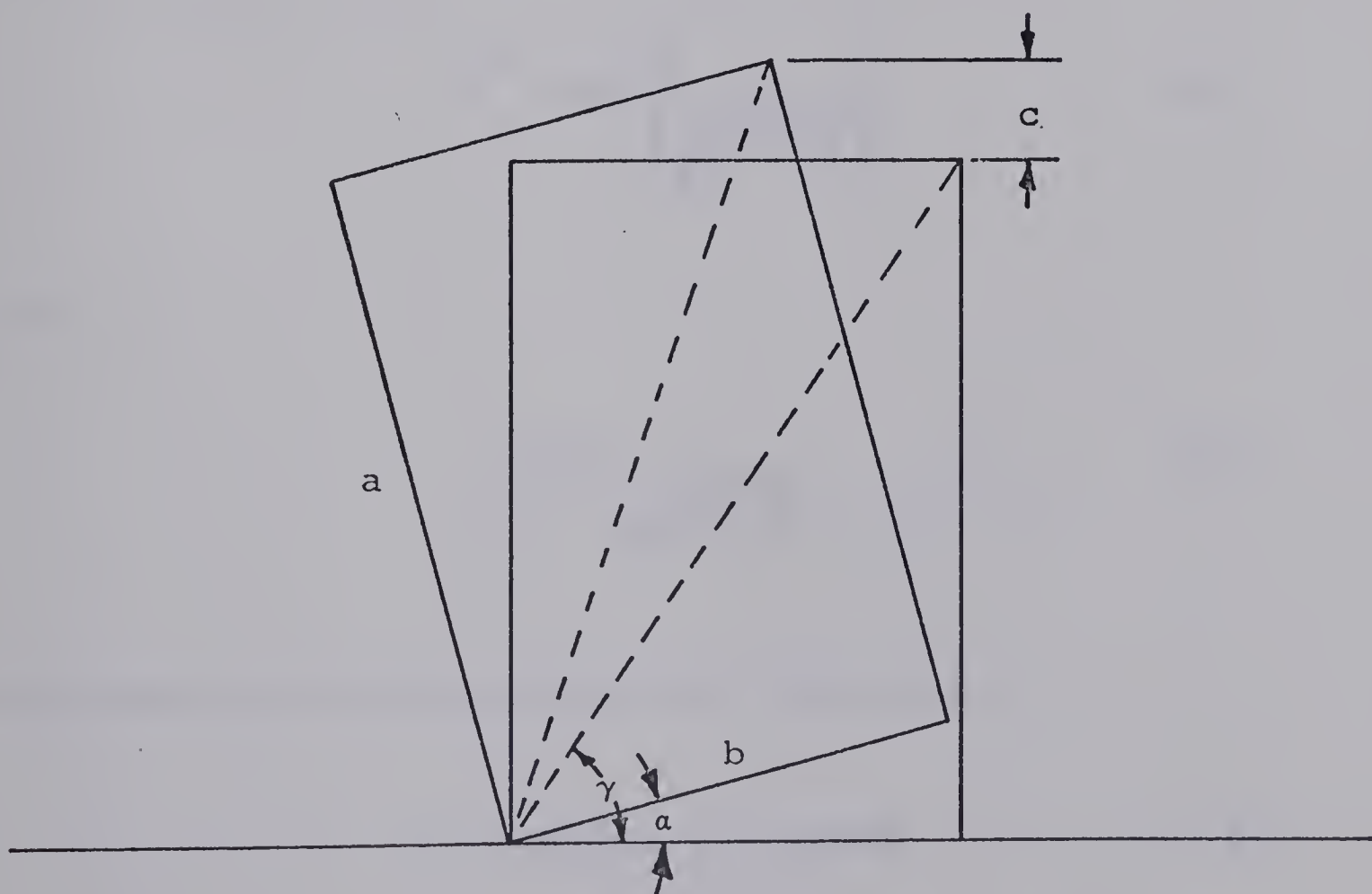


Fig. 8.2. Vertical Mechanical Dilation

$$\alpha = 90 - \gamma$$

/

but:

$$\gamma = \cos^{-1} \left(\frac{b}{\sqrt{a^2 + b^2}} \right) \quad 2a$$

or:

$$\cos \gamma = \frac{b}{\sqrt{a^2 + b^2}} \quad 2b$$

and:

$$\gamma = \sin^{-1} \left(\frac{a}{\sqrt{a^2 + b^2}} \right) \quad 2c$$

or:

$$\sin \gamma = \frac{a}{\sqrt{a^2 + b^2}} \quad 2d$$

The amount of vertical mechanical dilation is:

$$c = b \sin \alpha - a + a \cos \alpha \quad 3$$

by substituting 1 into 3, the maximum vertical dilation

is:

$$c_{max} = b \sin(90 - \gamma) - a + a \cos(90 - \gamma)$$

or:

$$c_{max} = b \cos \gamma - a + a \sin \gamma \quad 4$$

by substituting $2b$ and $2d$ into 4 :

$$c_{max} = \frac{b^2}{\sqrt{a^2 + b^2}} - a + \frac{a^2}{\sqrt{a^2 + b^2}} \quad 5$$

Let the aspect ratio of the columns be:

$$n = a/b \quad 6$$

therefore:

$$c_{max} = \frac{b^2}{\sqrt{n^2 b^2 + b^2}} - nb + \frac{n^2 b^2}{\sqrt{n^2 b^2 + b^2}} \quad 7a$$

or:

$$c_{max} = \frac{b^2 (n^2 + 1) - nb}{b \sqrt{n^2 + 1}} \quad 7b$$

or:

$$c_{max} = b \sqrt{n^2 + 1} - nb \quad 7c$$

Therefore, as the aspect ratio, n , increases, the maximum vertical mechanical dilation, c_{max} , decreases.

If the deformation and crushing of the block corners at the kink-band hinge is u , then the possibility exists that the width of the kink-band can be defined by the condition:

$$c_{max} - u \leq 0$$

However, further testing must be conducted to determine the validity of this statement.

APPENDIX IV

PROBLEMS AND IMPROVEMENTS IN THE DISCRETE ELEMENT METHOD

9.1. INTRODUCTION

The discrete element method developed by P. Cundall (1974) is on line on the AMDAHL 470 V/6 at the University of Alberta. The operating system under which this graphics package runs is the Michigan Terminal System (MTS). This system has on-line terminal support in a time-sharing mode. So far as interactive graphics are concerned, this system meets its foremost requirement, interaction. The analysis is performed by the user interacting on-line with the graphics display (i.e. in the running mode).

9.2. IMPLEMENTATION

It was important that the implementation allowed for as much flexibility as possible so as not to hinder the incorporation of a particular feature at a later date. Program modification is much easier if it in itself is quite comprehensible. This usually means good documentation and the use of a higher level language such as FORTRAN, PL/1 or ALGOL. What one loses in efficiency, one gains in flexibility and clarity.

The basic programming is available in Cundall's report. The theory and supporting program logic developed was assumed to be fairly well tested and remains intact in the

University of Alberta version. Also, the form of any program is determined heavily by the underlying data structures. The latter also remained intact so that reprogramming of the existing program logic was avoided. However, several design improvements were made to improve efficiencies in computer storage and run time.

9.3. MAJOR IMPROVEMENTS TO CUNDALL'S VERSION

9.3.1. HIGH LEVEL PROGRAMMING LANGUAGE

As a result of implementing the rock mass behavior program on a full size computer installation, a number of high level programming language compilers were made available. The use of ALGOL W over assembler language has all the automatic advantages of a high level language. Generally, the program became many more times readable to both the programmer and the less involved user. Increased readability facilitated any on going changes, improvements and extensions to the program. This must be a prime consideration in the design of any non-production, prototype program.

9.3.2. GENERAL PURPOSE GRAPHICS PACKAGE

The Integrated Graphics package used has the distinct advantage of availing to the programmer a very wide range of graphical manipulations. It frees the programmer from the details of the particular

graphics device used. All graphics within the program have a uniform design; indeed the graphics routines combined form a graphics language. Integrated Graphic's concept of pictures, sub-pictures and objects was extremely useful for the selection of commands from menus and for the various operations performed on the individual blocks.

9.3.3. DESIGN IMPROVEMENTS

a) CORNER BOXING SCHEME: The concept of classifying corners into boxes which divide up the 2-D space was retained and improved. Boxes were indexed by a 2-D co-ordinate system which was derived directly from their actual positioned value in reference to a x-y co-ordinate plane. This removed any limit to the bounds within which a corner could be classified. This is in direct contrast to Cundall's constrained scheme as reported on pages 62 - 63 of his report. This restrictive scheme required the removal (elimination) of rock blocks which had reached the edge of the display area whether or not they were still a significant part of the dynamics.

In addition to the above, the actual size of the boxes was made variable. A rough, inline calculation was made for each rock mass geometry in order to generate an optimal box size. The idea was to maintain a uniform number of boxes per edge of a block

regardless how fine or coarse the input structure should be. This would in turn result in a less variable number of searches for contacts per edge from one application to another. In other words, the boxing scheme retains a more or less optimal level of efficiency.

b) USE OF COMMAND MENUS: The presentation of all user commands in the form of displayed command menus which may be interactively selected, greatly facilitates the operation of the program. The previous function key operation of the program required a certain amount of training and practice by the user.

c) PICTURE SCALING: The present adaption allows the user to scale any rectangular region of the whole rock block system to full screen size while retaining proper aspect. This allows close inspection of the dynamics of a localized area within the system. The advantages of such a feature quickly becomes apparent once used.

d) LINE SEGMENT DEFINITION: The automatic definition of end 1 when displaying attached segments is a simple aid to manual input.

9.3.4. PROGRAMMING IMPROVEMENTS

a) LINE SEGMENT SORT ALGORITHMS: The sort algorithm used to sort segments of a new line into ascending order according to one of the co-ordinates

of the endpoint was improved. A Bubble Sort was used by Cundall which simply ripples the largest value of the ordered vector down to the end of the vector, one at a time. He failed to notice that after each "ripple", one need do one less comparison than the last time. For a n -element vector, $(n-1)$ comparisons were made on each ripple. In this case the number of comparisons (sorts), k , would vary as follows:

$$(n-1) \leq k \leq n(n-1)$$

or:

$$(n-1) \leq k \lesssim n^2$$

The sort algorithm was rewritten so that the range of comparisons was halved to:

$$(n-1) \leq k \leq n(n-1)/2.$$

b) DEAD END BACKUP: When a "dead end" situation arose in the scan of line segments forming a simple block, the original program abandoned the scan all together, eliminating the last segment (dead end). The scan was then restarted right from the beginning, redoing all the work which was just done in an attempt to build a block without the last dead end. The

program for block building was rewritten so that when a dead end occurred, the scan simply backed up one segment, then restarted having eliminated the dead end. Obviously, this is much more efficient.

c) BOX SCANNING FOR CONTACTS: As shown on page 78 in Cundall's report, all boxes within the rectangular region encompassing the edge were checked for corners which may be in contact. This search was reprogrammed, with the aid of the new boxing scheme, so that only those boxes along the edge were scanned for possible contacts.

9.4. CONCLUSION

Two problems arose which did not allow the use of Cundall's improved package for the caving study. The first problem concerned numerical instability and critical damping, which expressed itself by inter-penetration of blocks (i.e. a contact between blocks was not detected). Neither sufficient time nor current expertise was available to examine this problem and optimize the damping constants.

Secondly, but more significantly, the costs of running the improved program on a high-speed, time-sharing basis, rather than on a low-speed dedicated system, as Cundall had available, grew at an exponential rate with increase in the number of blocks drawn.

Though major improvements in program efficiency and the

development of a user-oriented system were made, the adaptation of the program to a time-shared mode is costly. It is suitable for demonstrating displacement mechanisms of a small number of blocks but is prohibitively expensive for simulating real rock masses containing hundreds of joint blocks.

Further information on the interactive graphics - discrete element program is available from Dr. B. Stimpson, Dept. of Mineral Engineering, The University of Alberta, Edmonton, Alberta, Canada.

B30246